Latvijas Universitāte
Cietvielu fizikas institūts

Roberts Zabels

# ĀTRO JONU IZRAISĪTIE STRUKTŪRAS UN MIKROMEHĀNISKO ĪPAŠĪBU MODIFIKĀCIJAS PROCESI PLATZONAS JONU KRISTĀLOS

Promocijas darbs
(publikāciju kopa)

Doktora grāda iegūšanai fizikas nozarē
Apakšnozare: cietvielu fizika

Rīga, 2015

# ĀTRO JONU IZRAISĪTIE STRUKTŪRAS UN MIKROMEHĀNISKO ĪPAŠĪBU MODIFIKĀCIJAS PROCESI PLATZONAS JONU KRISTĀLOS

## ANOTĀCIJA

Parādīts, ka ātro jonu izraisītajās struktūras un mikromehānisko īpašību izmaiņās LiF kristālos nozīmīgu ieguldījumu dod prizmatisko dislokāciju cilpu veidošanās. Atrasts, ka dislokāciju aizmetņi veidojas jau individuālos jonu trekos, bet dislokāciju struktūra intensīvi formējas treku pārklāšanās stadijā. LiF kristālos iegūta apstarošanas virzienā orientēta mozaīkas tipa nanostruktūra, apstarojot tos ar augstas enerģijas smagajiem joniem (U, Au, Kr, Xe) un noskaidroti tās veidošanās nosacījumi. Parādīts, ka apstarošana ar augstām ātro jonu dozām noved pie plastiskās deformācijas mehānisma maiņas no dislokāciju mehānisma uz deformācijas norisi lokalizēto bīdes zonu veidošanās ceļā. Pētīti ātro jonu izraisītie efekti MgO kā radiācijas izturīgā un pielietojumiem aktuālā materiālā. Novērota elastīgo sadursmju un elektronisko ierosinājumu mehānismu līdzdalība mikromehānisko īpašību modifikācijā.

**Atslēgas vārdi:** *LiF, MgO, nanoindentēšana, ātrie joni, dislokācijas*

# SWIFT-ION-INDUCED MODIFICATIONS OF STRUCTURE AND MICROMECHANICAL PROPERTIES IN WIDE-GAP IONIC CRYSTALS

## ANNOTATION

It has been shown that a major role in changes of structural and micromechanical properties in LiF crystals caused by swift ions is assigned to formation of prismatic dislocation loops. It has been found that dislocation seedlings are formed already in individual ion tracks but intense formation of a dislocation structure occurs in the stage of track overlapping. In LiF a mosaic-type nanostructure oriented in the direction of the ion beam has been obtained by irradiation with energetic heavy ions (U, Au, Kr, Xe). The prerequisites for its formation have been determined. It has been show that irradiation with high doses leads to change in the mechanism of plastic deformation – from dislocation glide to shear banding. Swift ion caused effects in MgO as a radiation resistant and application oriented material have been studied. A co-participation of elastic collisions and electronic excitations in modification of micromechanical properties has been observed.

**Key words:** *LiF, MgO, nanoindentation, swift ions, dislocations*

# PUBLIKĀCIJU SARAKSTS

1. J. Maniks, I. Manika, R. Grants, **R. Zabels**, K. Schwartz, M. Sorokin, R.M. Papaleo, Nanostructuring and hardening of LiF crystals irradiated with 3-15 MeV Au ions, *Applied Physics A: Materials Science and Processing*, 104 (2011) 1121-1128.
2. J. Maniks, I. Manika, **R. Zabels,** R. Grants, K. Schwartz, M. Sorokin, Modification of the structure and nano-mechanical properties of LiF crystals under irradiation with swift heavy ions, *Materials Science (Medžiagotyra),* 17 (2011) 223.
3. J. Maniks, I. Manika, **R. Zabels**, R. Grants, E. Tamanis, K. Schwartz, Nanostructuring and strengthening of LiF crystals by swift heavy ions: AFM, XRD and nanoindentation study, *Nuclear Instruments and Methods in Physics Research, Section B: Beam Interactions with Materials and Atoms*, 282 (2012) 81-84.
4. A. Dauletbekova, J. Maniks, I. Manika, **R. Zabels**, A.T. Akilbekov, M.V. Zdorovets, Y. Bikhert, K. Schwartz, Color centers and nanodefects in LiF crystals irradiated with 150 MeV Kr ions, *Nuclear Instruments and Methods in Physics Research, Section B: Beam Interactions with Materials and Atoms*, 286 (2012) 56-60.
5. J. Maniks, **R. Zabels**, I. Manika, Shear banding mechanism of plastic deformation in LiF irradiated with swift heavy ions, *IOP Conference Series: Materials Science and Engineering*, 38 (2012) 012017.
6. I. Manika, J. Maniks, **R. Zabels**, K. Schwartz, R. Grants, A. Dauletbekova, A. Rusakova, M. Zdorovets, Modification of LiF structure by irradiation with swift heavy ions under oblique incidence, *IOP Conference Series: Materials Science and Engineering*, 49 (2013) 012011.
7. **R. Zabels**, I. Manika, K. Schwartz, J. Maniks, R. Grants, MeV-GeV ion induced dislocation loops in LiF crystals, *Nuclear Instruments and Methods in Physics Research, Section B: Beam Interactions with Materials and Atoms*, 326 (2014) 318.
8. **R. Zabels**, I. Manika, K. Schwartz, J. Maniks, R. Grants, M. Sorokin, M. Zdorovets, Depth profiles of indentation hardness and dislocation mobility in MgO single crystals irradiated with swift $^{84}$Kr and $^{14}$N ions, 2015. gada 30. martā akceptēts publicēšanai žurnālā *Applied physics A.*,
   DOI: 10.1007/s00339-015-9145-9

Appl Phys A (2011) 104:1121–1128
DOI 10.1007/s00339-011-6387-z

**Applied Physics A**
**Materials Science & Processing**

# Nanostructuring and hardening of LiF crystals irradiated with 3–15 MeV Au ions

**J. Maniks · I. Manika · R. Grants · R. Zabels · K. Schwartz · M. Sorokin · R.M. Papaleo**

Received: 15 July 2010 / Accepted: 15 March 2011 / Published online: 14 April 2011


**Abstract** Modifications of the structure and mechanical properties in LiF crystals irradiated with MeV-energy Au ions have been studied using nanoindentation, atomic force microscopy and optical spectroscopy. The nanostructuring of crystals under a high-fluence irradiation (above $10^{13}$ ions/cm$^2$) was observed. Nanoindentation tests show a strong ion-induced increase of hardness (up to 150–200%), which is related to the high volume concentration of complex color centers, defect aggregates, dislocation loops and grain boundaries acting as strong barriers for dislocations. From the depth profiling of the hardness and energy loss it follows that both nuclear and electronic stopping mechanisms of MeV Au ions contribute to the creation of damage and hardening. Whereas the electronic stopping is dominating in the near-surface region, the effect of elastic displacements prevails in deeper layers close to the projectile range.

J. Maniks (✉) · I. Manika · R. Grants · R. Zabels
Institute of Solid State Physics, University of Latvia, 8 Kengaraga Str., 1063 Riga, Latvia
e-mail: manik@latnet.lv
Fax: +371-671-32778

I. Manika
e-mail: manik@latnet.lv

R. Grants
e-mail: rolchix@gmail.com

R. Zabels
e-mail: rzabels@gmail.com

K. Schwartz
GSI Helmholtz Zentrum für Schwerionenforschung, Planckstr. 1, 64291 Darmstadt, Germany
e-mail: K.Schwartz@gsi.de

M. Sorokin
Russian Research Centre 'Kurchatov Institute', Moscow, Russia
e-mail: m40@lab2.ru

R.M. Papaleo
Faculty of Physics, PUCRS, Av. Ipiranga 6681, Porto Alegre, RS, Brazil
e-mail: papaleo@pucrs.br

## 1 Introduction

Beams of swift heavy ions with MeV–GeV energy have increasingly gained an interest for their application in a structural modification of materials and an improvement of their optical, electrical and other properties [1].

Peculiarities of a heavy-ion interaction with dielectrics are a fast energy deposition in a time scale shorter than the defect creation time, a high excitation density and a high gradient of absorbed energy in the ion track [2–5]. In LiF crystals heavy ions create fast electrons, which after a thermal relaxation induce electronic excitations of the lattice (excitons, electron–hole pairs). These lattice excitations after self trapping produce $F$–$H$ Frenkel pairs (where the $F$ center is an anion vacancy with a localized electron ($v_a{}^+e$) and the $H$ center is an interstitial halogen molecule $X_2^-$). A higher dose (fluence) of the irradiation at room temperature leads to the transformation of primary $F$ and $H$ centers into more complex electron ($F_2$, $F_3$, $F_4$) and hole ($V_3$) centers (the $V_3$ center is a three-halide molecule $X_3^- = X^0X^-X^0$ in the lattice), halogen molecules ($H + H \rightarrow X_2$) and their clusters ($nX_2$) [2, 6].

An irradiation of LiF with ions in the MeV energy range shows some peculiarities relative to GeV ions. The MeV ions exhibit a comparable or higher elastic (nuclear) energy loss [6, 7]. Nevertheless, a more detailed analysis of the energy deposition of displaced atoms (recoils) shows that even for 3-MeV Au ions, where the elastic energy loss is twice the electronic one, the interaction of recoils with the crystal leads to a 66% fraction of the energy deposited into the

**Table 1** Energy ($E_{ion}$) and charge ($q$) of incident Au ions, calculated inelastic (ionization) energy loss fraction (% of $E_{ion}$) and range ($R$) for Au ions of different energies in LiF

| $E_{ion}$, MeV | Ion charge $q$ | Inelastic losses, % of $E_{ion}$ | | | Ion range $R$, μm |
|---|---|---|---|---|---|
| | | Ions | Recoils | Total | |
| 3 | +2 | 30.9 | 35.5 | 66.4 | 0.67 |
| 5 | +2 | 38.7 | 33.4 | 72.1 | 1.14 |
| 10 | +4 | 49.9 | 29.2 | 79.1 | 2.29 |
| 12 | +4 | 53.0 | 28.0 | 81.0 | 2.75 |
| 15 | +6 | 58.5 | 24.4 | 82.9 | 3.49 |

electronic subsystem [8]. Having a projected range of a few micrometers, the MeV ions induce a volume concentration of color centers more than one order of magnitude higher than the GeV-energy ions with the same absorbed energy. The high volume concentration of primary Frenkel pairs, on the one hand, leads to a high electron–hole center recombination and, on the other hand, to more efficient coagulation processes leading to a formation of $F_n$ centers as well as halogen molecules ($X_2$) and their aggregates [6]. These processes strongly depend on flux (beam current density) and fluence [9]. The coagulation of ion-induced defects produces strong modifications in the structure and properties of the target material. A high-fluence irradiation of LiF with swift heavy ions induces a pronounced increase of the indentation hardness which is sensitive to defect aggregates as strong obstacles for dislocations [10]. Indentation tests can provide information about defect aggregates on the surface as well as in the bulk of irradiated crystals.

In the presented study the modification of the structure and mechanical properties of LiF crystals irradiated with 3–15 MeV Au ions has been performed using optical absorption spectroscopy, nanoindentation, chemical etching and atomic force microscopy.

## 2 Experimental

Experiments were performed on nominally pure LiF single crystals grown from the melt in an inert atmosphere (Korth Kristalle, Germany). Main trace impurities were Mg and Na with the concentration of 20 ppm. The density of grown-in dislocations in the non-irradiated samples was about $5 \times 10^4$ cm$^{-2}$. Thin platelets were cleaved from a crystal block along the (100) planes. Crystals were irradiated at the Tandetron accelerator in Porto Alegre (Brazil) with 3-, 5-, 10- , 12- and 15-MeV Au ions at fluences of $10^{12}$–$2 \times 10^{14}$ ions/cm$^2$ and ion beam current densities ($i_{beam}$) from 6.2 to 150 nA/cm$^2$. The flux ($\varphi$) can be estimated as $\varphi = 6.24 \times 10^9 \times i_{beam}/q$ ions cm$^{-2}$ s$^{-1}$, where $q$ is the charge of the ion (Table 1). In order to compare effects induced by MeV- and GeV-ion irradiations, LiF samples were irradiated at the UNILAC linear accelerator of the GSI, Darmstadt with 2.2-GeV Au ions at a fluence of $10^{12}$ ions/cm$^2$ with a flux of $\sim 10^8$ ions cm$^{-2}$ s$^{-1}$. All irradiations were performed at room temperature and under normal incidence of the ions to the (100) cleavage face of the crystals. The irradiation parameters for LiF crystals and also the values of inelastic energy loss fraction (% of $E_{ion}$) and range ($R$) for Au ions which were calculated using the SRIM 2010 code [7] are presented in Table 1.

Optical spectroscopy was performed using a double-beam spectrometer (ATI Unicam UV4) in the spectral range of 190–700 nm. In this study only electron color centers ($F$, $F_2$, $F_3$, $F_4$) were tested, whereas the complementary $V_3$ centers have absorption in the vacuum UV spectral region (maximum at 114 nm) inaccessible with our equipment.

Nanoindentation tests were performed by a MTS G200 nanoindenter with a Berkovich diamond tip (curvature <20 nm) using the basic and continuous stiffness measurement techniques. Measurements were conducted at a load resolution <50 nN, a displacement resolution ≥1 nm, a strain rate of 0.05 s$^{-1}$ and a harmonic frequency of 45 Hz. The nanoindenter was calibrated using a reference sample of fused silica. The hardness, Young's modulus and standard deviation of the measurements were calculated from experimentally obtained loading–unloading curves by the MTS TestWorks 4 software. Results were averaged from 10 individual measurements. Indentation tests were conducted on the irradiated surface in ambient air at room temperature. The depth profiles of hardness and modulus were obtained from the indentation tests on sample cross sections prepared by cleaving perpendicular to the irradiated surface. The distance of indents from the irradiated surface was measured by optical microscopy. The structural defects in irradiated crystals were revealed by chemical etching in a saturated aqueous $FeCl_3$ solution. The surface topography was studied with a Veeco CPII atomic force microscope in tapping mode using standard silicon probes with a tip radius of 10 nm.

## 3 Results

### 3.1 Color centers

The irradiation with 3–15 MeV Au ions in LiF produces Frenkel pairs ($F$–$H$) with a high volume concentration. This is illustrated in Fig. 1 for LiF irradiated with 15-MeV Au ions to a fluence of $5 \times 10^{13}$ ions/cm$^2$ at two different flux ($\varphi$) values ($\varphi_1 = 6.5 \times 10^{10}$ and $\varphi_2 = 1.6 \times 10^{11}$ ions/cm$^2$ s). At the larger flux the number of created color centers is higher due to the enhanced formation of di-halide molecules

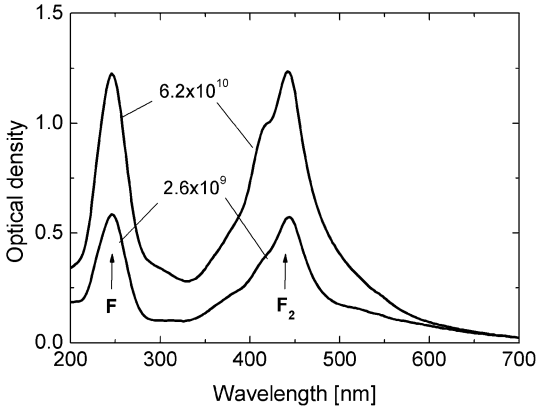


**Fig. 1** Optical absorption spectra for LiF crystals irradiated with 15-MeV Au ions at fluence $5 \times 10^{13}$ ions/cm$^2$. The ion beam flux values were $2.6 \times 10^9$ ions cm$^{-2}$ s$^{-1}$ and $6.2 \times 10^{10}$ ions cm$^{-2}$ s$^{-1}$

and their clusters, which prevents the recombination of mobile $H$ centers with electron color centers [6].

The concentrations of $F$ and $F_2$ centers can be estimated from the absorption spectra using the Smakula–Dexter formula [4]

$$n_F = 9.48 \times 10^{15} \times D_F \tag{1}$$

and

$$n_{F_2} = 4.42 \times 10^{15} \times D_{F_2}, \tag{2}$$

where $D_F$ and $D_{F_2}$ are the optical densities at the maximum of the absorption spectra for $F$ (250 nm) and $F_2$ (445 nm) centers, respectively. According to (1), the number of created $F$ centers for the higher flux (Fig. 1) is $n_F = 1.2 \times 10^{16}$ cm$^{-2}$ with the volume concentration $N_F = n_F/R \sim 3.4 \times 10^{19}$ cm$^{-3}$. Such volume concentration is much higher than in crystals irradiated with GeV Au ions having the same absorbed energy [4, 5]. The high value of $N_F$ stimulates the formation of $F_n$ centers. We can estimate the concentration for $F_n$ centers using the formula (2) with the approximation that the $F_2$ centers are dominating. The ratio $n_{F_2}/n_F = 0.47$, which is also remarkably higher than for GeV Au ions with the same absorbed energy (cf. [4], where $n_{F_2}/n_F = 0.2$). At a higher flux the efficiency of $F$ center aggregation increases and higher concentrations of $F_3$ and $F_4$ centers are produced according to the reactions $F_2 + F \rightarrow F_3$ and $F_3 + F \rightarrow F_4$. The maxima of the absorption spectra of $F_3$ centers are at 317 and 377 nm and for $F_4$ centers at 518 and 540 nm, respectively. The increased concentrations of $F_3$ and $F_4$ centers lead to an extension of the absorption around the $F_2$ peak (Fig. 1).

Taking into account the high volume concentration of defect aggregates in crystals irradiated with 3–15 MeV Au ions, we can expect a stronger ion-induced effect on mechanical properties.

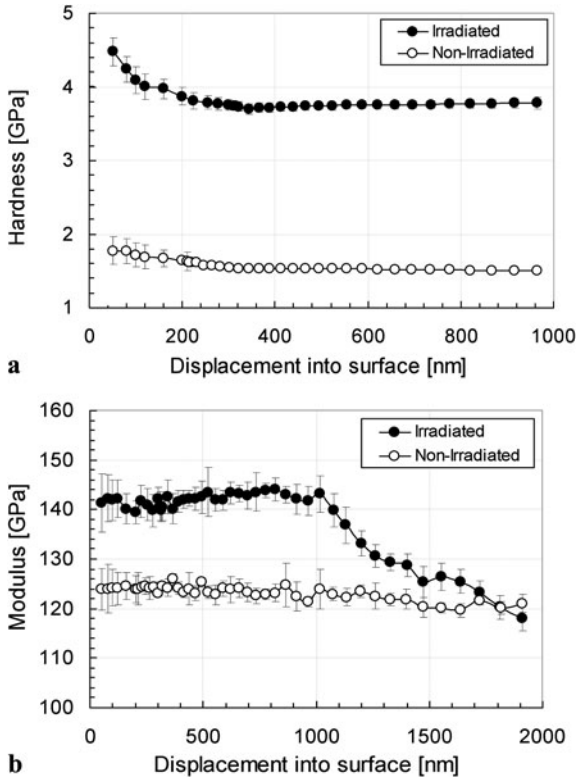


**Fig. 2** Hardness (**a**) and Young's modulus (**b**) on the irradiated surface as a function of indentation depth for samples irradiated with 15-MeV Au ions at the fluence of $5 \times 10^{13}$ ions/cm$^2$. The measured values for a non-irradiated LiF crystal are reported for comparison

### 3.2 Ion-induced changes of hardness and modulus

Nanoindentation tests showed a remarkable ion-induced increase of hardness which depends on the fluence and the ion energy. In order to exclude the effect of a softer bulk material, measurements were performed in a limited indentation depth range ($\leq 0.3$ of the thickness of the irradiated layer) in accordance with the recommendations for a given hardness ratio of irradiated and non-irradiated material [11].

Figure 2 demonstrates a typical result for the sample irradiated with 15-MeV Au ions. The hardness on the irradiated surface exceeds the hardness of a non-irradiated crystal by 150%, providing the evidence of a severe ion-induced damage and a formation of strong obstacles for dislocations. The ion-induced change of Young's modulus is comparatively small (about 15%, Fig. 2b) and lies in the typical range for stress-induced variations of modulus. Moreover, the sign of the effect changes from positive on the irradiated surface to negative in deeper layers, thus following the change of ion-induced stresses from compressive on the surface to tensile at the vicinity of the interface between irradiated and non-irradiated areas.

The dependence of hardness on fluence for all applied ion energies is shown in Fig. 3. The ion-induced hardening

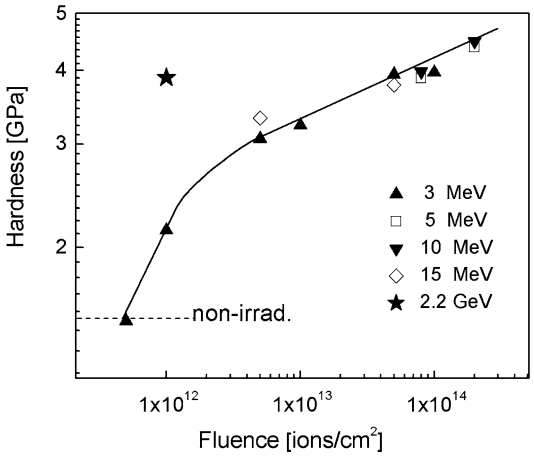


**Fig. 3** Hardness as a function of fluence for LiF irradiated with 3-, 5-, 10- and 15-MeV Au ions. The irradiation is performed at an ion beam current density of 100 nA/cm$^2$. The measured value for the irradiation with 2.2-GeV Au ions is also reported

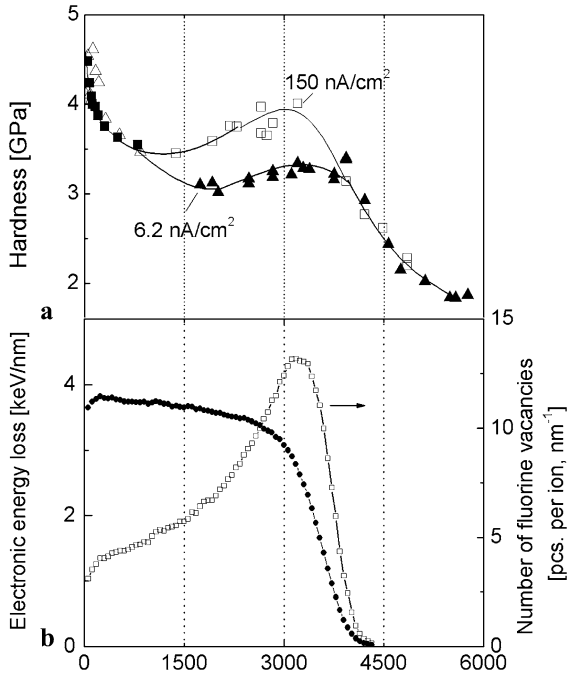


**Fig. 4** (**a**) The depth profile of hardness of LiF irradiated with 15-MeV Au ions; the density of ion beam current was 6.2 and 150 nA/cm$^2$; (**b**) the calculated depth profiles of electronic energy loss (*circles*, *left-hand axis*) and fluorine vacancies, created by elastic displacements (*open squares*, *right-hand axis*)

is observed at fluences above the threshold of $10^{12}$ ions/cm$^2$. The hardness increases with the fluence and saturates at the fluence of $10^{14}$ ions/cm$^2$. The saturation value of hardness ($\sim$4.5 GPa) exceeds by a factor of three the hardness of a virgin crystal. The hardness data for all applied ion energies settle on a common curve, thus indicating that the ion-induced hardening is nearly independent of energy. Obviously, such behavior emerges from the fact that the local deposited energy ($E/R$) in the investigated range of ion energies is almost constant (see Table 1). However, an increase of the energy leads to an increase of the depth of the hardened layer in accordance with the change of the ion range.

Depth profiles of the hardness were measured on the cross section of irradiated crystals. A detailed study was performed on samples irradiated with 15-MeV Au ions with the flux of 2.6 and 6.2 ions cm$^{-2}$ s$^{-1}$. To access the near-surface region, results are supplemented with the hardness–indentation depth data from measurements on the irradiated surface. Hardness as a function of the distance from the irradiated surface is plotted in Fig. 4a. The hardness curve displays two maxima: (1) on the irradiated surface and (2) close to the end of the ion pass. A stronger hardening on the surface is typical for irradiations with swift heavy ions [10]. The hardening maximum in bulk is sensitive to the ion beam current density and increases with the current. The hardened zone is slightly extended beyond the projectile range. In order to compare the nanoindentation data with the fraction of the energy actually absorbed by the target material, we used the SRIM code in the mode of a detailed calculation with full damage cascades as described in [8]. It was taken into account that the primary knocked target atoms have the energy high enough to deposit a considerable fraction of the energy in inelastic collisions inside the material. The calculated data of the electronic energy loss contributed both by projectile ions and recoils and the calculated profile of fluorine vacancies created by elastic displacements for 15-MeV Au ions are plotted in Fig. 4b. From the comparison of depth profiles of the hardness and the energy loss, it follows that both nuclear and electronic stopping mechanisms of MeV Au ions contribute to the creation of damage and hardening. Whereas the electronic stopping is dominating in the near-surface region, the effect of elastic displacements prevails in deeper layers close to the projectile range.

To compare effects produced by MeV and GeV ions, the nanoindentation tests were performed also on LiF samples irradiated with 2.2-GeV Au ions at the fluence of $10^{12}$ ions/cm$^2$, at which ion tracks strongly overlap and the effect of the ion-induced hardening saturates. An observed increase in the hardness in the case of the GeV-ion irradiation reaches up to 3.9 GPa, which is in accordance to the previous research results [10]. To achieve the same hardening by MeV ions a higher fluence is required (see Fig. 3) but the absorbed energy in comparison to GeV ions is lower. The irradiation at an ion beam current density of 100 nA/cm$^2$ corresponds to the flux of $3.12 \times 10^{11}$ ions cm$^{-2}$ s$^{-1}$ for 3- and 5-MeV, $1.56 \times 10^{11}$ ions cm$^{-2}$ s$^{-1}$ for 10-MeV and $10^{11}$ ions cm$^{-2}$ s$^{-1}$ for 15-MeV Au ions. The flux for 2.2-GeV Au ions was $\varphi \approx 10^8$ ions cm$^{-2}$ s$^{-1}$. The absorbed ion energy $E_{\text{ion}} \times \Phi$ for 2.2-GeV Au ions ($\Phi = 10^{12}$ ions/cm$^2$) is $2.2 \times 10^{21}$ eV/cm$^2$ and for 3-MeV Au ions ($\Phi = 10^{14}$ ions/cm$^2$) is $3 \times 10^{20}$ eV/cm$^2$.

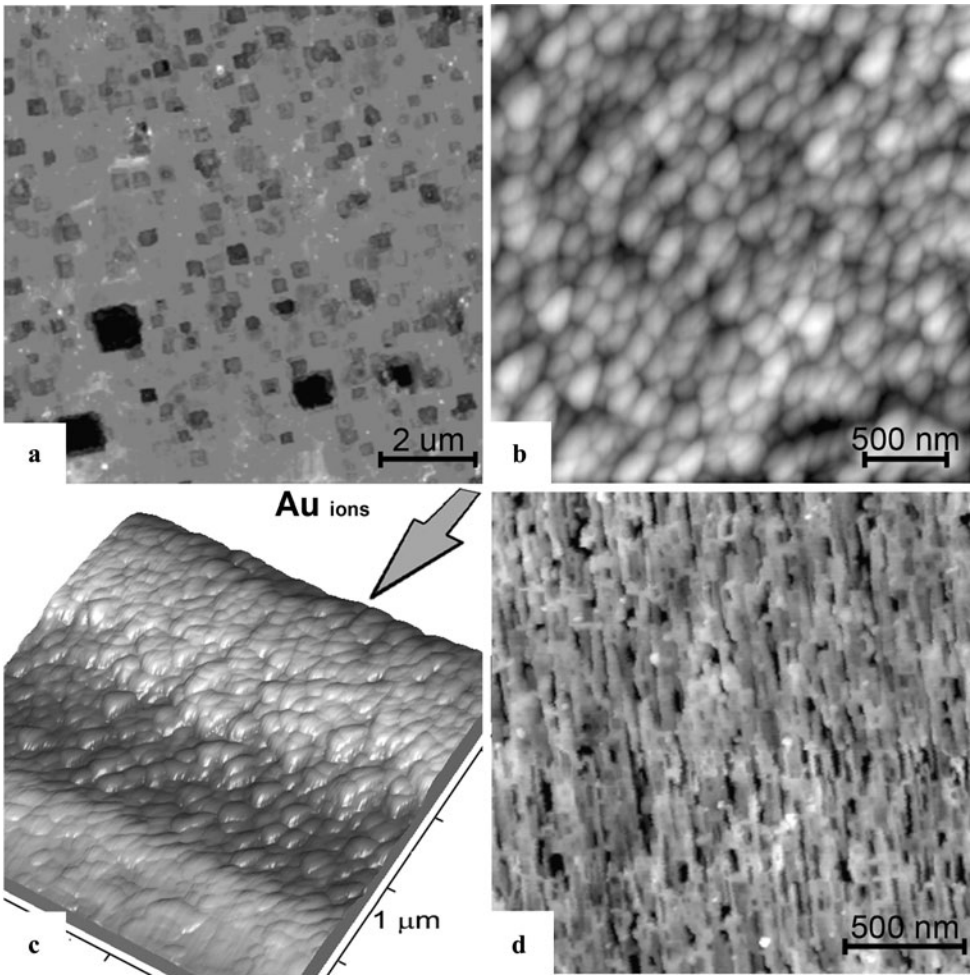


**Fig. 5** AFM images of the irradiated surface: (**a**) after irradiation with 3-MeV Au ions at $\Phi = 10^{12}$ ions/cm$^2$ and (**b**) after irradiation with 15-MeV Au ions at $\Phi = 5 \times 10^{13}$ ions/cm$^2$; AFM images of the sample's cross section: (**c**) after irradiation with 15-MeV Au ions at $\Phi = 5 \times 10^{13}$ ions/cm$^2$ and (**d**) after irradiation with 2.2-GeV Au ions at $\Phi = 10^{12}$ ions/cm$^2$

### 3.3 Ion-induced modifications of structure

Investigations of the structure were performed on the irradiated surface and on the cross section of samples prepared by cleaving perpendicular to the irradiated surface. Detailed studies were performed on samples irradiated with 3- and 15-MeV Au ions. In order to reveal structural defects, samples were treated by a chemical etching. The results of the optical and atomic force microscopy (AFM) study showed that the density of dislocations in non-irradiated crystals varies in the range of $5 \times 10^4$ to $10^6$ cm$^{-2}$ depending on a cleavage procedure. After an irradiation at fluences up to $5 \times 10^{12}$ ions/cm$^2$, a large amount of new dislocations was revealed (Fig. 5a). Their density increased with the fluence and reached about $10^9$ cm$^{-2}$. Etch pits of ion-induced dislocations were smaller compared to those for pre-existing dislocations. In many cases etch pits were flat bottomed, as is typical for prismatic dislocations of vacancy and interstitial types. The identical orientation of dislocation etch pits gives the evidence for a maintained single-crystalline structure of the irradiated samples.

After the irradiation at the fluence $10^{13}$ ions/cm$^2$ first indications a nanostructuring were observed. At the fluence $5 \times 10^{13}$ ions/cm$^2$ the irradiated layer became uniformly nanostructured. AFM images of the irradiated surface show a structure consisting of clusters with the size of 50–150 nm (Fig. 5b). The three-dimensional image of the sample's cross section shows the irradiated layer consisting of columnar grains (Fig. 5c). The thickness of the nanostructured layer (∼3.5 μm) coincides with the calculated range of 15-MeV Au ions in LiF. The formation of a nanostructure in LiF samples was also observed under the irradiation with 2.2-GeV-energy Au ions. The irradiated layer consists of long columnar grains with a cross section of about 50–100 nm (Fig. 5d). Its structure on the irradiated surface is similar to that shown in Fig. 5b.

The thermal stability of nanostructures was assessed by annealing irradiated samples at 750 K for 10 min. A recovery of the structure and the hardness after the annealing was observed. An exception was the samples irradiated at the highest current density (150 nA/cm$^2$) for which a small residual effect of hardening and an increased density of dislocations was observed.

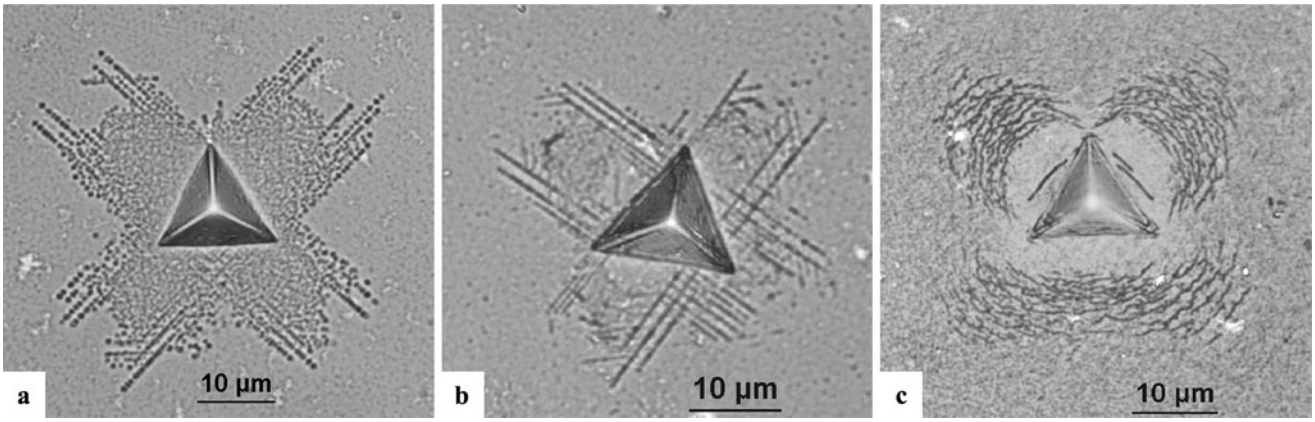


**Fig. 6** Optical images of the deformation zone around indents (after chemical etching): (**a**) on the virgin surface, (**b**) and (**c**) on surfaces irradiated with 3-MeV Au ions at the fluences of $10^{12}$ and $5 \times 10^{13}$ ions/cm$^2$, respectively

Figure 6 shows the evolution of the deformation zone at the indentation test. In non-irradiated samples a typical dislocation rosette is formed, confirming the dislocation gliding on {110} planes along the ⟨110⟩ axis. After an irradiation at moderate fluences, a dislocation rosette shows indications of a dislocation hindering. In samples, which were nanostructured under the high-fluence irradiation, no preferable directions of the deformation were observed, and the deformation mode was similar to that for isotropic solids where the maximum of stress and deformation is produced against the centers of indenter faces (Fig. 6c). A crack pattern around the indent is formed, indicating immobilization of dislocations by radiation defects.

## 4 Discussion

The optical absorption spectra for LiF irradiated with Au ions of MeV energy show the formation of a broad spectrum of damage products, such as single $F$ centers, $F_2$, $F_3$, $F_4$, as well as $F_3^+$ etc. The concentration of produced $F_n$ centers and defect aggregates achieved by an irradiation with 3–15 MeV ions is higher than that for GeV Au ions [6, 8, 9]. The structural study reveals additional defects, such as dislocations and grain boundaries.

A strong ion-induced increase of the indentation hardness as a structure-sensitive characteristic is observed. The deformation at the indentation test occurs under a high local stress and the produced dislocations are moving at a high velocity (up to $10^5$ cm/s [12]) that allows surmounting point defects, single color centers and other comparatively weak obstacles. As a result, single defects play a minor role in the ion-induced hardening. However, weak obstacles can reduce the mobility of dislocations moving at low velocity, as follows from measurements of the arm length of a dislocation pattern around indents [10, 13]. The nanohardness is sensitive mainly to dislocations, closely spaced aggregates of radiation defects and grain boundaries. According to the additivity rule, the resulting hardening is a superposition of different strengthening phenomena.

Discrete obstacles, particularly in the form of precipitates, aggregates of point defects of various types and even nanoscale cavities can alter the hardness by the dispersion strengthening mechanism. According to Orowan's model, the stress ($\sigma$) required for a dislocation to pass an array of particles spaced at the distance $\lambda$ is given by

$$\sigma = \sigma_0 + \frac{\alpha G b}{\lambda}, \tag{3}$$

where $\sigma_0$ is the yield strength of the non-irradiated crystal, $G$ is the shear modulus, $b$ denotes the Burgers vector and $\alpha$ characterizes the obstacle strength [14]. An identical relation holds for the indentation hardness. Brief estimates performed by (3) using the hardness of the matrix $H_0 = 1.5$ GPa, $G = 45.8$ GPa, $b = 2.84 \times 10^{-10}$ m and $\alpha = 1$ show that a detectable increase of the hardness is expected at the average obstacle spacing $\lambda < 200$ nm. Such conditions are fulfilled at high-fluence irradiations at the stage of track overlapping.

The strength properties of crystalline solids strongly depend on the density of dislocations. It is well established that dislocation loops of vacancy and interstitial types are formed in alkali-halide crystals by different kinds of high-dose irradiation under conditions of saturation and an aggregation of single defects [15, 16]. Another source of dislocations are the ion-induced elastic stresses, which in irradiated samples can reach a critical value [17]. Accumulation of dislocations under a high-fluence irradiation leads to a formation of dislocation networks and their transformation to grain boundaries. Such evolution of the structure ensures a reduction of ion-induced elastic stresses. Ion-induced dislocations cause an increase of the flow stress and the hardness. The flow

stress ($\tau$) is related to the density of dislocations ($\rho$) through Tailor's relationship

$$\tau = \tau_{\mathrm{m}} + \beta G b \sqrt{\rho}, \tag{4}$$

where $G$ is the shear modulus of the matrix and $\tau_{\mathrm{m}}$ is its flow stress; $\beta$ is a constant, which varies in the range of 0.05–1.5 [14]. Estimates by (4) show that strength properties markedly increase at dislocation densities above $10^7$ cm$^{-2}$. This limit of the created dislocation density is surpassed in irradiation experiments presented here.

The nanostructuring of LiF under the irradiation creates a large volume fraction of boundaries. Grain boundaries serve as obstacles for dislocations and have a significant impact on mechanical properties, e.g. yield strength and hardness. For many materials the yield strength ($\sigma$) is related to a grain size ($d$) through the Hall–Petch equation

$$\sigma = \sigma_0 + k d^{-1/2}, \tag{5}$$

where $\sigma_0$ and $k$ are constants [18, 19].

As shown in Fig. 3, the hardness of the nanostructured LiF saturates at about 4.5 GPa. Obviously, further increase of the hardness is limited due to the initiation of a brittle fracture in the indentation zone as shown in Fig. 6c. However, a remarkable hardening is observed before the stage of a uniform nanostructuring that confirms a considerable strengthening by dislocations, colloids and other aggregates of point defects.

The dislocations and grain boundaries serve as sinks for mobile radiation defects and seeds for a nucleation and a growth of defect aggregates, thus affecting the aggregation and annihilation processes of single defects. Besides, the segregation of defects on dislocations and grain boundaries reduces their mobility and facilitates the ion-induced hardening.

The irradiation effects are largely controlled by the energy absorbed in the target material and by concentrations of point defects which are introduced during displacement cascades. A comparison between depth profiles of hardness and energy loss is given in Fig. 4. A stronger hardening on the irradiated surface can be related to a higher electronic energy loss at a vicinity to the surface and partially also to specific surface processes. The collision of high-energy ions with the crystal surface causes a variety of phenomena, such as a sputtering of target atoms and a segregation of mobile radiation defects on the surface. The above-mentioned processes can lead to the compositional and structural change. Additional modifications could be caused during the post-irradiation stage by the environmental attack. The second maximum of hardness is observed in the bulk of the irradiated layer close to the end of the ion path, where a production of vacancies and interstitials in displacement cascades displays a maximum and an aggregation of single defects is facilitated. As shown in Fig. 4a, this maximum increases with the ion beam current. Such effect can be explained by the noticeable rise of the creation efficiency for the aggregates of $F$ centers and intrinsic lithium colloids under conditions when a high fluence is accumulated with a high flux of ions [8, 9]. At high flux and fluence the concentration of $H$ centers is high and the interaction between them takes place. Such interaction leads to a formation of hole centers, di-halide molecules and fluorine bubbles and reduces the number of free $H$ centers which are able to recombine with $F$ centers. As a result, the concentration of $F$ centers increases and their aggregation is facilitated.

Structural modifications of LiF are of a special interest. In contrast to many insulators, LiF does not amorphize even under a high dose of irradiation. This property is characteristic for materials with a strong ionic bonding. An irradiation with swift ions typically leads to the formation of a composite-like structure in which the crystalline LiF matrix is interwoven with linear ion tracks and embedded with nanometer-sized defect aggregates. Studies of the nanostructuring are concerned mainly with modifications of the surface topography, including an ion-induced formation of hillock- or crater-type nanostructures and figures of ion sputtering [20, 21]. Fragmentation processes, which lead to the reduction of the grain size, are observed in polycrystalline LiF films under the irradiation with MeV-energy Au ions [22]. The present study shows that the high-fluence irradiation of LiF single crystals with MeV–GeV Au ions leads to the formation of the bulk nanostructure consisting of grains with nanoscale dimensions.

## 5 Conclusion

The ratio of concentrations of complex $F_n$ to single $F$ centers in LiF crystals irradiated with 3–15 MeV Au ions is higher than in case of GeV Au ions with a similar absorbed energy. This explains higher changes in mechanical properties under the MeV-ion irradiation. The strong hardening (up to 150–200%) of LiF crystals under the irradiation with MeV-energy Au ions is observed. Structural studies reveal the formation of dislocations and nanostructuring under the high-fluence irradiation. The ion-induced hardening is related to dislocation impeding by assemblies of defect aggregates, such as dislocation loops of vacancy and interstitial types, grain boundaries, molecular fluorine clusters, lithium colloids etc.

Both nuclear and electronic stopping mechanisms of MeV Au ions in LiF contribute to the damage creation and hardening. Whereas the electronic stopping is dominating in the near-surface region, the effect of elastic displacements prevails in deeper layers, close to the projectile range.

**Acknowledgements** This research was partly supported by the Latvian Government grant no. 09.1548 M. Sorokin greatly acknowledges support from the Russian Foundation for Basic Research (grant nos. 08-08-00603 and 09-08-12196).

## References

1. M. Toulemonde, C. Trautmann, E. Balanzat, K. Hjort, A. Weidlinger, Nucl. Instrum. Methods B **256**, 346 (2007)
2. N. Itoh, A.M. Stoneham, *Materials Modification by Electronic Excitations* (Cambridge University Press, Cambridge, 2001)
3. N. Itoh, D.M. Duffy, S. Khakshouri, A.M. Stoneham, J. Phys., Condens. Matter **21**, 474205 (2009)
4. K. Schwartz, A.E. Volkov, M.V. Sorokin, C. Trautmann, K.-O. Voss, R. Neumann, M. Lang, Phys. Rev. B **78**, 0241120 (2008)
5. C. Trautmann, K. Schwartz, J.M. Costantini, T. Steckenreiter, M. Tolulemonde, Nucl. Instrum. Methods B **146**, 367 (1998)
6. K. Schwartz, M.V. Sorokin, A. Lushchik, Ch. Lushchik, E. Vasil´chenko, R.M. Papaleo, D. de Souza, A.E. Volkov, K.-O. Voss, R. Neumann, C. Trautmann, Nucl. Instrum. Methods B **266**, 2736 (2008)
7. J.F. Ziegler, P. Biersack, U. Littmark, *The Stopping and Range of Ions in Matter* (Pergamon, New York, 1985). SRIM—version 2010.01
8. M.V. Sorokin, R.M. Papaleo, K. Schwartz, Appl. Phys. A **97**, 143 (2009)
9. A. Lushchik, Ch. Lushchik, K. Schwartz, E. Vasil´chenko, R. Papaleo, M. Sorokin, A.E. Volkov, R. Neumann, C. Trautmann, Phys. Rev. B **76**, 054114 (2007)
10. I. Manika, J. Maniks, K. Schwartz, J. Phys. D, Appl. Phys. **41**, 074008 (2008)
11. I. Manika, J. Maniks, Thin Solid Films **144**, 257 (1992)
12. W.G. Johnston, J.J. Gilman, J. Appl. Phys. **30**, 129 (1959)
13. A.A. Urusovskaya, G.G. Knab, Phys. Status Solidi A **80**, 59 (1975)
14. F.R.N. Nabarro, M.S. Duesbery (eds.), *Dislocations in Solids*, vol. 10 (Elsevier, Amsterdam, 1996)
15. Y. Kawamata, J. Phys. **12**, C502 (1976)
16. L.W. Hobbs, J. Phys. **34**, C9-227 (1973)
17. I. Manika, J. Maniks, K. Schwartz, M. Toulemonde, C. Trautmann, Nucl. Instrum. Methods B **209**, 93 (2003)
18. E.O. Hall, Proc. Phys. Soc. Ser. B **64**, 747 (1951)
19. H. Gleiter, B. Chalmers, *High-Angle Grain Boundaries* (Oxford, Pergamon, 1972)
20. A. Müller, R. Neumann, K. Schwartz, C. Trautmann, Nucl. Instrum. Methods B **146**, 393 (1998)
21. V. Mussi, F. Granone, T. Marolo, R.M. Montereali, C. Boragno, F. Buatier de Mongeot, U. Valbusa, Appl. Phys. Lett. **88**, 103116 (2006)
22. M. Kumar, F. Singh, S.A. Khan, A. Tripathi, D.K. Avasthi, A.C. Pandey, J. Phys. D, Appl. Phys. **39**, 2935 (2006)

# Modification of the Structure and Nano-Mechanical Properties of LiF Crystals Under Irradiation with Swift Heavy Ions

**Jānis MANIKS [1]*, Ilze MANIKA [1], Roberts ZABELS [1], Rolands GRANTS [1], Kurt SCHWARTZ [2], Michael SOROKIN [3]**

[1] *ISSP, University of Latvia, 8 Kengaraga Str., LV 1063, Riga, Latvia*
[2] *GSI, Darmstadt, Planckstrasse 1, D-64219 Darmstadt, Germany*
[3] *Russian Research Centre "Kurchatov Institute", Moscow, Russia*

crossref http://dx.doi.org/10.5755/j01.ms.17.3.583

*Received 01 October 2010; accepted 02 July 2011*

The modifications of the structure and hardness of LiF crystals under high-fluence irradiation with MeV- and GeV-energy Au ions have been studied using nanoindentation and atomic force microscopy. The formation of ion-induced dislocations and bulk nanostructures consisting of grains with nanoscale dimensions (50 nm – 100 nm) has been observed. The structural modifications are accompanied by a strong ion-induced hardening which is related to dislocation impeding by assemblies of defect aggregates, dislocation loops of vacancy and interstitial types and grain boundaries. For MeV ions, the modifications are localized in a thin surface layer (few μm) where much higher density of deposited energy is reached and deeper stage of aggregation of radiation defects is achieved than for GeV ions with the same absorbed energy.

*Keywords*: LiF crystals, MeV-energy ions, nanostructuring, nanoindentation, hardening.

## 1. INTRODUCTION

The modifications of the structure of materials on the micro- and nanometer scale and an improvement of their optical, electrical, mechanical and other properties by the irradiation with beams of swift heavy ions are of importance from both the fundamental and technological standpoint. During the recent decades the attention was focused mainly on damage processes induced by swift heavy ions in the GeV-energy range [1 – 5]. The GeV- ion-induced effects have been investigated in all classes of materials, ranging from metals, semiconductors and insulators to living cells. A large number of studies have been made on LiF, which is widely used as a model material exhibiting high sensitivity to irradiation and high stability of radiation defects at room temperature. Besides, LiF is a material of technological importance in the areas of dosimeter and optical devices.

The main peculiarity of interaction of GeV-energy ions with dielectrics, such as LiF is the localization of damage in ion tracks [2, 5]. At low or moderate fluences the irradiation typically leads to the formation of far-standing tracks embedded in LiF matrix. At high fluences tracks overlap that leads to the formation of additional defect aggregates via the saturation and coagulation of single defects. At this stage the structural damage leads to the strong increase of structure-sensitive mechanical properties, such as indentation hardness [6 – 10].

Irradiation of LiF with ions in the MeV-energy range, which deposit a significant fraction of their energy via elastic collisions with the target atoms (nuclear energy loss), shows some peculiarities relative to GeV ions [11 – 13]. Having a projected range of few micrometers, the MeV ions induce more than one order of a magnitude higher volume concentration of colour centres than the GeV-energy ions with the same absorbed energy. The high volume concentration of primary Frenkel pairs, on the one hand, leads to a high electron-hole centre recombination, and, on the other hand, to more efficient coagulation processes leading to the formation of $F_n$-centres as well as halogen molecules ($X_2$) and their aggregates. These processes strongly depend on the fluence and flux (beam current density). For MeV ions, the modifications are localized within a thin surface layer, where a much higher density of the deposited energy is reached and a deeper stage of aggregation of radiation defects is achieved. It is of interest to compare effects induced by MeV and GeV ions. In the present work modifications of the structure and nano-mehanical properties of LiF crystals under irradiation with MeV- and GeV-energy Au ions are studied using nanoindentation, AFM and chemical etching techniques.

## 2. EXPERIMENTAL

Experiments were performed on nominally pure LiF single crystals (Korth Kristalle, Germany). Main trace impurities were Mg and Na with the concentration of 20 ppm. The density of dislocations in the non-irradiated samples was about $10^5$ cm$^{-2}$. Samples of 10×5 mm$^2$ with the thickness between 0.5 mm and 1 mm were cleaved from a crystal block along the (100) planes. The crystals were irradiated at the Tandetron accelerator in Porto Alegre (Brasil) with 3-, 5-, 10-, 12-, and 15-MeV Au ions at fluences of ($10^{12} – 2\times10^{14}$) ions/cm$^2$ and ion beam current densities $I_{beam}$ from 6.2 nA/cm$^2$ to 150 nA/cm$^2$. The flux ($\varphi$) can be estimated as:

$$\varphi\ [\text{ions cm}^{-2}\ \text{s}^{-1}] = 6.24\times10^9\times i_{beam}/q, \quad (1)$$

where $q$ is the charge of the ion. In order to compare effects induced by MeV and GeV ion irradiations, LiF samples were irradiated at the UNILAC linear accelerator

*Corresponding author Tel.: +371-67-261132; fax: +371-67-132778.
E-mail address: *manik@latnet.lv* (J. Maniks)

of the GSI, Darmstadt with 2187-MeV Au ions at a fluences of $2\times10^{11}-10^{12}$ ions/cm$^2$ with a flux of ~$10^8$ ions cm$^{-2}$ s$^{-1}$. All irradiations were performed at room temperature and under normal incidence of the ions to the (100) cleavage face of the crystals. The range and energy loss of incident Au ions of different energy in LiF were calculated using SRIM 2010 [14] (Table 1).

**Table 1.** Energy, range, electronic energy losses and density of deposited energy of Au ions in LiF

| $E_{ion}$, MeV | Ion range $R$, μm | Electronic energy losses, % of $E_{ion}$ | Density of deposited energy ($E_{ion}/R$), MeV/ μm |
|---|---|---|---|
| 3 | 0.67 | 66.4 | 4.47 |
| 5 | 1.14 | 72.1 | 4.39 |
| 10 | 2.29 | 79.1 | 4.37 |
| 12 | 2.75 | 81.0 | 4.36 |
| 15 | 3.49 | 82.9 | 4.30 |
| 2187 | 92 | 99 | 23.7 |

Characterization of the surface morphology and the structure of the irradiated layer were performed using AFM (Veeco, CPII), optical microscopy and chemical etching techniques. In order to reveal ion-induced structural defects, the $FeCl_3$ solution as a suitable etchant was used.

Nanoindentation tests were performed by MTS G200 nanoindenter with a Berkovich diamond tip (curvature < 20 nm) using the basic and continuous stiffness measurement techniques. The measurements were conducted at the load resolution <50 nN, displacement resolution ≥ 1 nm, strain rate 0.05 s$^{-1}$ and harmonic frequency 45 Hz. The nanoindenter was calibrated using a reference sample of fused silica. The hardness, Young's modulus and standard deviation of the measurements were calculated from the experimentally obtained loading-unloading curves by the MTS TestWorks 4 software. The results were averaged from 10 individual measurements. The indentation tests were conducted in ambient air at room temperature.

## 3. RESULTS

### 3.1. Evolution of the structure of LiF crystals under irradiation with MeV and GeV Au ions

The evolution of structure of LiF crystals irradiated with 3- and 15-MeV Au ions is shown in Fig. 1, a – d. The irradiation with fluences $(10^{12}-10^{13})$ ions/cm$^2$ results in formation of a large amount of ion-induced dislocations (Fig. 1, a – b). Compared with grown-in dislocations, the size of etch pits of ion-induced dislocations was smaller. The density of dislocations increased with the fluence and reached up to $5\times10^9$ cm$^{-2}$ that strongly exceeds the density of dislocations in virgin crystals (~$10^5$ cm$^{-2}$).

After irradiation with $(5\times10^{13}-10^{14})$ ions/cm$^2$ the irradiated layer becomes uniformly nanostructured. The AFM images from the cross-section of irradiated crystal prepared by cleaving along the ion pass show a structure consisting of columnar LiF grains with the size of 100 nm – 150 nm (Fig. 1, c and d). The thickness of the nanostructured layer (Fig. 1, c) coincides with the range of 15-MeV ions given in Table 1.

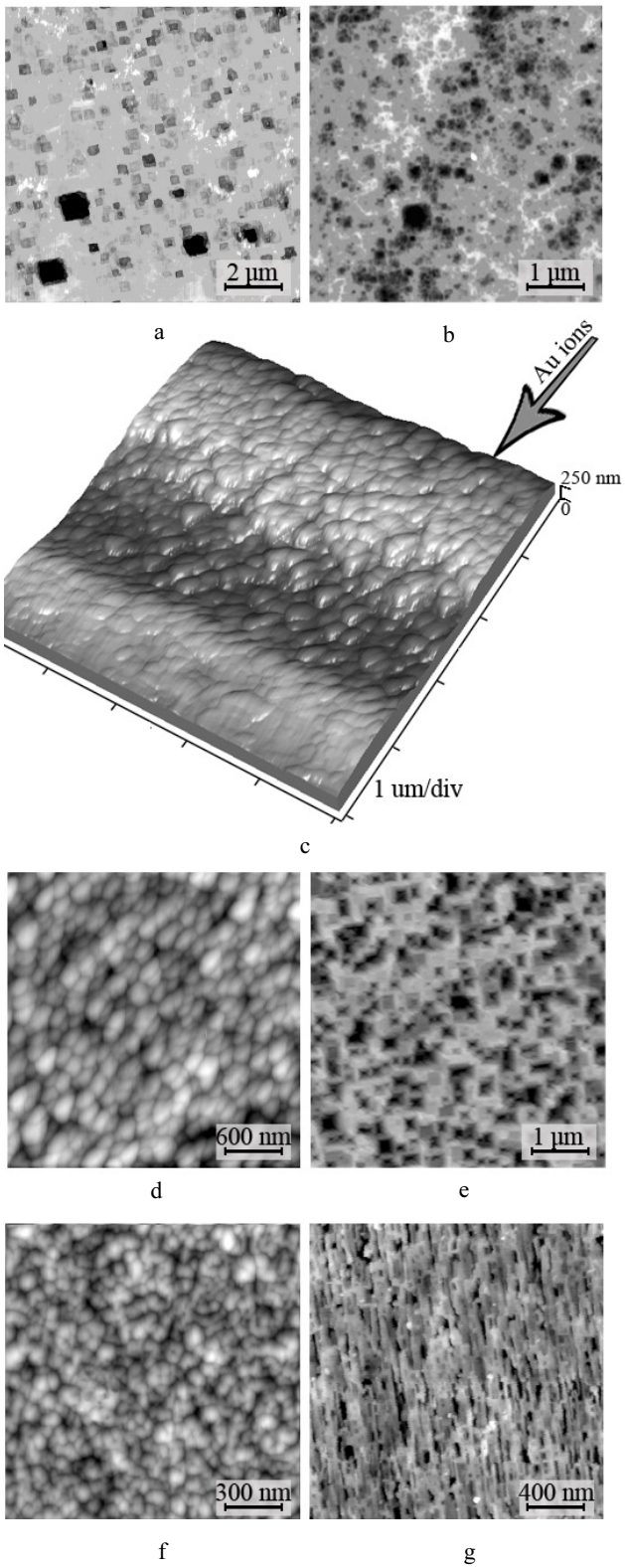


**Fig. 1.** AFM images of the irradiated LiF surface (after chemical etching): a – 3 MeV, $10^{12}$ Au/cm$^2$. The dark large etch pits denote the grown-in dislocations; b – 3 MeV, $10^{13}$ Au/cm$^2$; c – 15 MeV, $5\times10^{13}$ Au/cm$^2$ (3D- view of the sample's cross-section); d – 15 MeV, $5\times10^{13}$ Au/cm$^2$; e – the same sample, after annealing at 750 K for 10 min; f – 2187 MeV, $10^{12}$ Au/cm$^2$, g – 2187 MeV, $10^{12}$ Au/cm$^2$ (view of the sample's cross section)

The selective chemical etching of crystals irradiated with GeV Au ions, for which the energy loss surpasses a threshold of 10 keV/nm, reveals ion tracks [15]. As in the case of dislocations, etching of ion tracks results in etch pits of a pyramidal shape. The etchable tracks exhibit a complex structure: a narrow (few nm) core region, consisting of closely spaced small aggregates of radiation defects, and surrounding halo zone consisting mainly of single electron and hole centres [5].

The observation of ion-induced dislocations on the surface irradiated with GeV Au ions becomes impossible due to the background of etchable tracks. We performed the experiments on samples irradiated with lighter ions (Ni) for which the energy loss is known to be below the threshold for the track etching [15]. The results showed formation of ion-induced dislocations, which density at fluence of $10^{10}$ ions/cm$^2$ reached about $10^8$ cm$^{-2}$. Obviously, similar or more intense formation of dislocations could be expected also for GeV Au ions.

The high-fluence irradiation of crystals with GeV Au ions resulted in the nanostructuring of irradiated layer (Fig. 1, f and g). The nanostructure consists of long columnar grains with the width of 50 nm – 100 nm.

The thermal stability of nanostructures formed under irradiation with MeV and GeV Au ions was investigated. The annealing above 810 K was required for the full recovery of the structure and properties. In all cases the nanostructure was transformed into the dislocation-reach structure during the initial stage of annealing (Fig. 1, e). After annealing the orientation of dislocation etch pits and dislocation rosettes around imprints coincided with those for single crystals.

### 3.2. Ion-induced change of hardness and modulus

Nanoindentation tests showed a significant increase of the hardness of samples irradiated with MeV-energy ions (Fig. 2, a).

It should be taken into account that for a hard layer on a softer substrate the true hardness can be obtained in a limited indentation depth range. In order to exclude the effect of a softer bulk material, the indentation depth $< 0.3$ of the ion range for a given hardness ratio of irradiated layer and virgin bulk material is recommended [16]. Such condition is fulfilled in the plateau region of the hardness-indentation depth curves (Fig. 2).

The hardness sorely depends on the applied fluence. The effect of hardening is observed above the threshold fluence of $5\times10^{11}$ ions/cm$^2$. The hardness increases with fluence and above $10^{14}$ ions/cm$^2$ bends towards saturation at about 4.5 GPa, which exceeds the hardness of a virgin crystal by a factor of three. A further increase of hardness is limited due to transition of plastic deformation mechanisms from the dislocation related to those characteristic to nanostructured materials, which are facilitated by grain boundaries and a free volume.

The corresponding ion-induced change of Young's modulus is comparatively small (~15 %) (Fig. 2, b) and lies in the typical range for stress-induced variations of modulus. Moreover, the sign of the effect changes from a positive on the irradiated surface to a negative in deeper layers thus following the change of ion-induced long-range stresses from compressive on the surface to tensile at the vicinity of interface between the irradiated layer and non-irradiated crystal [8].

The hardness data for all applied ion energies settle on a common curve (Fig. 3) thus indicating that the ion-induced hardening is nearly independent of ion energy. Obviously, such behavior emerges from the fact that the local deposited energy ($E_{ion}/R$) in the investigated range of MeV-ion energies is almost constant (Table 1). However, the increase of ion energy leads to the increased thickness of hardened layer as it is evident from the increase of the plateau region of the corresponding hardness-indentation depth curves (Fig. 4). The variation of the thickness of hardened layer with the ion energy is related to the change of ion range.

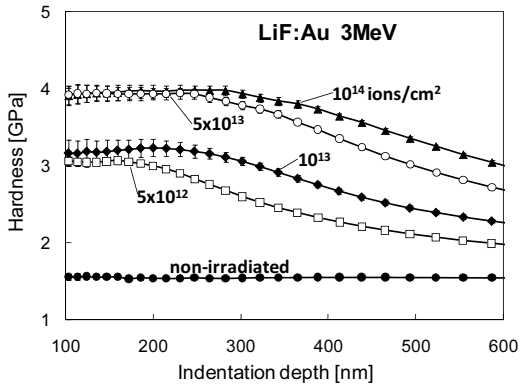


a

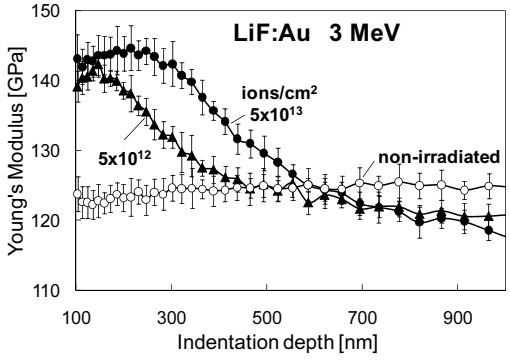


b

**Fig. 2.** Hardness (a) and Young's modulus (b) on the irradiated surface as a function of indentation depth for samples irradiated with 3 MeV Au ions at different fluences

To compare effects produced by MeV and GeV ions, a series of nanoindentation tests were conducted on LiF samples irradiated with 2187-MeV Au ions. The investigations were performed at the fluences ($2\times10^{11} – 10^{12}$) ions/cm$^2$. The results showed ion-induced hardening at fluences above the threshold of $5\times10^9$ ions/cm$^2$ at which the tracks of swift heavy ions start to overlap [9]. The hardness increases with fluence and at $10^{12}$ ions/cm$^2$ reaches about 3.9 GPa (Fig. 5). To achieve the same hardening by MeV ions, a higher fluence is required; however, the absorbed energy in comparison to GeV ions is lower. The irradiation at an ion beam current density of 100 nA/cm$^2$ corresponds to the flux of $3.12\times10^{11}$ ions cm$^{-2}$ s$^{-1}$ for 3- and 5-MeV,

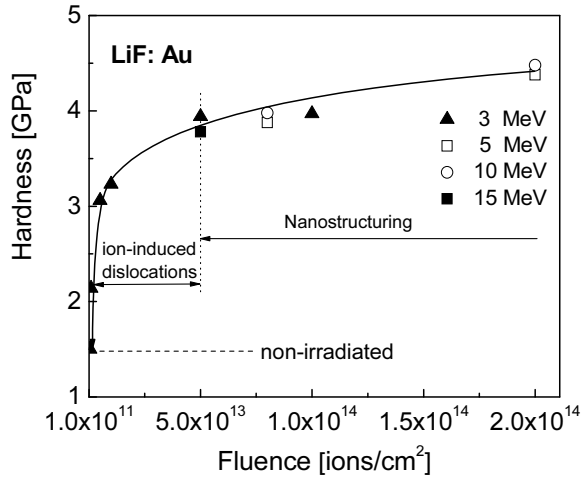


**Fig. 3.** Hardness as a function of fluence for different ion energies. The irradiations are performed at an ion beam current density of 100 nA/cm$^2$

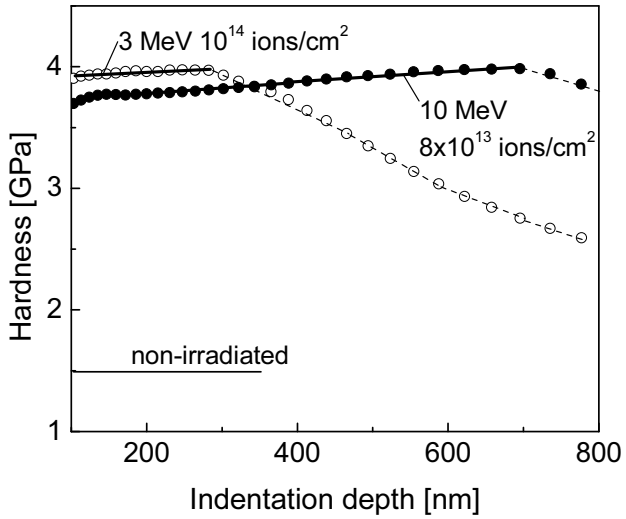


**Fig. 4.** Surface hardness as a function of indentation depth for samples irradiated with 3 MeV and 10 MeV Au ions under a comparable fluence. Solid curves denote the depth region where true hardness of the irradiated layer (not affected by a softer bulk material) is obtained

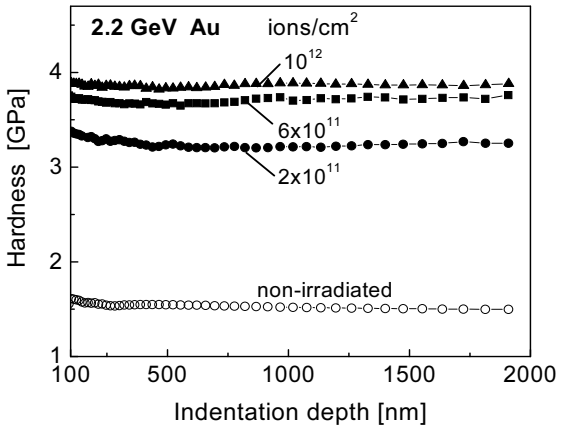


**Fig. 5.** Surface hardness as a function of indentation depth for samples irradiated with 2187 MeV Au ions at different fluences

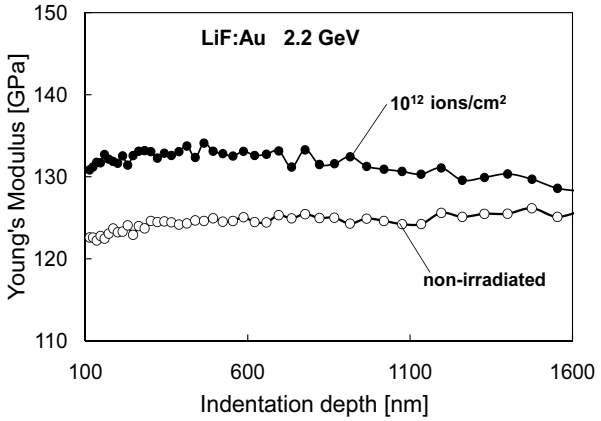


**Fig. 6.** Young's modulus as a function of indentation depth for samples irradiated with 2187 MeV Au ions at $10^{12}$ ions/cm$^2$

$1.56\times10^{11}$ ions cm$^{-2}$ s$^{-1}$ for 10 MeV, and $10^{11}$ ions cm$^{-2}$ s$^{-1}$ for 15-MeV Au ions. The flux for 2187-GeV Au ions was $\varphi \approx 10^8$ ions cm$^{-2}$ s$^{-1}$. The absorbed ion energy $E_{\text{ion}}\times\Phi$ for 2187-GeV Au ions ($\Phi = 10^{12}$ ions/cm$^2$) is $2.2\times10^{21}$ eV/cm$^2$ and for 3 MeV Au ions ($\Phi = 10^{14}$ ions/cm$^2$) is $3\times10^{20}$ eV/cm$^2$.

The nanoindentation tests on the surface irradiated with GeV Au ions show the increase of modulus by about 12 % (Fig. 6). We relate this effect to long-range compressive stresses generated in the irradiated layer due to swelling processes.

## 4. DISCUSSION

The damage produced in LiF by Au ions with energy in the GeV range is localized in ion tracks, which have a complex structure: the core region possessing a radius of 1 nm – 2 nm and consisting of small closely spaced aggregates of radiation defects, and surrounding halo region possessing a radius of 15 nm – 30 nm and consisting of point defects, such as *F* centres [5]. More complex structure is formed at the stage of track overlapping when ions penetrate into the pre-irradiated areas. Under such conditions the saturation and aggregation of single defects is known to occur. The formation of complex color centres, fluorine bubbles and other products of radiolysis is detected by optical absorption spectroscopy and other methods [1 – 5, 17]. Similar aggregation processes are observed under irradiation with MeV-energy ions. However, the MeV ions produce higher volume concentration of color centres than the GeV-energy ions with the same absorbed energy. [11 – 13].

Structural modifications of LiF under irradiation with swift ions are of a special interest. In contrast to many insulators LiF does not amorphize even under a high dose of irradiations. This property is characteristic for materials with a strong ionic bonding. An irradiation with swift ions at moderate fluences typically leads to the formation of a composite-like structure in which the linear ion tracks and nanometre-sized precipitates and other aggregates of radiation defects are embedded in the crystalline LiF matrix.

The nanostructuring processes in the irradiated LiF are not studied in detail. The research is concerned mainly

with modifications of the surface topography, including the ion-induced formation of surface hillocks and figures of ion sputtering [18, 19]. Information about fragmentation processes in the bulk of irradiated crystals is limited. The reduction of the grain size in polycrystalline LiF films exposed to irradiation with MeV-energy Au ions is reported [20].

The present study shows that the high-fluence irradiation of LiF single crystals with MeV- and GeV- Au ions leads to the formation of bulk nanostructure consisting of grains with nanoscale dimensions. The structural study demonstrates the formation of ion-induced dislocations just before the stage of nanostructuring. It is well established that dislocation loops of vacancy and interstitial types are formed in LiF crystals by aggregation of single defects under different kinds of high-dose irradiation [21]. Another source of dislocations is ion-induced long-range mechanical stresses, which in irradiated samples can reach a critical value [8]. Accumulation of dislocations leads to fragmentation and nanostructuring via formation of dislocation networks and their transformation to grain boundaries. The grain boundaries and dislocations serve as sinks for mobile radiation defects and seeds for nucleation and growth of defect aggregates thus affecting the aggregation and annihilation processes of single defects. On the other hand, the segregation of defects and growth of the defect agglomerates on dislocations facilitate their immobilization.

The observed structural modifications strongly affect the strength properties of irradiated LiF. Remarkable ion-induced increase of the nanohardness as a structure-sensitive characteristic is found to occur. The deformation at the nanoindentation test develops under a high local stress and produced dislocations are moving at a high velocity (up to $10^5$ cm/s [22]) that allows surmounting point defects, single colour centres and other comparatively weak obstacles. As a result, single defects play a minor role in the ion-induced hardening. However, the weak obstacles can reduce the mobility of dislocations moving at low velocity as it is observed in measurements of the arm length of dislocation rosettes around indents [9, 23].

The hardness is sensitive mainly to closely spaced aggregates of radiation defects, dislocations and grain boundaries. According to the additivity rule, the resulting hardening is a superposition of different strengthening phenomena.

The defect aggregates as strong obstacles for dislocations can alter the hardness mainly by the dispersion strengthening mechanism. Brief estimates performed using the Orowan's model [24] show that detectable increase of the hardness is expected at the average obstacle spacing $\lambda < 130$ nm. Such conditions can be reached at high-fluence irradiations at the stage of track overlapping.

According to the Tailor's model, the increase of flow stress (or hardness) scales with the dislocation density ($\rho$) as $\Delta\tau \sim \sqrt{\rho}$ [24]. Remarkable strengthening is expected at dislocation densities above $10^7$ cm$^{-2}$ – $10^8$ cm$^{-2}$. This limit is surpassed in irradiation experiments presented here.

The nanostructuring of LiF under the irradiation creates a large volume fraction of grain boundaries. Grain boundaries serve as obstacles for dislocations and have a significant impact on the strength and hardness. For many materials the hardness ($H$) varies with grain size as $H \sim d^{-1/2}$ [25], where $d$ is the average grain size. However, the result presented in Fig. 3 shows that a significant part of ion-induced hardening is reached before the stage of nanostructuring and confirms a strong contribution of dispersion strengthening and dislocation strengthening mechanisms. It should be taken into account that the hardness of irradiated LiF crystals saturates at about 4 GPa – 4.5 GPa due to the change in mechanisms of plastic deformation.

## 5. CONCLUSIONS

The present study shows that the high-fluence irradiation of LiF single crystals with MeV and GeV Au ions leads to the formation of bulk nanostructures consisting of grains with nanoscale dimensions. The nanoindentation tests demonstrate a strong ion induced hardening, which is ascribed to dislocation impeding by assemblies of defect aggregates, such as *H*-centre and vacancy clusters, dislocation loops of vacancy and interstitial types, and grain boundaries.

Irradiation with ions in the MeV-energy range, which deposit a significant fraction of their energy via elastic collisions with the target atoms (nuclear energy loss), shows some peculiarities relative to GeV ions. About two orders of magnitude higher threshold fluence for hardening is observed in the case of MeV ions. However, the ratio of concentrations of complex $F_n$ to single $F$ centres in LiF crystals irradiated with 3 MeV – 15 MeV Au ions is higher than in the case of GeV Au ions with a similar absorbed energy. This explains the higher localization of damage and higher changes in mechanical properties under the MeV-ion irradiation.

### *Acknowledgments*

This research was partly supported by the Latvian Government grant No.09.1548.

M. Sorokin greatly acknowledges support from the Russian Foundation for the Basic Research (Grants 08-08-00603 and 09-08-12196).

The authors thank R. Papaleo for the irradiations with MeV ions.

**REFERENCES**

1. **Itoh, N., Stoneham, A. M.** Materials Modification by Electronic Excitations *Radiation Effects and Defects in Solids* 155 (1 – 4) 2001: pp. 277 – 290.
2. **Schwartz, K., Trautmann, C., El-Said, A. S, Neumann, R., Toulemonde, M., Knolle, W.** Color-center Creation in LiF under Irradiation with Swift Heavy Ions: Dependence on Energy Loss and Fuence *Physical Review B* 70 2004: pp. 1841041 – 1841048.
3. **Bonanza, E., Buford, S., Cassimere, A., Coryphée, E., Portion, L., Gradin, J. P., Donavan, J. L., Margery, J.** Defect Creation in Alkali-halides under Dense Electronic Excitations: Experimental Results *Nuclear Instruments and Methods in Physics Research B* 91 1994: pp. 134 – 139.
4. **Toulemonde, M., Boffard, S., Studer, F.** Swift Heavy Ions in Insulating and Conducting Oxides: Tracks and Physical

Properties *Nuclear Instruments and Methods in Physics Research B* 91 1994: pp. 108 – 123.

5. **Schwartz, K., Trautmann, C., Steckenreiter, T., Geiß, O., Kramer, M.** Damage and Track Morphology in LiF Crystals Irradiated with GeV Ions *Physical Review B* 58 1998: pp. 11232 – 11240.
6. **Regel, L. L., Regel, V. R., Boriskin, S. E., Knab, G. G., Urusovskaya, A. A., Alekseeva, L. I., Klechkovskaya, V. V.** Influence of Irradiation with Heavy Ions on the Defect Structure and Mechanical Properties of LiF Crystals *Physica Status Solidi (a)* 73 1982: pp. 255 – 256.
7. **Kikuchi, A., Naramoto, H., Ozawa, K., Kazumata, Y.** Damage Profiles in Alkali Halides Irradiated with High-energy Heavy Ions *Nuclear Instruments and Methods in Physics Research B* 39 1989: pp. 724 – 727.
8. **Manika, I., Maniks, J., Schwartz, K, Toulemonde, M., Trautmann, C.** Hardening and Long-range Stress Formation in Lithium Fluoride Induced by Energetic Ions *Nuclear Instruments and Methods in Physics Research B* 209 2003: pp. 93 – 97.
9. **Manika, I., Maniks, J., Schwartz, K.** Swift-ion-induced Hardening and Reduction of Dislocation Mobility in LiF Crystals *Journal of Physics D: Applied Physics* 41 2008: pp. 074011 – 074015.
10. **Manika, I., Maniks, J.** Ion-induced Hardening in LiF: Energy Loss and Fluence Effects *Nuclear Instruments and Methods in Physics Research B* 245 2006: pp. 260 – 263.
11. **Schwartz, K., Sorokin, M. V., Lushchik, A., Lushchik, Ch., Vasil´chenko, E., Papaleo, R. M., de Souza, D., Volkov, A. E., Voss, K.-O., Neumann, R., Trautmann, C.** Color Center Creation in LiF Crystals Irradiated with 5- and 10-MeV Au Ions *Nuclear Instruments and. Methods in Physics Research B* 266 1998: pp. 2736 – 2740.
12. **Lushchik, A., Lushchik, Ch., Schwartz, K., Vasil´chenko, E., Papaleo, R., Sorokin, M., Volkov, A. E., Neumann, R., Trautmann, C.** Creation of Nanosize Defects in LiF Crystals under 5- and 10-MeV Au Ion Irradiation at Room Temperature *Physical Review B* 76 2007: pp 0541141 – 05411411.
13. **Sorokin, M. V., Papaleo, R. M., Schwartz, K.** Elastic Atomic Displacements and Color Center Creation in LiF Crystals Irradiated with 3-, 9- and 12-MeV Au Ions *Applied Physics A* 97 2009: pp.143 – 146.
14. **Ziegler, J. F., Biersack, P., Littmark, U.** The Stopping and Range of Ions in Matter. New York, Pergamon Press, 1985, SRIM - version 2010.01.
15. **Trautmann, C., Schwartz, K., Geiss, O.** Chemical Etching of Ion Tracks in LiF Crystals *Journal of Applied Physics* 83 (7) 1998: pp. 3560 – 3564.
16. **Manika, I., Maniks, J.** Effect of Substrate Hardness and Film Structure on Indentation Depth Criteria for Film Hardness Testing *Journal of Physics D: Applied Physics* 41 2008: pp. 0740081 – 0740086.
17. **Davidson, A. T., Schwartz, K., Comins, J. D., Kozakiewicz, E. G., Toulemonde, M., Trautmann, C.** Vacuum Ultraviolet Absorption and Ion Track Effects in LiF Crystals Irradiated with Swift Ions *Physical Review B* 66 2002: pp. 2141021 – 2141028.
18. **Müller, A., Neumann, R., Schwartz, K., Trautmann, C**. Heavy-ion Induced Modification of Lithium Fluoride Observed by Scanning Force Microscopy *Applied Physics A* 66 1998: pp. S1147 – S1150.
19. **Gebeshuber, I. C., Cernusca, S., Aumayr, F., Winter, H. P.** AFM Search for Slow MCI-produced Nanodefects on Atomically Clean Monocrystalline Insulator Surfaces *Nuclear Instruments and Methods in Physics Research B* 205 2003: pp. 751 – 757.
20. **Kumar, M., Singh, F., Khan, S. A., Tripathi, A., Avasthi, D. K., Pandey, A. C.** Swift Heavy Ion Induced Structural and Optical Modifications in LiF Thin Film *Journal of Physics D: Applied Physics* 38 2005: pp. 637 – 641.
21. **Kawamata, Y.** The Formation of Dislocation Loops and the Outgrows of Crystallites by Electron Irradiation of the Alkali Halide Foils *Journal de Physique* 12 1976: pp. C502 – C507.
22. **Johnston, W. G., Gilman, J. J.** Dislocation Velocities, Dislocation Densities and Plastic Flow in LiF Crystals *Journal of Applied Physics* 30 1959: pp. 129 – 141.
23. **Berzina, I. G., Berman, I. B.** Dislocation Mobility in Irradiated Crystals *Kristallographia* 9 1964: pp. 260 – 264 (in Russian).
24. **Kelly, A., Nicholson, R. B.** Precipitation Hardening. Ed. B. Chalmers, New York, Pergamon Press, 1963: 391 p.
25. Grain Boundaries and Interfaces. Eds. **Chaudhari, P., Matthews, J. W.** Amsterdam, North-Holland, 1972: 630 p.

Nuclear Instruments and Methods in Physics Research B 282 (2012) 81–84

Contents lists available at SciVerse ScienceDirect

Nuclear Instruments and Methods in Physics Research B

journal homepage: www.elsevier.com/locate/nimb

# Nanostructuring and strengthening of LiF crystals by swift heavy ions: AFM, XRD and nanoindentation study

J. Maniks [a,*], I. Manika [a], R. Zabels [a], R. Grants [a], E. Tamanis [b], K. Schwartz [c]

[a] ISSP, University of Latvia, 8 Kengaraga Str., LV 1063 Riga, Latvia
[b] University of Daugavpils, 1 Parades Str. LV5400 Daugavpils, Latvia
[c] GSI, Darmstadt, 1 Planckstrasse, D-64219 Darmstadt, Germany

ARTICLE INFO

*Article history:*
Available online 17 September 2011

*Keywords:*
LiF
Heavy ions
Nano-structuring
Dislocations
AFM
Nanoindentation

ABSTRACT

Modifications of the structure and micromechanical properties of LiF crystals under high-fluence irradiation ($10^{11}$–$10^{13}$ ions cm$^{-2}$) with swift C, Ti, Au and U ions of the specific energy of 11.1 MeV/u have been studied. In the case of heavy ions (U, Au), the AFM and SEM results reveal the bulk nanostructure consisting of columnar grains with nano-scale dimensions (50–100 nm). For lighter C ions the structure enriched with prismatic dislocation loops has been observed. High-resolution XRD reciprocal space maps for nanostructured LiF expose a mosaic-type structure with low-angle boundaries between grains.



## 1. Introduction

The development of nano-structured materials, which promise unique electronic, optical, mechanical and other properties, is an increasingly active area of research. Swift heavy ion (SHI) beams offer new possibilities in the modification of structure and properties. Until now the studies of ion-induced nanostructuring are concerned mainly with modifications of the surface topography, including creation of nano-sized hillock- or crater-like structures, nanoislands and figures attributed to ion sputtering [1–3].

Severe structural modifications, such as formation of latent tracks, aggregates of radiation defects, occurrence of amorphisation, phase transitions and interfacial mixing processes, are observed in the bulk of an irradiated material [3–5]. In connection with the formation of nanostructure the processes of structural fragmentation under the irradiation with SHI which have been observed in LiF films [6] are of special interest. The aim of the present study is to examine whether the SHI technique is applicable for the development of bulk nanostructures via ion-induced structural fragmentation. Alkali halides and other ionic crystals with a pure ionic bonding are promising candidates for the target material. Such materials, in contrast to many insulators, do not amorphize even under a high dose of irradiation. This allows us to study high-fluence processes responsible for the development of nano-structures. We have chosen LiF crystals due to their sensitivity to electronic excitations and stability of radiation defects at room temperature. Furthermore, our recent study performed on LiF crystals irradiated with 3–15 MeV Au ions demonstrates the possibility to create a bulk nanostructure consisting of LiF grains with nano-scale dimensions [7]. For ions with energy of few MeV, both nuclear and electronic stopping mechanisms contribute to the creation of damage and structural modification. A similar result was suggested to become apparent also under high-fluence irradiation with GeV ions, where interaction with the crystal is dominated by the electronic energy loss.

In this work modifications of the structure of LiF crystals exposed to high-fluence irradiation with the GeV range projectiles of different atomic mass (C, Ti, Au and U), for which the created damage varies in a wide range, have been studied. In order to obtain comparable results the irradiation for all ion species is performed at the same specific energy (11.1 MeV per nucleon). The AFM, SEM, HR XRD and nanoindentation techniques were used for the structural characterization of irradiated crystals.

## 2. Experimental

Experiments were performed on nominally pure LiF single crystals (Korth Kristalle, Germany). Main trace impurities were Mg and Na with the concentration of 20 ppm. The density of grown-in dislocations in the non-irradiated samples was about $5 \times 10^4$ cm$^{-2}$. Thin platelets were cleaved from a crystal block along the (100) planes. The samples were exposed to high-fluence irradiation ($10^{11}$–$10^{13}$ ions cm$^{-2}$) with swift $^{12}$C, $^{48}$Ti, $^{197}$Au and $^{238}$U ions of a specific energy of 11.1 MeV/u at the UNILAC linear accelerator

* Corresponding author. Tel.: +371 67261132; fax: +371 67132778.
*E-mail address:* manik@latnet.lv (J. Maniks).

0168-583X/$ - see front matter © 2011 Elsevier B.V. All rights reserved.
doi:10.1016/j.nimb.2011.08.042

of the GSI, Darmstadt, Germany. Throughout experiments the flux was kept at about $10^8$ ions $cm^{-2}$ $s^{-1}$. All irradiations were performed at room temperature and under normal incidence of the ions to the (100) cleaved face of crystals. The energy loss and the range of ions were calculated using SRIM 2008.04 [8].

Nanoindentation tests were performed by a MTS G200 nanoindenter with a Berkovich diamond tip (curvature <20 nm) using the basic and continuous stiffness measurement techniques. Measurements were conducted at the strain rate of 0.05 $s^{-1}$ and at the harmonic frequency of 45 Hz. The nanoindenter was calibrated using a reference sample of fused silica. The hardness, Young's modulus and standard deviation of the measurements were calculated from experimentally obtained loading – unloading curves by the MTS TestWorks 4 software. Results were averaged from 10 individual measurements. Indentation tests were conducted on the irradiated surface in ambient air at room temperature. The depth profiles of hardness and modulus were obtained from the indentation tests on sample cross-sections prepared by cleaving perpendicular to the irradiated surface. The distance of indents from the irradiated surface was measured by optical microscopy.

The structural defects in the irradiated crystals were revealed by a short-time chemical etching in a saturated aqueous $FeCl_3$ solution. The surface structure was studied using SEM and CPII (Veeco) atomic force microscope. The AFM images were obtained in a tapping mode using the standard silicon probes with a tip radius <10 nm. The XRD measurements were performed by a SmartLab (Rigaku) diffractometer in a high-resolution mode.

## 3. Results and discussion

### 3.1. Nanoindentation study

The nanoindentatioin was chosen as a structure sensitive technique, which ensures high locality of tests on the irradiated surface and on profile surfaces prepared by cleaving along the ion path. The nanoindentation tests after high-fluence irradiation of LiF showed ion-induced increase of hardness, confirming our earlier results [9]. Fig. 1 shows the depth profiles of hardness and energy loss in LiF irradiated with swift Au and C ions for which the ion-induced hardening reached 150% and 70%, respectively. The thickness of the hardened zone coincides with the calculated range of ions. An exception was the samples irradiated with C ions, for which the effect of hardening was observed also beyond the range of projectiles (Fig. 1(b)). This result is consistent with the reported propagation of coloring in the adjacent non-irradiated zone due to β irradiation resulting from the formation of $^{14}C$ isotope [10,11]. Generally, the nanoindentation tests show a remarkable increase of hardness, which points to a high volume concentration of strong obstacles for dislocations, such as defect aggregates, dislocations and grain boundaries. The mechanisms of ion-induced hardening are analysed in [7]. Quantitatively, the hardening effect at a constant fluence depends on the kind of projectiles and energy loss.

### 3.2. Structural study: SEM and AFM results

SEM and AFM studies showed no specific ion-induced structures on cleaved surfaces before etching. To reveal the microstructure of irradiated crystals, the samples were subjected to short-time (few s) selective chemical etching, which was successfully proven in the track core study [5]. Inspection of the topography on the irradiated surface revealed a strong modification of structure, which depends on the atomic mass of projectiles. In the case of lighter C ions, the SEM and AFM reveals numerous (up to $10^9$ $cm^{-2}$) square-based etch pits (Fig. 2(a) and Fig. 3(a)), which are typical for dislocations. A part of them was of a

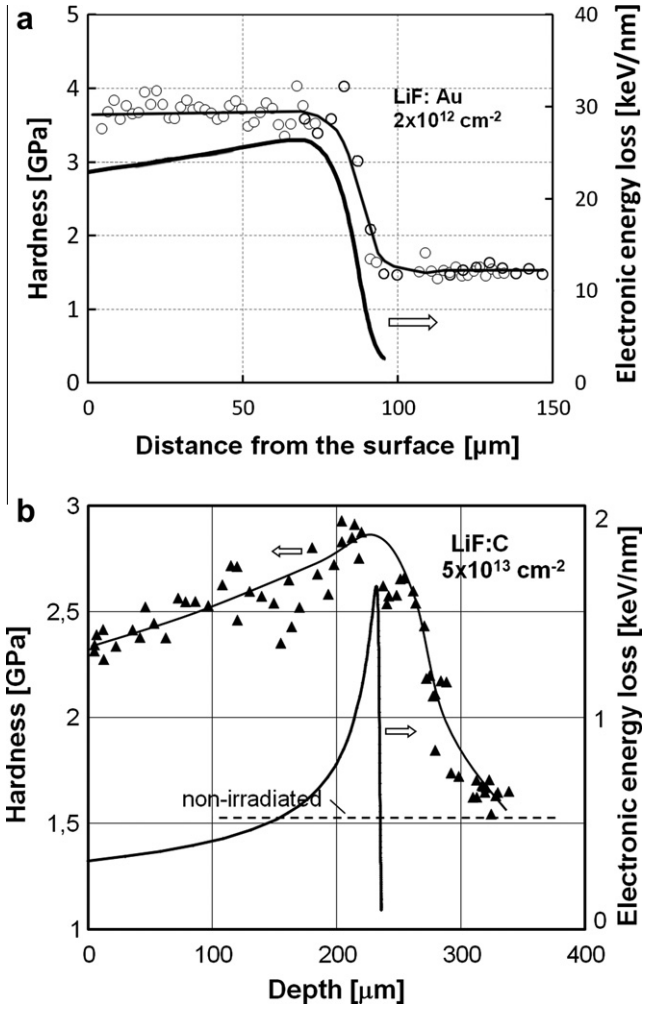


**Fig. 1.** The depth profiles of hardness and energy loss for LiF irradiated with $2 \times 10^{12}$ $cm^{-2}$ Au ions (a) and $5 \times 10^{13}$ $cm^{-2}$ C ions (b).

flat-bottomed shape. We relate such etch pits to prismatic dislocation loops. It is well established that the prismatic dislocation loops whose Burgers vector has a component normal to their plane are formed in LiF and other alkali halides through clustering of interstitials or vacancies that are generated by the irradiation. A typical example is the observation of prismatic dislocation loops under the irradiation with high-energy electrons inside TEM [12,13]. In contrast to edge and screw dislocations, which are linear extended defects, the prismatic dislocation loops exhibit small size (around 100 nm).

In the case of heavy ions (Au and U), the AFM study on the irradiated surface reveals nano-scale (50–100 nm) grains confined by boundaries (Fig. 2(b–c)). The same structure on profile surfaces prepared by cleaving along the ion pass shows columnar grains extended in the direction of ion flux (Fig. 3(c)). The observed nanostructure includes also some amount of dislocation etch pits. For ions with an intermediate atomic mass (Ti), a mixed structure consisting of dislocations and nano-grains was observed.

The irradiation of LiF with swift heavy ions is accompanied by swelling and generation of long-range stresses [14]. For heavy ions (U and Au), numerous dislocations beyond the range of projectiles are observed (Fig. 3(b)) giving the evidence for a high level of ion-induced stresses. In the case of lighter C ions, the boundary region between the irradiated and non-irradiated parts is free from dislocations (Fig. 3(a)) confirming that the ion-induced stresses are below the threshold for generation of dislocations.

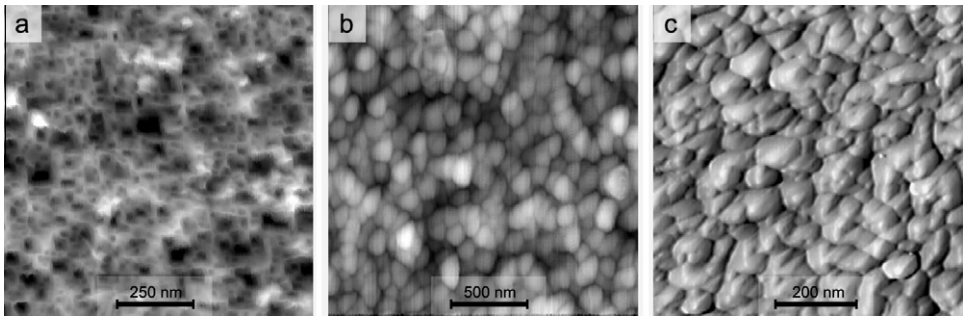


**Fig. 2.** The AFM micrographs from the LiF surface after irradiation with $5 \times 10^{13}$ cm$^{-2}$ C ions (a), $4 \times 10^{11}$ cm$^{-2}$ U ions (b) and $2 \times 10^{12}$ cm$^{-2}$ Au ions (c).

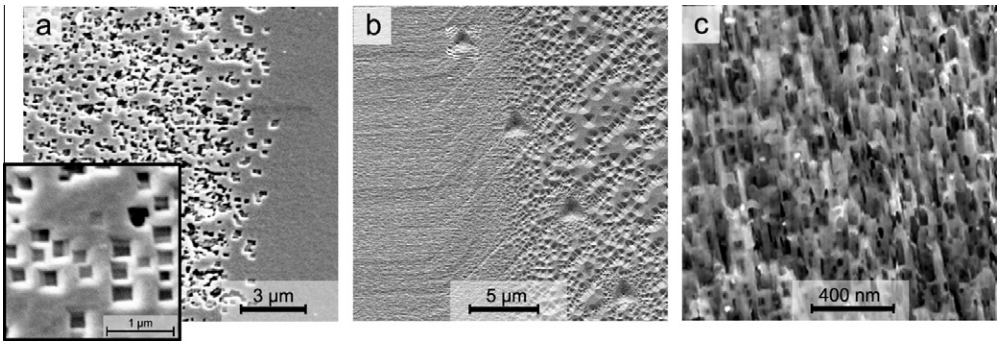


**Fig. 3.** The AFM micrographs of profile surfaces prepared by cleaving along the ion path (after etching): (a) dislocation rich zone (overall and detailed view) formed after irradiation with C ions to fluence $5 \times 10^{13}$ ions cm$^{-2}$, (b) unirradiated (right) and irradiated (left) zone for Au ions at fluence $2 \times 10^{12}$ ions·cm$^{-2}$; triangles denote the imprints performed during nanoindentation test, (c) nanostructured zone formed by irradiation with U ions to fluence $4 \times 10^{11}$ ions cm$^{-2}$.

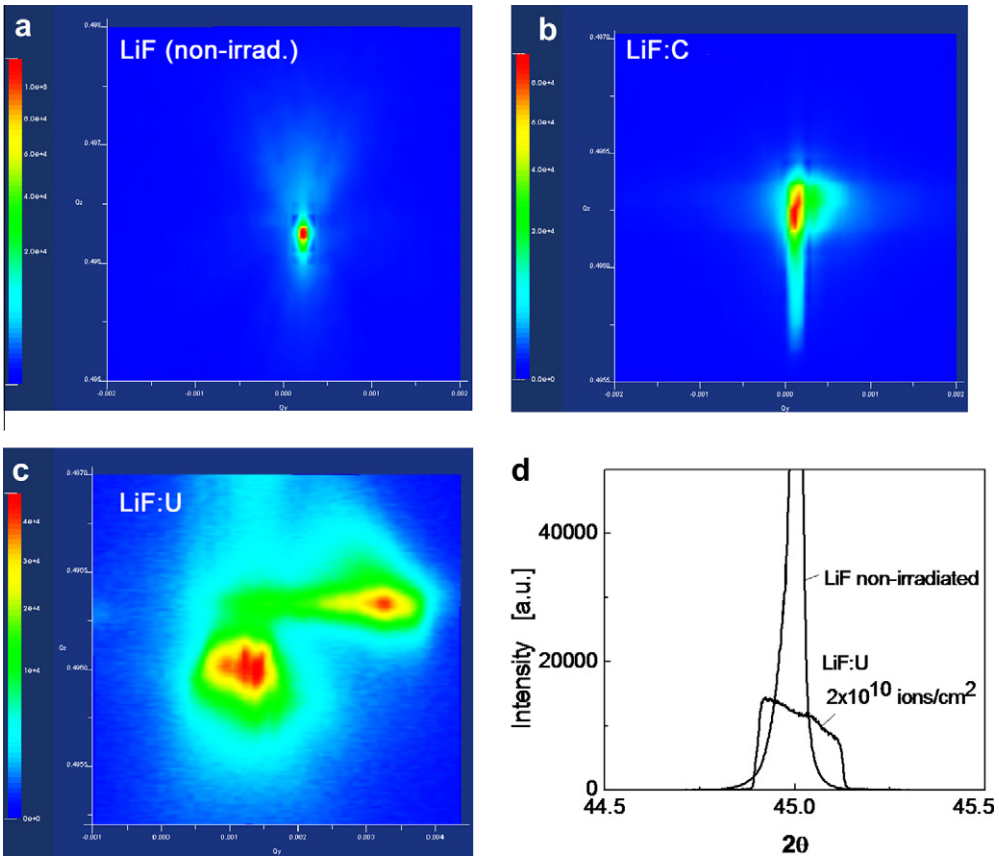


**Fig. 4.** XRD reciprocal space maps for LiF crystals (a) non-irradiated, (b) irradiated with $10^{12}$ cm$^{-2}$ C ions, (c) nano-structured under irradiation with $4 \times 10^{11}$ cm$^{-2}$ U ions. (d) X-ray diffraction pattern before and after irradiation with $4 \times 10^{11}$ cm$^{-2}$ U ions.

As shown by the structural study, the self-organized nanostructuring via fragmentation is observed at high-fluence irradiation when the stage of saturation and aggregation of primary radiation defects is well developed. During this stage the aggregate-centers and different types of defect aggregates, such as dislocations, small precipitates, voids and halogen bubbles are known to be created. The interaction of the stress fields of ion tracks, dislocations and defect clusters leads to the ordering of defects and formation of grain boundaries reducing the size of crystallites.

The grain boundaries and dislocations serve as sinks for mobile radiation defects and seeds for nucleation and growth of defect aggregates thus affecting the aggregation and annihilation processes of single defects during irradiation. As a result, the boundaries and dislocations become decorated with radiated defects and their clusters. The segregation of defects and defect agglomerates on dislocations facilitate their immobilization and strengthening of the irradiated crystal.

### 3.3. High-resolution XRD results

The high-resolution XRD reciprocal space mapping (RSM) provides quantitative information about the variation of interplanar distance and lattice tilting of the irradiated samples. Fig. 4(a–c) shows the results for the unirradiated crystal and for samples irradiated with C and U ions plotted in Cartesian coordinates. The broadening along the $q_z$ direction indicates the variation of the interplanar distance while the broadening along the $q_y$ direction characterizes the tilting of grains and their size reduction. In the irradiated samples results show the increase of the interplanar distance up to $\sim$0.1%. Such effect can be related to generation of prismatic dislocations, internal and long-range stresses [14,15]. In the nanostructured samples both the tilting of grains and variation of the interplanar distance were found to appear (Fig. 4(c)). The estimates give low tilting angles that indicate the formation of a mosaic-type nano-structure. The fragmentation in LiF crystals and reduction of the size of coherent domains was detected by XRD measurements also under neutron irradiation [16].

Fig. 4(d) shows the X-ray diffraction pattern before and after irradiation with $4 \times 10^{11}$ U ions. The data are deduced from the high-resolution XRD measurements. As seen, the diffraction peak intensity in the irradiated sample is drastically decreased pointing to an ion-induced deterioration of crystallinity due to nanostructuring.

## 4. Conclusion

The results obtained in the course of this study confirm the potential of high-fluence SHI irradiation for creating bulk nanostructures in LiF crystals and related materials. From the AFM and SEM study it follows that the obtained nanostructure consists of columnar LiF grains with dimensions 50–100 nm.

A detailed HR XRD reciprocal space mapping of the nanostructure confirms its mosaic nature with low angle boundaries between grains. Consequently, the obtained nanostructure cannot be characterized as polycrystalline. It is composed rather of subgrains or mosaic blocks.

The irradiation of LiF with lighter C ions leads to the formation of a dislocation-rich structure. No nanostructuring was observed under irradiation with C ions even when the fluence reached $5 \times 10^{13}$ cm$^{-2}$.

The observed structural modifications strongly affect the structure-sensitive strength properties of the irradiated LiF. Both the nanostructure and dislocation rich structure show remarkable hardening that gives evidence for the high volume concentration of strong obstacles for dislocations.

From the obtained results the relationship between the energy loss of ions and developed structures can be seen. Further experiments are required to establish the quantitative limits.

## Acknowledgements

This work has been supported by the European Social Fund within the project «Support for Doctoral Studies at University of Latvia» and by the Latvian Government Grant No. 09.1548.

## References

[1] M. Toulemonde, C. Trautmann, E. Balanzat, K. Hjort, A. Weidinger, Nucl. Instr. Meth. B 216 (2004) 1.
[2] R. Neumann, Nucl. Instr. Meth. B 151 (1999) 42.
[3] I.P. Jain, G. Agarwal, Surf. Sci. Rep. 66 (2011) 77.
[4] K. Schwartz, C. Trautmann, T. Steckenreiter, O. Geiss, M. Kramer, Phys. Rev. B 58 (1998) 11232.
5 S. Abu Saleh, Y. Eyal, Nucl. Instr. Meth. B209 (2003) 113.
[6] M. Kumar, F. Singh, S.A. Khan, A. Tripathi, D.K. Avasthi, A.C. Pandey, J. Phys. D: Appl. Phys. 39 (2006) 2935.
[7] J. Maniks, I. Manika, R. Grants, R. Zabels, K. Schwartz, M. Sorokin, R.M. Papaleo, Appl. Phys. A. 104 (2011) 1121.
[8] J.F. Ziegler, J.P. Biersack, U. Littmark, The Stopping and Range of Ions in Solids, Pergamon, New York, 1985.
[9] I. Manika, J. Maniks, K. Schwartz, J. Phys. D: Appl. Phys. 41 (2008) 074008.
[10] A. Kikuchi, H. Naramoto, K. Ozawa, Y. Kazumata, Nucl. Instr. Meth. B39 (1989) 724.
[11] V.R. Regel, L.I. Alekseeva, A.A. Urusovskaya, G.G. Knab, G.V. Sotserdotova, Radiat. Eff. 82 (1984) 157.
[12] L.W. Hobbs, J. Phys. 34 (1973) C9–C227.
[13] Y. Kawamata, J. Phys. 37 (1976) C7–C502.
[14] I. Manika, J. Maniks, K. Schwartz, M. Toulemonde, C. Trautmann, Nucl. Instr. Meth. B209 (2003) 93.
[15] D.T. Keating, A.N. Goland, J. Appl. Phys. 44 (1973) 3784.
[16] K. Kubo, Y. Hamaguchi, H. Motohashi, J. Phys. Jap. 19 (1964) 1105.

Nuclear Instruments and Methods in Physics Research B 286 (2012) 56–60

Contents lists available at SciVerse ScienceDirect

Nuclear Instruments and Methods in Physics Research B

journal homepage: www.elsevier.com/locate/nimb

# Color centers and nanodefects in LiF crystals irradiated with 150 MeV Kr ions

A. Dauletbekova [a,*], J. Maniks [b], I. Manika [b], R. Zabels [b], A.T. Aklibekov [a], M.V. Zdorovets [c], Y. Bikhert [a], K. Schwartz [d]

[a] L.N. Gumilyov Eurasian National University, 5, Munaitpassov Str., 010008 Astana, Kazakhstan
[b] ISSP, University of Latvia, 8 Kengaraga Str., LV-1063 Riga, Latvia
[c] Institute of Nuclear Physics, ½, Abylaikhan Av., 010008 Astana, Kazakhstan
[d] GSI, Darmstadt, 1 Planckstrasse, D-64291 Darmstadt, Germany

ARTICLE INFO

*Article history:*
Received 31 July 2011
Received in revised form 21 November 2011
Available online 30 December 2011

*Keywords:*
Ionic crystals
Radiation damage
Color centers
Ion tracks
Thermal annealing
Nanodefects

ABSTRACT

The modifications of structure, optical and nano-mechanical properties of LiF crystals after irradiation with 150-MeV $Kr^{+14}$ ions at a fluence of $6 \times 10^{12}$ ions $cm^{-2}$ have been studied using optical absorption spectroscopy, scanning electron and atomic force microscopy, and nanoindentation. Optical spectroscopy shows the saturation of *F* centers and a comparatively high number of $F_n$ centers. AFM and SEM imaging reveals a nanostructured region with columnar nanocrystallites (size 30–90 nm). Nanostructuring occurs in depths up to 10 μm, where the ion energy loss surpasses a critical threshold of about 10 keV/nm. At a lower energy loss a zone enriched with dislocations is observed. Structural changes are accompanied by a substantial increase of hardness. The recovery processes of structure and properties under annealing have been studied.



## 1. Introduction

Swift heavy ion (SHI) irradiation is a promising technique for the creation of nanostructures in solids and thin films. Significant progress has been achieved in building nano-structures on irradiated surfaces, such as nano-sized hillocks, nanoislands and etching figures formed by ion sputtering [1,2]. In a wide class of materials irradiation with SHI leads to substantial structural modifications within the bulk. On a nanometer scale ions induce different type of radiation damage including formation of single defects and defect clusters, latent tracks as well as phase transitions, amorphization and interfacial mixing [3–5]. Recent studies show that the nanostructuring in the bulk of solids can be achieved by irradiation to high-fluences ensuring the saturation, aggregation and ordering of radiation defects [6,7]. Such studies are performed mainly on ionic solids like alkali halides which are promising materials for the development of bulk nanostructures because of their high resistance to amorphization, even at high-fluence irradiation.

The creation of color centers in ionic crystals under SHI irradiation depends on the ion energy and energy loss ($dE/dx$), irradiation temperature, and fluence ($\Phi$) [8,9]. With increasing fluence, when the overlapping of ion tracks occurs, single *F* centers reach saturation and further irradiation leads to their decrease, whereas complex $F_n$ centers continue to increase in numbers. The saturation of *F* centers via $\Phi$ depends at a given temperature on the ion energy and $dE/dx$. For 150 MeV Kr ions it takes place at about $\Phi \sim 10^{12}$ ions/$cm^2$ corresponding to a volume concentration of *F* centers $N_F \geqslant 10^{19}$ $cm^{-3}$. It was shown that the creation of *F* centers strongly depends on the ion beam current (nA/$cm^2$) or flux (ions/$cm^2$ s). At high flux values the efficiency of color center creation increases, especially for complex $F_n$ centers [10,11]. This should result also in fluorine molecule clusters ($nX_2$) and stimulate the formation of nanoscale defects [7,12,13].

The present research focuses on the modification of structure, optical and nano-mechanical properties in LiF irradiated with 150-MeV $Kr^{+14}$ ions using scanning electron and atomic force microscopy, nanoindentation and optical absorption spectroscopy. The latter was used for studying the evolution of color centers during thermal annealing. LiF is chosen as an appropriate target material because of its high sensitivity to electronic excitations, stability of radiation defects at room temperature and the simplicity of sample preparation by cleaving. Taking into account that self-organized nanostructuring under irradiation with SHI is linked to ion-induced stresses [6] which depend on the kind of projectiles and energy loss, 150 MeV Kr ions are ideal projectiles as their energy loss ($dE/dx$) is well above the critical threshold for the track-core damage formation during some part of their trajectory. Generally, heavy ions (e.g. U, Pb and Au) are known to cause more substantial structural modifications and changes in properties as compared to lighter ions [14]. However, the lighter Kr projectiles are preferable

* Corresponding author. Tel.: +7 7172342013; fax: +7 7172 353812.
*E-mail address:* alma_dauletbek@mail.ru (A. Dauletbekova).

0168-583X/$ - see front matter © 2011 Elsevier B.V. All rights reserved.
doi:10.1016/j.nimb.2011.12.030

because of lower undesirable effects of swelling and long-range stress.

In this study, the formation of a bulk nanostructure is investigated with respect to $dE/dx$ along the Kr ion range. To assess the thermal stability of obtained nanostructures, the recovery of structure and nano-hardness has been studied in conjunction with the thermal annealing experiments.

## 2. Experiment

For the experiments high quality LiF crystals grown from the melt in vacuum (Optical Institute (GOI) St. Petersburg, Russia) were used. About 1 mm thick platelets of $10 \times 10$ mm$^2$ were irradiated at room temperature (RT) normal to one of the (0 0 1) cleaving planes with 150 MeV $Kr^{+14}$ ions (range $R = 17.5$ μm, $dE/dx = 12$ keV/nm [15]). Irradiations were performed at the DC-60 cyclotron accelerator (Astana, Kazakhstan). Samples irradiated to fluence of $6 \times 10^{12}$ ions/cm$^2$ at an ion beam current density of 180 nA/cm$^2$ ($8 \times 10^{10}$ ions/cm$^2$ s) were chosen for the research as this fluence ensures saturation of $F$ centers. Online temperature measurements in LiF samples showed slightly elevated temperatures ($T_{irr} \approx 360$ K) during irradiation with 150 MeV Kr ions at the beam current of 180 nA/cm$^2$.

Optical measurements were carried out with the spectrometer СФ-103 in the spectral range of 1.8 eV (700 nm)–6.2 eV (200 nm) corresponding to the absorption of the main electronic color centers ($F, F_2, F_3, F_4$) in LiF. In the absorption spectra the peaks of $F$ and $F_2$ centers are dominating [3,10].

Nanoindentation tests were performed using a MTS G200 nanoindenter with a Berkovich diamond tip (curvature <20 nm) applying the basic and continuous stiffness measurement techniques. Measurements were conducted at a strain rate of 0.05 s$^{-1}$ and harmonic frequency of 45 Hz. The nanoindenter was calibrated using a reference sample of fused silica. The mean hardness and Young's modulus including the standard deviation were calculated from experimentally obtained loading–unloading curves by the MTS TestWorks 4 software. Results were averaged from 10 individual measurements. Indentation tests were conducted on the irradiated surface in ambient air at room temperature. The depth profiles of hardness were obtained from the indentation tests on sample cross-sections prepared by cleaving perpendicular to the irradiated surface. The distance of indents from the irradiated surface was measured by optical microscopy.

Structural defects in the irradiated crystals were revealed by a short-time selective chemical etching in a saturated aqueous $FeCl_3$ solution. The surface topography was studied using SEM and CPII (Veeco) atomic force microscope. The AFM images were obtained in a contact mode using the standard silicon probes with a tip radius <10 nm.

## 3. Results and discussion

### 3.1. Structural study

The investigation of structural modifications after irradiation was performed on the cross-sections prepared by cleaving LiF along the ion path (normal to the irradiated (1 0 0) surface). The cleavage surfaces before etching showed no micro-structural elements other than cleavage steps.

An overview of the irradiated zone after chemical etching is shown in Fig. 1(a) and in the inset of Fig. 2. A substantial change in structure is observed up to 17.5 μm depth which coincides with the ion range $R$. Two zones exhibiting different types of structural features are clearly seen: (1) the nanostructured zone consisting of small columnar grains (zone 1 in Fig. 1(a)), and (2) the zone with

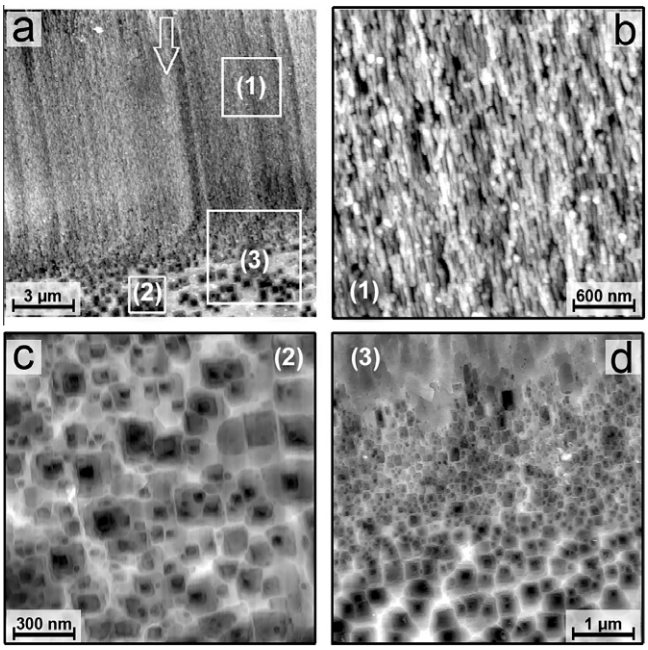


**Fig. 1.** AFM micrographs (topography) of LiF samples irradiated with 150 MeV Kr ions at a fluence of $6 \times 10^{12}$ ions cm$^{-2}$ and cleaved along the ion pass: (a) Overall view, the arrow denotes the direction of ion flux, (b) the nanostructured zone, (c) the dislocation-rich zone, (d) a transitional region between zones (1) and (2). The structure was revealed by chemical etching.

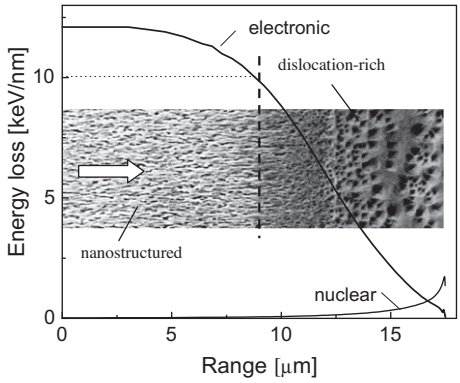


**Fig. 2.** The depth distribution profile of electronic and nuclear energy loss for150 MeV Kr ions in LiF calculated by SRIM.2008.04. The inset shows SEM image (profile view) of the irradiated zone. The arrow denotes the direction of ion flux.

numerous square-based etch pits (zone 2 in Fig. 1(a)), which are typical for dislocations. Between the nanostructured and dislocation-rich zones we can see approximately 2 μm wide transitional region (3) which is depicted in Fig. 1(d).

An AFM image of the nanostructured zone at a higher magnification is presented in Fig. 1(b). The size (cross section) of grains estimated from the AFM images is in the range of 30–90 nm. It should be noted that this value slightly overestimates the grain size due to the finite size of the AFM tip.

Fig. 1(c) presents a detailed view of the dislocation-rich zone. The average density of dislocation etch pits in this zone, estimated from the AFM images, is about $5 \times 10^9$ cm$^{-2}$, which is approximately 4 orders of magnitude higher than the grown-in dislocations. A part of the dislocation etch pits is flat-bottomed which can be ascribed to prismatic dislocations of interstitial or vacancy type. It is well known that prismatic dislocation loops are formed in LiF and other alkali halides through the clustering of interstitials

or vacancies that are generated by the irradiation. The observation of prismatic dislocation loops in alkali halides under irradiation with high-energy electrons inside a TEM was reported earlier in [16,17]. A variation of etch pit size is observed along the ion range (Fig. 1(d)). This effect can be related to variance in etching rate which depends on the density of radiation defects.

The result of the structural modifications along the ion path is compared with the calculated energy loss evolution in Fig. 2. The stopping of 150 MeV Kr ions in LiF is dominated by the electronic energy loss. The nanostructure forms in a depth range where the electronic energy loss exceeds the threshold of 10 keV/nm. At the end of ion path, where the energy loss decreases below this limit, the formation of a dislocation-rich structure has been observed.

A significant role in self-organized nanostructuring is played by ion-induced internal stresses, which facilitate processes of defect ordering and crystal fragmentation in heavily irradiated LiF [6]. It is well established that in LiF at the energy loss above 10 keV/nm ion tracks exhibit core damage and can be visualized by etching technique due to a local stress field introduced by a track in a surrounding lattice [3]. Obviously, an accumulation of internal stresses during irradiation to fluence of $6 \times 10^{12}$ ions cm$^{-2}$ facilitates nanostructuring. The decisive role of stresses associated with tracks manifests also in their columnar shape extended along the direction of ion flux.

The structure of zone 2 (Fig. 1(c)) is formed by tracks exhibiting only the halo zone. At the fluence of $6 \times 10^{12}$ the overlapping of the halo regions occurs that leads to saturation and aggregation of single defects. The structural study reveals ion-induced formation of dislocations in this zone. In this case the applied fluence is too low for the nanostructuring via formation of dislocation networks and their transformation into grain boundaries.

A similar columnar nanostructure has been observed for LiF irradiated with GeV-energy U and Au ions, but was absent after high-fluence irradiation with lighter C ions due to substantially lower energy loss, below the threshold required for core damage [18]. A XRD reciprocal space mapping analysis of the nanostructure induced by U and Au ions showed the presence of a mosaic-type structure with low-angle boundaries between the domains. Likely, a similar type of nanostructure, which is composed rather by subgrains or domains of the mosaic structure, is formed also by irradiation with 150 MeV Kr ions.

### 3.2. Nanoindentation study

Nanoindentation as a structure sensitive technique is well suited for nano-mechanical characterization of nanostructures complementary to the AFM study of nanostructures. The measurements of nanohardness and Young's modulus were performed on samples irradiated with Kr ions to fluence $\Phi = 6 \times 10^{12}$ ions/cm$^2$ at the flux of $8 \times 10^{10}$ ions/cm$^2$ s. The measurements on the irradiated surface show a strong ion-induced increase of hardness (Fig. 3), which is typical for high-fluence irradiation of LiF with SHI [14]. The relative increase of hardness exceeds 200% compared to that for the unirradiated sample. The ion-induced increase of Young's modulus on the irradiated surface is comparatively small (about 20%) and could be ascribed to stress-related effects. The swelling-induced compressive long range stresses could be responsible for the observed increase of modulus. The increase of hardness confirms a substantial structural modification, while the permanence of modulus points to the maintained crystallinity of samples after irradiation.

The nanoindentation tests on the surfaces cleaved along the ion trajectory demonstrate a remarkable ion-induced hardening both – in the nanostructured and dislocation-rich zones (Fig. 4). The maximum hardening was observed in the nanostructured zone and adjacent transitional region. Starting at depth of about 11 μm, hardness gradually decreases and at the end of ion range reaches the hardness of unirradiated crystal.

The comparison of the nanoindentation results in the near-surface layer and profile surfaces (Figs. 3 and 4) shows that swift ions cause a slightly stronger hardening on the irradiated surface.

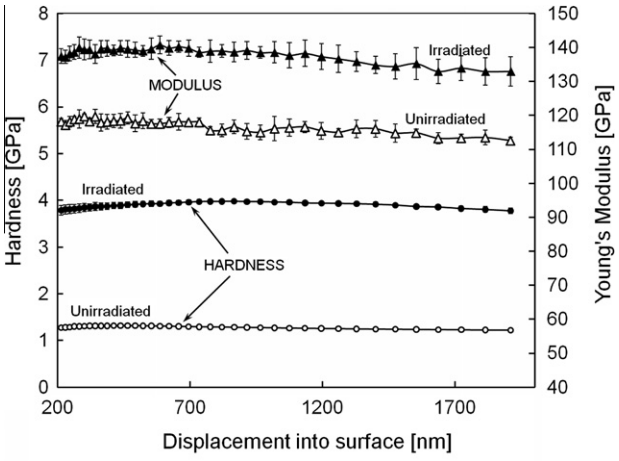


**Fig. 3.** Hardness and Young's modulus on the irradiated LiF surface as a function of indentation depth for sample irradiated with 150 MeV Kr ions at the fluence $6 \times 10^{12}$ ions/cm$^2$. The measured values for a non-irradiated LiF crystal are reported for comparison.

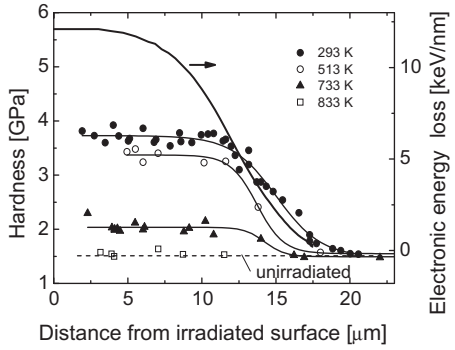


**Fig. 4.** The depth distribution profiles of hardness for LiF after room-temperature irradiation with 150 MeV Kr ions at fluence $6 \times 10^{12}$ ions cm$^{-2}$ and after annealing at 513 K, 733 K and 833 K for 20 min. The surface was prepared by cleaving the irradiated sample along the ion path. The values for a non-irradiated LiF crystal are reported for comparison.

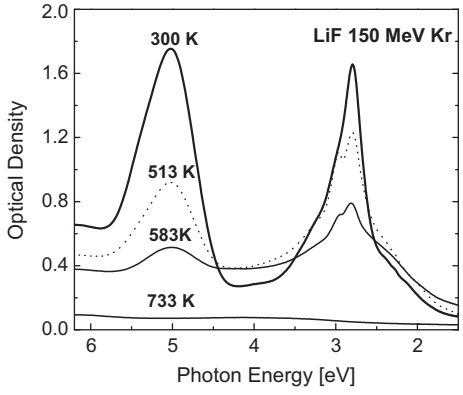


**Fig. 5.** Absorption spectra of LiF crystals irradiated with 150 MeV Kr ions at a fluence $\Phi = 6 \times 10^{12}$ ions/cm$^2$ with a flux of $8 \times 10^{10}$ ions/cm$^2$·s at room temperature and after thermal annealing at 513 K, 583 K, and 733 K.

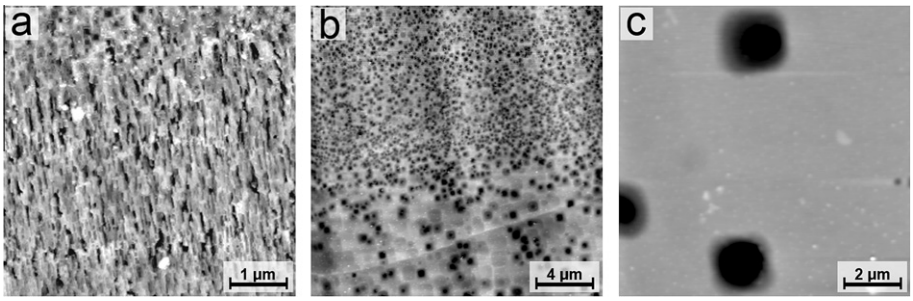


**Fig. 6.** The AFM micrographs of LiF crystals irradiated with 150 MeV Kr ions to fluence of $\Phi = 6 \times 10^{12}$ ions/cm$^2$ at room temperature and annealed at (a) 513 K, (b) 733 K, and (c) 833 K for 20 min.

Such behavior has been observed for heavy ion projectiles [14]. This difference can be caused by various factors like sputtering-induced compositional changes on the irradiated surface, the sink nature of surface for mobile radiation defects and environmental attack in the post-irradiation stage.

Generally, nanoindentation tests give the evidence for the high volume concentration of strong obstacles for dislocations, such as defect aggregates, dislocations, grain and subgrain boundaries. The behavior of ion-induced hardening is in agreement with the results of structural study. The mechanisms of hardening are analyzed and discussed in [14,18].

### 3.3. Thermal annealing

Thermal stability of various defects in LiF irradiated with heavy ions depends on the ion energy loss and fluence [19]. During thermal annealing two different processes take place: (1) the decomposition of $V_3$ centers with $H$ center production; (2) diffusion of single $F$ centers with the following formation of complex electron color centers according to the reactions $F + F_n \rightarrow F_{n+1}$, e.g. $F + F \rightarrow F_2$, $F + F_2 \rightarrow F_3$ etc. The annealing process depends on the initial defect structure in the irradiated LiF crystal and on the annealing temperature. Optical absorption spectra of LiF crystals irradiated with 150 MeV Kr ions at room temperature and after different steps of thermal annealing are shown in Fig. 5. At $T < 500$ K $F$ centers are not mobile and the decomposition of $V_3$ centers leads to the recombination with electron centers according to $F + H \rightarrow 0$. At a higher temperature besides the recombination of electron color centers with $H$ centers also the coagulation of electron and hole centers is possible ($F + F_n \rightarrow F_{n+1}$ or $H + H \rightarrow X_2$). Heating at 733 K leads to a complete annealing of $F$ and $F_n$ centers and only a residual absorption of aggregate centers (Li, and possible contaminants) is present.

The AFM studies on as-irradiated and annealed LiF crystals show that the nanostructure created in LiF by the high-fluence irradiation with swift Kr ions is thermally stable at temperatures up to about 500 K (Fig. 6(a). At higher temperatures the nanostructure is transformed into a dislocation-rich structure (Fig. 6(b)) and further increase of temperature leads to the recovery by reduction of the dislocation density (Fig. 6(c)).

The recovery of hardness during annealing is initiated at a temperature above 500 K and completed at 833 K (Fig. 4). The Arrhenius type plot of hardness recovery (%) versus ($1/T$) gives an activation energy of $0.2 \pm 0.03$ eV in the temperature range of 513–833 K. This value is close to the activation energy for the $H$-center migration in LiF obtained by other authors [20]. It is also close to the activation energy estimated from the indentation hardness data for LiF crystals irradiated with 790-MeV Kr ions [21]. In the case of $F$ centers, the activation energy is known to be considerably higher ($\sim$1.5 eV). The obtained result points to the essential role of interstitial halogen defects in the hardening. Since $H$ centers become mobile at lower temperatures, the stable configuration of interstitial halogen defects at room temperature are $H$-center aggregates. Obviously, the annealing above 530 K leads to a thermal decomposition of $H$-center aggregates. The created single $H$ centers can annihilate with $F$ centers, which are substantially less mobile, or they can decay on the surface by emitting a neutral halogen atom or molecule.

Taking into account the heating of samples under ion beam the results of annealing are also of importance for making a decision for a reasonable choice of the ion beam current density and irradiation time. From the obtained data it follows that the ion-beam induced temperature increase in the sample to about 360 K during irradiation at the current density of 180 nA/cm$^2$ is insufficient for annealing of defects.

## 4. Conclusions

AFM and SEM investigation on etched LiF crystals irradiated with 150 MeV Kr ions confirmed the formation of bulk nanostructures consisting of columnar grains with nanoscale dimensions (30–90 nm). The nanostructure forms (1) under high-fluence irradiation ($6 \times 10^{12}$ ions/cm$^2$) at which the saturation of $F$ centers and aggregation stage of radiation defects is reached, and (2) above a threshold of energy loss $dE/dx > 10$ keV/nm for the track core damage.

Annealing experiments showed that the nanostructure is thermally stable up to temperatures of 500 K. Further increase of annealing temperature leads to transition from nanostructure to dislocation-type structure which is restored to the original state at about 830 K. At the same temperature the recovery of hardness by the decomposition of H-center aggregates is achieved.

Comparing our results with previous data leads to the conclusion that the nanostructuring can be considered as a stress-driven ordering of ion-induced defects and their clusters. The stress field of ion tracks exhibiting core damage is suggested to play a decisive role in the self-organized nanostructuring.

At an energy loss $dE/dx < 10$ keV/nm, ion-induced dislocations are created. The formation of prismatic dislocations by clustering of interstitials or vacancies at this stage is suggested.

## References

[1] M. Toulemonde, C. Trautmann, E. Balanzat, K. Hjort, A. Weidinger, Nucl. Instrum. Methods B 216 (2004) 1.
[2] R. Neumann, Nucl. Instrum. Methods B 151 (1999) 42.
[3] K. Schwartz, C. Trautmann, T. Steckenreiter, O. Geiss, M. Kramer, Phys. Rev. B 58 (1998) 11232.
[4] S. Abu Saleh, Y. Eyal, J. Appl. Crystallogr. 40 (2007) 71.
[5] I.P. Jain, G. Agarwal, Surf. Sci. Rep. 66 (2011) 77.
[6] M. Kumar, F. Singh, S.A. Khan, V. Baranwal, S. Kumar, D.C. Agarwal, A.M. Siddiqui, A. Tripathi, A. Gupta, D.K. Avasthi, A.C. Pandey, Phys. D: Appl. Phys. 38 (2005) 637.

[7] J. Maniks, I. Manika, R. Grants, R. Zabels, K. Schwartz, M. Sorokin, R.M. Papaleo, Appl. Phys. A 104 (2011) 1121.
[8] N. Itoh, D.M. Duffy, S. Khabakshouri, A.M. Stoneham, J. Phys.: Condens. Matter 21 (2009) 474205.
[9] K. Schwartz, A.E. Volkov, M.V. Sorokin, C. Trautmann, K.-O. Voss, R. Neumann, M. Lang, Phys. Rev. B 78 (2008) 024120.
[10] A. Dauletbekova, A. Akilbekov, M. Zdorovets, Phys. Status Solidi B 247 (2010) 1227.
[11] A. Dauletbekova, A. Akilbekov, M. Zdorovets, A.F. Vasíĺeva, D.A. Akilbekova, Nucl. Instrum. Methods B 268 (2010) 3005.
[12] K. Schwartz, M.V. Sorokin, A. Lushchik, Ch. Lushchik, E. Vasilchenko, R.M. Papaleo, D. de Souza, A.E. Volkov, K.-O. Voss, R. Neumann, C. Trautmann, Nucl. Instrum. Methods B 266 (2008) 2736.
[13] A.B. Lidiard, Z. Phys. Chem. 208 (1998) 219.
[14] I. Manika, J. Maniks, K. Schwartz, J. Phys. D: Appl. Phys. 41 (2008) 074008.
[15] J.F. Ziegler, J.P. Biersack, U. Littmark, The Stopping and Range of Ions in Solids, Pergamon, New York, 1985.
[16] Y. Kawamata, J. Phys. 37 (1976) C7–C502.
[17] L.W. Hobbs, J. Phys. 34 (1973) C9–C227.
[18] J. Maniks, I. Manika, R. Zabels, R. Grants, E. Tamanis, K. Schwartz, Nucl. Instrum. Methods B (2011) doi: 10.1016/j.nimb.2011.08.042.
[19] K. Schwartz, A.E. Volkov, M.V. Sorokin, R. Neumann, C. Trautmann, Phys. Rev. B 82 (2010) 144116.
[20] N. Seifert, W. Husinsky, G. Betz, Phys. Rev. B 43 (1991) 6723.
[21] Manika, J., Maniks, P., Kulis, L., Gailite,, In: Rosental, A., (Ed.), Proceedings of SPIE 5946, 2005, 59460B-1.

IOP Conf. Series: Materials Science and Engineering **38** (2012) 012017 doi:10.1088/1757-899X/38/1/012017

# Shear banding mechanism of plastic deformation in LiF irradiated with swift heavy ions

**J Maniks[1], R Zabels, I Manika**
Institute of Solid State Physics, University of Latvia, Latvia

E-mail: manik@latnet.lv

**Abstract.** The effect of ion irradiation on the behavior of plastic deformation at micro- and nanoindentation on (001) face of LiF has been investigated. The irradiation was performed using heavy ions (U, Au, Ti and S) with energy in the range from 3 MeV to 2 GeV at fluences up to $5x10^{13}$ ions/cm$^2$. In non-irradiated LiF, the indentation produces dislocation gliding on the {110} planes along the <100> and <110> directions. At high fluence irradiation, the resource of the dislocation slip along the preferable directions becomes exhausted due to immobilization of dislocations by radiation defects and their aggregates. The present study demonstrates the change of the mechanism of plastic deformation from homogenous dislocation slip to localized shear banding in samples irradiated to high fluences. The factors facilitating of the localization of deformation have been analyzed.

## 1. Introduction

Modification of the structure, physical and mechanical properties of solids irradiated with swift heavy ions (SHI) is a topic that has attracted considerable interest over recent decades. Numerous papers have been devoted to radiation damage studies in lithium fluoride and related solids with strong ionic bonding [1]. Such materials maintain crystallinity even under conditions of severe irradiation. However, nanostructuring on surface and in bulk of LiF samples accompanied by strong (up to threefold) increase of hardness under irradiation with SHI was reported [2, 3]. The ion- induced change of the mechanism of plastic deformation is suggested [4].

In this work the behavior of plastic deformation at indentation on LiF crystals irradiated with SHI to high fluences has been investigated.

## 2. Experimental

Irradiations were performed on LiF crystals (Korth Kristalle, Germany) to high fluences ($10^{11}$-$10^{13}$ ions/cm$^2$) using $^{238}$U, $^{197}$Au, $^{49}$Ti and $^{32}$S ions. Exposure to high energy (GeV) ion radiation was performed at the UNILAC linear accelerator within GSI, Darmstadt, Germany. A portion of LiF samples were irradiated with Au ions in the 3-15 MeV energy range at the Tandetron accelerator in Porto Alegre, Brasil.
For the indentation measurements two methods were utilized. The instrumented indentation was performed using nanoindentation unit MTS Nano G200 with a Berkovich diamond tip. For higher loads a microhardness tester PMT-3 with a precision loading mechanism and Vickers diamond indenter was used.

[1] To whom any correspondence should be addressed

Structural defects around the indentation imprints were revealed by a chemical etching in saturated aqueous $FeCl_3$ solution. The surface was studied using optical and atomic force microscopy.

## 3. Results

### *3.1 Nanoindentation study*

Figure 1 shows MeV ion-induced hardening in LiF and evolution of the deformation pattern around indents. Substantial changes in hardness and deformation mode are observed at high fluences (>$10^{13}$ ions/cm$^2$), when saturation and aggregation of radiation defects occur.

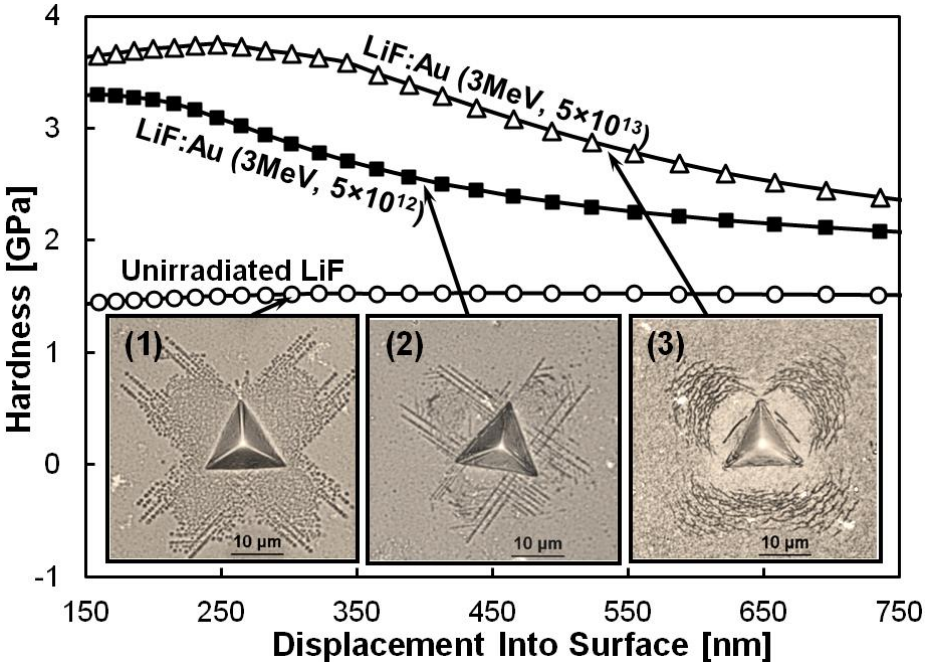


**Figure 1.** Hardness as a function of indenter penetration depth for LiF samples irradiated with 3 MeV $^{197}$Au ions. The inset shows optical images of imprints and deformation zone after chemical etching.

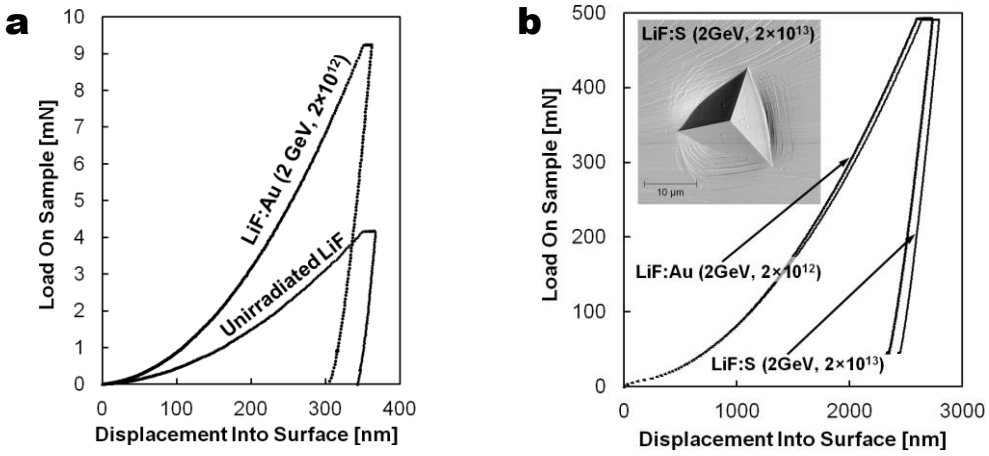

**Figure 2.** Load-Displacement data from instrumented indentation on LiF (a) – before and after irradiation with 2 GeV Au ions, (b) on LiF irradiated with Au and S ions. The inset shows the AFM image of deformation zone around the imprint for the sample irradiated with S ions.

Figure 2a shows loading-unloading curves for unirradiated and with Au ions irradiated LiF. The indentation has been performed at identical depth – 350 nm. When relative values of plasticity are compared, the irradiated material is only by 10% less plastic than the unirradiated crystal – 81.2% versus 92% plasticity. Fig.2 b contains a comparison of Load-Displacement data for LiF samples irradiated with 2 GeV Au ions at $2\times10^{12}$ ions/cm$^2$ and S ions at $2\times10^{13}$ ions/cm$^2$. In both cases the radiation dose was similar – 2.75 MGy. Light S ions cause comparable structural changes, which reflect both on hardness as well as plasticity. Even the high load of 500 mN didn't cause failure of these highly irradiated materials – no signs of brittleness could be observed on the loading curves. The inset of Fig.2 b shows Berkovich imprint on the sulphur irradiated LiF – shear bands around indent are clearly visible, similar as in the case of Au ions. Regarding hardness, GeV ions produce similar effects of hardening as MeV ions – only the modified layer is thicker – proportional to the ion penetration depth.

*3.2 Structural study of the deformation zone*

In an unirradiated LiF, the rows of dislocation etch pits can be seen extending along the <100> and <110> directions (Fig.1, inset 1) which are the directions of easy glide for dislocations [5]. The reduction of the dislocation arm length with increasing the fluence is observed. At high fluences the change of the deformation pattern from classic rosette formed by dislocation slip to a pattern of localized shear banding in zones of maximum stress against the centre of indenter faces has been observed (Fig.1, inset 3, inset of Fig.2b). The transition stage between them shows features characteristic to both – dislocation gliding as well as localized deformation (fig.1, inset 2, Fig3 b).

Deformation bands around an imprint on heavily irradiated LiF become very similar to those observed in amorphous metals (Fig.3 a). After such irradiation the material maintains a reasonable plasticity. No cracks are formed at light loads. Brittle cracking is observed only in heavily irradiated samples at high loads (Fig.3c).

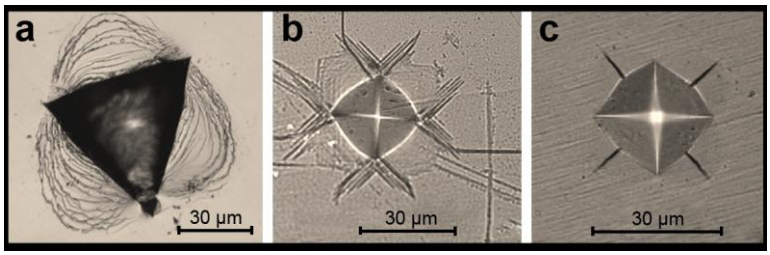


**Figure 3.** Deformation zones around imprints on (a) metallic glass [6], (b) LiF irradiated with 0.6 GeV Ti ions, fluence $5\times10^{12}$ cm$^{-2}$, (c) LiF irradiated with 2 GeV U ions, fluence $5\times10^{12}$ cm$^{-2}$.

## 4. Discussion

The swift-ion-induced damage processes in LiF are localized in tracks exhibiting comparatively large (up to few tens on nm) halo region of point defects. At room temperature the most significant type of defects are F centers, $F_2$ centers and complementary hole centers [1]. At high-fluences, the tracks overlap that leads to saturation and aggregation of point defects. The interaction of dislocations with defect aggregates as strong obstacles affects the deformation behavior and leads to increase of indentation hardness. Single defects as weak obstacles play a minor role [7]. The investigation of the structure of deformation zone in irradiated crystals (see inset of Fig.1 and Fig.2 a, b) shows a change of the mechanism of plastic deformation. The typical for LiF mechanism of dislocation glide is replaced by the mechanism of localized shear banding. In a transition stage the two mechanisms coexist.

The shear banding mechanism at definite conditions is observed for different materials, such as irradiated metals [8], nanocrystalline materials [9] and metallic glass [6]. Shear banding mechanism was reported also for LiF crystals at high temperature deformation [10]. In the latter case the deformation is ensured by thermo-activated climb of dislocations over obstacles. In our experiments performed at room temperature the contribution of thermo-activated processes to deformation is small as it follows from negligible indentation creep observed for irradiated crystals.

Formation of localized shear bands in irradiated metals is based on a specific mechanism named the channeling of deformation, which includes periodical formation of defect-free local zones followed by softening [4]. In such case, the instability of deformation is observed and cyclic bursts appear on the loading curves at indentation. Formation of defect free zones during deformation is never observed for ionic crystals. Confirming this, the loading curves on irradiated LiF show no signs of plastic instability.

Shear banding is well known as a main mechanism of plastic deformation in metallic glasses, were movement of assembles of atoms under high stresses becomes possible due to free volume in the structure of glassy materials. A noticeable contribution of similar non-dislocation mechanisms of deformation is suggested also for crystalline solids including LiF [11]. Appearance of the deformation zone in irradiated LiF and metallic glass is quite similar (see Fig.3 a). It should be taken into account that LiF crystals exhibit comparatively strong ion-induced effect of swelling that indicates formation of free volume. So, favorable conditions for the contribution of non-dislocation plasticity exist also for LiF crystals irradiated to high fluences. On the other hand, the nanostructuring of LiF under irradiation with SHI is observed [2, 3]. In nanostructured materials the deformation can be ensured by grain boundary sliding. A high concentration of ion-induced glissile prismatic dislocations facilitates such deformation mode.

The development of shear banding is known to occur without strain-hardening. Its initiation leads to saturation of hardness in irradiated crystals. Further increase of fluence shows small or no effect on flow stress or hardness. The present work and our earlier results show that the upper limit of hardness in ion-irradiated LiF reaches about 4 – 4.5 GPa.

## 5. Conclusion

In LiF crystals irradiated to high-fluences the change of the mechanism of plastic deformation from homogenous dislocation glide to localized shear banding is observed. Generally, the results indicate a complex nature of plastic deformation of ion-irradiated LiF. The non-dislocation mechanisms of deformation and grain boundary sliding are suggested to contribute the shear banding. The initiation of the shear banding mechanism limits further ion-induced increase of hardness. The irradiated crystals maintain reasonable plasticity. It follows from the obtained results that formation of localized shear bands at indentation is facilitated by ion-induced strengthening, which ensures high applied mechanical stress, swelling-induced formation of free volume and ion-induced nanostructuring.

**Acknowledgements:** This work has been supported by the Latvian government grant No 09.1548 and European Social Fund within the project «Support for Doctoral Studies at University of Latvia».

## References

[1] Perez A, Balanzat E and Dural J 1990 *Phys Rev B* **41** 3943
[2] Maniks J, Manika I, Grants R, Zabels R, Schwartz K, Sorokin M and Papaleo RM 2011 *Appl Phys A* **104** 1121
[3] Maniks J, Manika I, Zabels R, Grants R, Tamanis E and Schwartz K 2012 *Nucl. Instr. Meth. B* **282** 81
[4] Manika I, Maniks J, Schwartz K, Toulemonde M and Trautmann C 2003 *Nucl. Instr. Meth. B* **209** 93
[5] Nadgorny EM and Stepanov AV 1963 *Soviet Phys Solid State* **5** 732
[6] Keryvin V 2007 *Acta Mater* **55** 2565
[7] Manika I, Maniks J and Schwartz K 2008 *J Phys D: Appl Phys* **41** 074008
[8] Byun T and Hashimoto N 2006 *Nucl Eng & Technol.* **38** 619

[9] Meyers MA, Mishra A and Benson DJ 2006 *Progr Mater Sci* **51** 427
[10] Skvorcova NP 1996 *Cryst Res Technol* **31** 373
[11] Golovin YuI, Tyurin AI and Farber BYa 2002 *Mater Sci* **37** 895

# Modification of LiF structure by irradiation with swift heavy ions under oblique incidence

**I. Manika[1], J. Maniks[1], R. Zabels[1], K. Schwartz[2], R. Grants[1], A. Dauletbekova[3], A.Rusakova[3], M. Zdorovets[4]**
[1]Institute of Solid State Physics, University of Latvia, Riga, Latvia
[2]GSI Helmholtz Centre, Planckstr 1, 64291 Darmstadt, Germany
[3]L.N. Gumilyov Eurasian National University, Astana, Kazakhstan
[4]Institute of Nuclear Physics, Kazakhstan

E-mail: manik@latnet.lv

**Abstract.** The structural modifications of LiF irradiated with swift heavy ions under oblique angles have been investigated using AFM, SEM, chemical etching, nanoindentation and optical absorption spectroscopy. LiF crystals were irradiated under incidence angles of 30 and 70 degrees with 2.2 GeV Au (fluence $5\times10^{11}$ ions·cm$^{-2}$) and 150 MeV Kr ions (fluence $10^{12}$-$10^{14}$ ions·cm$^{-2}$). Structural study on sample cross-sections shows that two damage regions – (1) nanostructured zone and (2) dislocation - rich zone, which are typical for irradiations at normal incidence, appear also in samples irradiated under oblique angles. However in the latter case a more complex structure is formed that leads to stronger ion-induced hardening.

## 1. Introduction

The modifications of the structure of materials on the micro- and nanometer scale and an improvement of their properties by irradiation with swift heavy ions (SHI) are of importance on both the fundamental and technological standpoint. High fluence irradiation of ionic crystals with SHI leads to severe structural modifications including formation of latent tracks and surface and bulk nanostructures [1-3]. A significant role in the self-organized nanostructuring play stress fields of extended defects (such as tracks and dislocations) as well as crystallographic orientation. The latter is of special importance for ionic crystals which maintain crystallinity even under high-fluence irradiation. In the majority of studies the ion beam has been oriented normal to the crystal surface and tracks propagate along particular crystallographic direction. Peculiarities of track damage were observed at irradiation of crystal surfaces under grazing incidence of ion beam [4].

In this study the structural modifications in the bulk of LiF crystals irradiated under oblique incidence of ions has been investigated using AFM, SEM, chemical etching, nanoindentation and optical absorption spectroscopy. Irradiation was performed with 2.2 GeV Au ions, which in LiF produce complex tracks consisting of core region containing small defect aggregates and a surrounding halo region where mostly single defects are created [1]. Such tracks similar to dislocations exhibit stress field and can be revealed by selective chemical etching. In this study also 150 MeV Kr ions have been used which are attractive in a way that the threshold of energy loss for the core damage is surpassed only in a certain part of the ion range. As a result, two distinctively different in structure regions on the etched profile surfaces are observed [3].

## 2. Experimental

Irradiations were performed on nominally pure LiF crystals (Korth Kristalle, Germany) at the UNILAC linear accelerator of the GSI Darmstadt with 2.2 GeV Au ions at dose of $5\times10^{11}$ ions·cm$^{-2}$ under normal and oblique (30 degrees) incidence to the (100) cleavage face and at the cyclotron DC-60 (Astana, Kazakhstan) with 150 MeV $^{84}Kr^{+14}$ ions in the fluence range $10^{11}$ - $10^{14}$ ions·cm$^{-2}$ under incidence angles of 30 and 70 degrees. All irradiations were performed at room temperature. Ion tracks and dislocations were revealed using chemical etching

## 3. Results and discussion

### *3.1 Dependence of the thickness of irradiated layer on angle of incidence*

The thickness of the irradiated layer in the case of normally and under oblique incidence irradiated samples was estimated from optical microscopy of etched profile surfaces. The irradiated layer can be observed as striated structure oriented along the direction of the ion beam. For the normally irradiated samples the thickness of the irradiated layer coincided with the ion range R, which was calculated using the SRIM code [5]. For the samples irradiated under oblique angles the damaged layer was thinner. Its thickness is in agreement with the estimates performed from the geometrical considerations as h= Rsinα , where α is the angle of incidence (Fig. 1). The result confirms the independence of ion range of the ion incidence angle. Besides, samples which are inclined against ion beam receive correspondingly lower ion fluence due to projection of exposure over larger area.

The results of optical absorption spectroscopy for simultaneously irradiated samples under normal and oblique incidences are also in agreement with this model. Weaker coloration was found in samples irradiated under lower angles of incidence (Fig. 2). Spectra for all samples were similar and showed F, $F_2$ and $F_n$ absorption bands typical for high fluence irradiations [1,3].

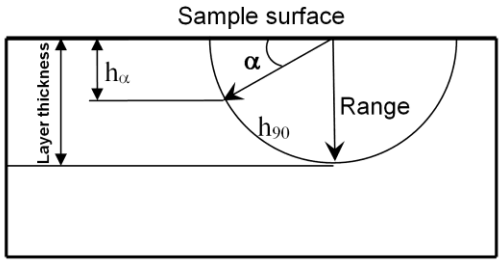


**Figure 1.** The thickness of the irradiated layer in dependence on the incidence angle of ions (scheme).

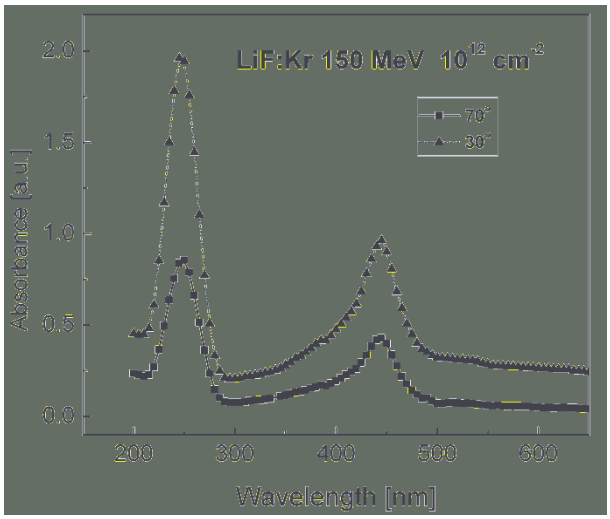


**Figure 2.** Absorption spectra for LiF crystals irradiated with150 MeV Kr ions at $10^{12}$ ions·cm$^{-2}$ under$70^0$ and $30^0$ incidence.

### *3.2 Structural study on the irradiated surface*

On the surfaces irradiated with Au and Kr projectiles etchable tracks were observed (Fig. 3a). Such result was expected because in both cases the energy loss for the ions surpasses the critical threshold of 10 keV/nm for core damage and track etching [1]. For the samples irradiated under oblique angle also the etch pits of tracks were tilted (Fig. 3a, inset).

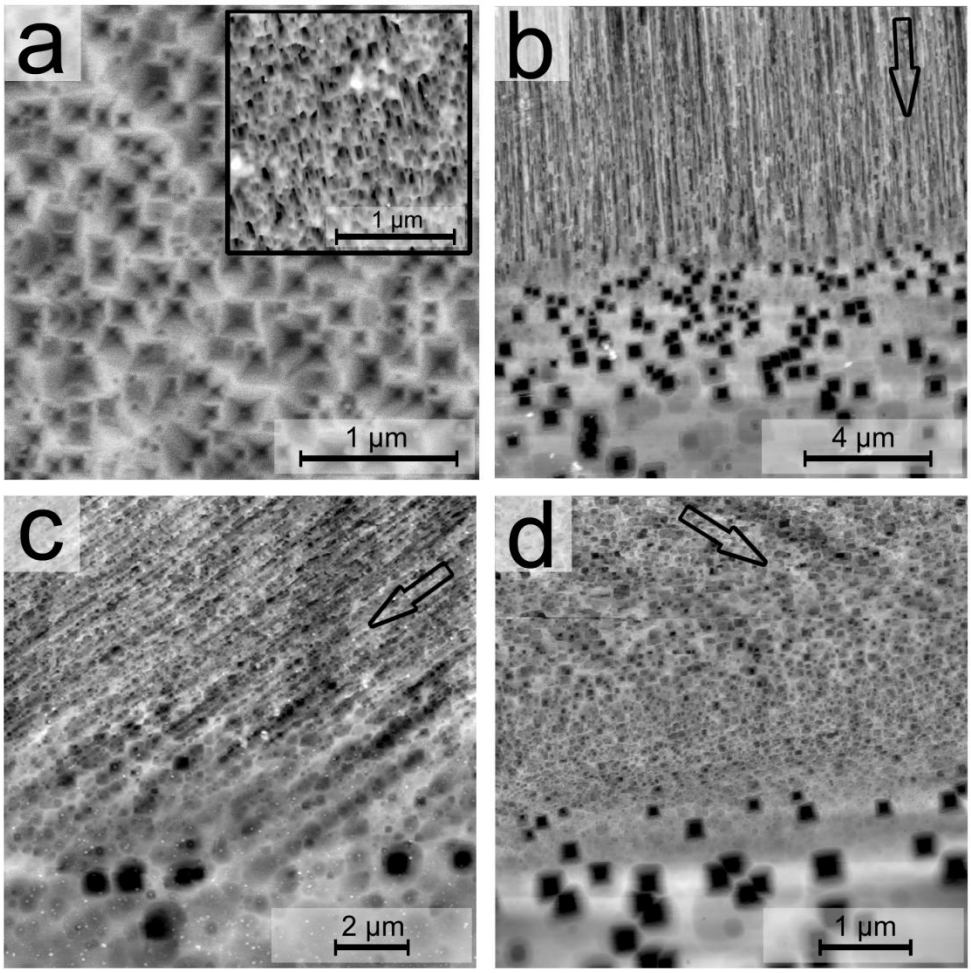


**Figure 3.** Damage structures created under normal and oblique incidence of ions (AFM and SEM images): (a) – etching of Au tracks on normally irradiated surface; fluence $5x10^{11}$ ions·cm$^{-2}$. Inset shows etched tracks under $30^o$ incidence; (b) - profile surface, normal irradiation with Kr ions at $10^{12}$ ions·cm$^{-2}$; (c) profile surface, Au ions under $30^o$ incidence , fluence $2.5x10^{11}$ ions·cm$^{-2}$; (d) profile surface, irradiation with Kr ions under $30^o$ incidence at $10^{12}$ ions·cm$^{-2}$. Arrows show the direction of irradiation.

*3.3 Structural study on the cross-sections of samples*

The structural study was performed on cross sections prepared by cleaving perpendicular to irradiated (001) face. At all irradiations under oblique angles the total thickness of irradiated layer was lower than the ion range and varied with the incidence angle as described in section *3.1*.

Our previous studies showed that at high fluence irradiation with Kr ions under normal angle, two regions exhibiting different types of structural features appear: (1) the nanostructured zone which can be characterized as mosaic type structure with small subgrains and (2) the zone containing numerous ion-induced dislocations (Fig. 3b) [2,3]. The two structural types were obtained also for all investigated incidence angles of Kr ions. The proportion of their extension was approximately the same as for irradiations under normal angle. Figure 3d shows the structure formed on profile surface of sample irradiated with Kr ions at the angle of $30^0$.

In the case of Au ions, the energy loss of which in LiF strongly exceeds that for Kr ions, the high fluence irradiation under normal and oblique angles in a dominant part of the irradiation zone creates a typical for nanostructures striated relief oriented in the direction of incoming ions (Fig. 3c)

### *3.4 Nanoindentation measurements*

Nanoindentation testing on normally irradiated surface revealed substantial increase of hardness in agreement with our earlier results [2,3]. Nevertheless in samples irradiated under oblique angle the hardening effect was stronger despite of the lower received irradiation dose (Fig. 4). Taking into account that hardness is sensitive to defect aggregates, the result points to certain difference in their ordering in dependence of irradiation angle. In agreement with the scheme (Fig. 1), the thickness of the hardened zone at oblique irradiation ($30^0$) is about half of that for perpendicularly irradiated sample

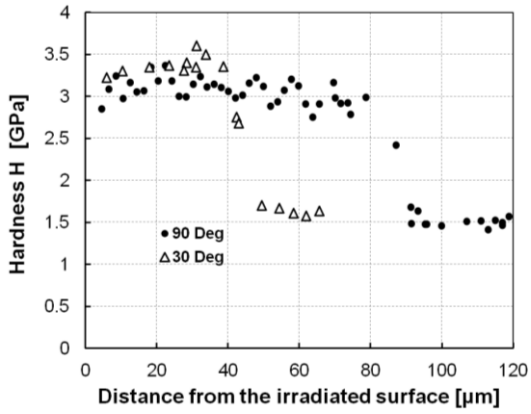


**Figure 4.** Hardness *vs.* indentation depth on profile surface of samples irradiated with Au ions under $90^0$ (solid symbols) and $30^0$ (open symbols) incidence angle. The fluence was $5x10^{11}$ and $2.5\ x10^{11}$ ions·cm$^{-2}$, correspondingly.

## 4. Conclusion

The thickness of irradiated layer varies with the incidence angle of ions. Maximum thickness which equals to the calculated ion range R is observed at irradiation perpendicularly to the (001) surface of a sample. The thickness of the irradiated layer decreases with decreasing of the incidence angle as h= R sinα in agreement with geometrical considerations. The results confirm that the ion range is independent of the incidence angle of ions.

Structural study shows that two zones of structural damage – nanostructured zone and dislocation rich zone, which are typical for irradiations at normal incidence [2,3], appear also in samples irradiated under oblique angles. The extension of these zones depends on energy loss of projectiles.

The irradiated layer for all investigated incidence angles exhibits increased hardness that gives evidence for formation of defect aggregates, such as dislocations and other extended defects.

## Acknowledgments

The research is carried out within the framework of the ERAF project Nr. 2010/0253/2DP / 2.1.1.1.0/10/APIA/VIAA//079**.**

R.Zabels acknowledges the financial support from the European Social Fund within the project «Support for Doctoral Studies at University of Latvia».

## References

[1] Trautmann C, Schwartz K, Costantini JM, Steckenreiter T, Toulemonde M. Nucl. Instr. and Meth. B **146** (1998)367-378.
[2] Maniks J, Manika I, Zabels R, Grants R, Tamanis E, Schwartz K. Nucl. Instr. and Meth. B **282** (2012) 81
[3] Dauletbekova A, Maniks J, Manika I, Zabels R, Aklibekov AT, Zdorovets MV, Bikert Y, Schwartz K. Nucl. Instr. and Meth. B**286** (2012) 56-60
[4] Vorobyova IV. Nucl. Instr. and Meth. B **198** (2002) 119-128.
[5] Ziegler JF, Biersack P, and Littmark U. The Stopping and Range of Ions in Matter, Pergamon Press, New York (1985).

Nuclear Instruments and Methods in Physics Research B 326 (2014) 318–321

Contents lists available at ScienceDirect

Nuclear Instruments and Methods in Physics Research B

journal homepage: www.elsevier.com/locate/nimb

# MeV–GeV ion induced dislocation loops in LiF crystals

R. Zabels [a,*], I. Manika [a], K. Schwartz [b], J. Maniks [a], R. Grants [a]

[a] Institute of Solid State Physics, University of Latvia, 8 Kengaraga str., Riga LV-1063, Latvia
[b] GSI Helmholtzzentrum für Schwerionenforschung, Planckstr. 1, 64291 Darmstadt, Germany

ARTICLE INFO

*Article history:*
Received 28 June 2013
Received in revised form 24 September 2013
Accepted 2 October 2013
Available online 22 January 2014

*Keywords:*
LiF crystal
U and S ion irradiation
Dislocations
Chemical etching
AFM

ABSTRACT

Formation of prismatic dislocation loops and evolution of dislocation structure in LiF crystals irradiated with swift $^{238}$U and $^{36}$S ions of specific energy 11 MeV/u at fluences up to $10^{13}$ ions cm$^{-2}$ has been investigated using chemical etching and AFM. It has been shown that prismatic dislocations are formed in the stage of track overlapping above threshold fluences $\Phi \approx 10^{9}$ U cm$^{-2}$ and $\Phi \approx 10^{10}$ S cm$^{-2}$. The diameter of dislocation loops reaches 600–1000 nm for $^{238}$U ions and 200 nm for $^{36}$S ions. The dislocations created by $^{238}$U ions are arranged in rows along the direction of ion beam, whereas $^{36}$S ions create freely distributed dislocation loops each of them being oriented along the ion beam. The role of dislocations in ion-induced nanostructuring and hardening is discussed.



## 1. Introduction

Irradiation with swift heavy ions (SHI) is an effective way for modification of structure, surface topography, electrical, mechanical and other properties of materials [1,2]. Structural changes in irradiated materials intensively occur under high-fluence irradiation which ensures the saturation and aggregation of primary radiation defects [3–7]. A significant attention during recent decades has been devoted to study of extended defects in alkali halides, which maintain their single-crystalline state even at very high irradiation doses. Nevertheless relatively few experimental and theoretical studies touch the question about formation of dislocations. Recently we found a strong contribution of SHI-induced dislocations in modifications of structure and mechanical properties of LiF crystals [2,8,9]. Still there are many open questions regarding formation of dislocations and their role in damage processes.

In the present study formation of SHI- induced dislocations in heavily irradiated LiF single crystals has been investigated by means of chemical etching and AFM. For the irradiation $^{36}$S and $^{238}$U projectiles have been chosen, which form tracks with different morphology [10].

## 2. Experimental

Nominally pure LiF crystals (Korth Kristalle, Germany) with the initial density of dislocations around $5 \times 10^{4}$ cm$^{-2}$ were irradiated at UNILAC (GSI Darmstadt, Germany) with $^{238}$U ions and at GANIL Caen (France) with $^{36}$S ions (specific energy of 11.1 MeV/u for both ions). Fluences from $5 \times 10^{7}$ ions cm$^{-2}$ to $10^{13}$ ions cm$^{-2}$ were achieved. Irradiations were conducted at room temperature perpendicular to (001) face. In the structural investigations selective chemical etching complemented by atomic force microscopy (AFM) imaging were used. Investigations were performed on (001) profile surfaces which were obtained by cleaving the samples in the direction of ion beam.

## 3. Results

### 3.1. Formation of dislocations in LiF crystals under irradiation with $^{238}$U ions

Previous studies show that substantial structural changes including formation of etchable tracks, dislocations and nanostructures in LiF crystals are caused by irradiation with heavy ions [2,8,11]. An open question remains if dislocations are created in a single ion track or under conditions of track overlapping. To clarify this, a structural study on LiF crystals irradiated with uranium ions in the fluence range $10^{7}$–$10^{10}$ ions cm$^{-2}$, which includes both – formation of single tracks as well as stages of their overlapping, was performed. The results are shown in Fig. 1.

On samples irradiated at low fluences (up to $10^{8}$ U cm$^{-2}$), where single tracks are formed, no typical square-shaped dislocation etch pits are observed. However, a row of small etching pits with rounded shape is revealed in the trajectory of each ion track (Fig. 1a). This indicates the presence of very small defect

* Corresponding author.
*E-mail address:* rzabels@gmail.com (R. Zabels).

0168-583X/$ - see front matter © 2014 Elsevier B.V. All rights reserved.
http://dx.doi.org/10.1016/j.nimb.2013.10.043

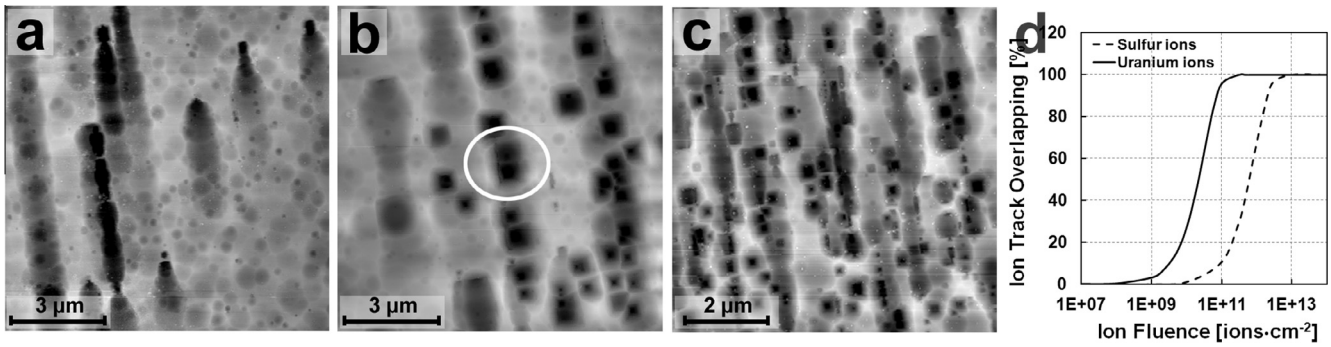


**Fig. 1.** Dislocation etch pits on LiF profile surfaces irradiated with 2.6 GeV $^{238}$U ions at different fluences: (a) $\Phi = 10^8$ ions cm$^{-2}$, (b) $\Phi = 10^9$ ions cm$^{-2}$; dislocation loop marked by circle, (c) $\Phi = 5 \times 10^9$ ions cm$^{-2}$ and (d) – calculated track overlapping *vs.* fluence for $^{238}$U and $^{36}$S ions, correspondingly.

aggregates, which might serve as nuclei for the growth of dislocations. A different result was obtained at higher fluences at which overlapping of tracks becomes possible.

The overlapped area of tracks can be estimated from the Poisson law as $A = A_0(1 - \exp(-\pi r_F^2 \times \Phi)$ where $\Phi$ is the ion fluence and $r_F$ is the Thevenard radius, which is deduced from the optical absorption data [12]. The calculated curves of track overlapping ($A/A_0$) for $^{238}$U and $^{36}$S ions are shown in Fig. 1d. As seen, the overlapping for $^{238}$U tracks appears at fluences above $10^9$ ions cm$^{-2}$ and for $^{36}$S tracks at fluences above $10^{10}$ ions cm$^{-2}$. The positions of the overlapping curves differ by an order of magnitude due to difference in the track radii.

Fig. 1b shows structural changes in the crystal irradiated to fluence $10^9$ U cm$^{-2}$. Such fluence corresponds to the initial stage of track overlapping (overlapping around 4% (Fig. 1d)). Few rows of square shaped etch pits aligned in the direction of ion beam were observed on the investigated profile surfaces. The distance between these rows substantially exceeds the average distance between ion tracks (about 0.3 μm) calculated as $d = 2\ (\pi \times \Phi)^{-1/2}$ where $\Phi$ is the fluence. Therefore, it can be assumed, that etch pits of dislocations are formed in areas where some ion tracks overlap i.e. intersect previously irradiated regions. The role of overlapping becomes evident at even higher fluences ($5 \times 10^9$ U cm$^{-2}$) where comprehensive formation of dislocation is observed (Fig. 1c). The results allow us to conclude that dislocations forming classical square shaped etch pits appear under conditions of track overlapping. Their alignment in rows along the direction of ion beam is associated with a similar alignment of dislocation nuclei in individual tracks and also with ordering influence of the mechanical stress field of ion tracks. Such stress field is characteristic only for tracks of heavy ions exhibiting core damage [10]. In the tail of the ion range where energy loss is insufficient to form tracks with core damage, arrangement of etch pits drastically changes from ordered in rows to freely distributed.

When dislocation loop intersects the surface under investigation, it creates a mutually related pair of etch pits – as it is schematically shown in Fig. 2f. The distance between the etch pits approximately characterizes the size of the loop. During chemical etching of small loops the pits might merge forming elongated rectangles or even almost square shaped etch pits.

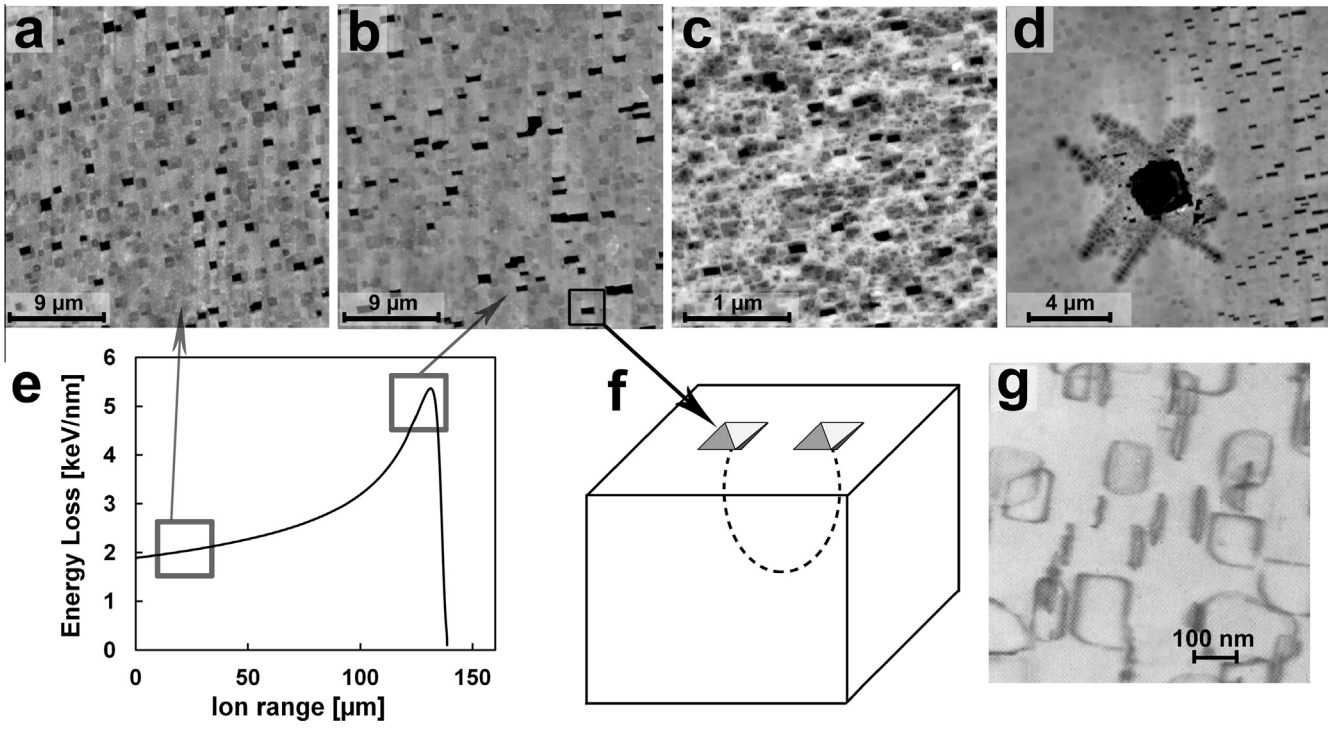


**Fig. 2.** (a) and (b) – view of etched profile surface, fluence $\Phi = 10^{12}$ S cm$^{-2}$ ; AFM images were taken from near-surface region and from Bragg maximum correspondingly, (c) view of etched profile surface , $\Phi = 4 \times 10^{13}$ S cm$^{-2}$, (d) – redistribution of dislocations near local indentation on profile surface irradiated with $^{36}$S ions, (e) – calculated electronic energy loss in LiF irradiated with 410 MeV $^{36}$S ions, (f) schematic of etched dislocation loop, (g) – TEM image of dislocation loops from Ref. [7].

In the case of $^{238}$U ions the largest loops create well separated pairs of etch pits (Fig. 1b, marked by circle) which are oriented along the direction of ion beam. The distance between them (the size of loop) reaches 600–1000 nm.

### 3.2. Formation of dislocations under irradiation with $^{36}$S ions

Selective chemical etching in LiF crystals irradiated with low fluences (<$10^{10}$ S cm$^{-2}$) didn't reveal classical square-shaped dislocation etch pits. At low fluences only small etching pits are revealed in the ion trajectory. However, the contrast of etching is much lower than in the case of $^{238}$U ions. In this fluence range the average distances between ion tracks (>113 nm) substantially exceed the diameter of tracks (about 12 nm) and the overlapping effect of tracks can be ignored. Our previous studies show that irradiation with sulfur ions at low fluences also does not cause changes in mechanical properties – hardness and dislocation mobility, which are sensitive to defect aggregates [13].

After irradiation to higher fluences ($10^{12}$ S cm$^{-2}$) numerous freely arranged dislocation etch pits occur on profile surfaces. The AFM images, which have been obtained in various regions of the ion trajectory, where is notable differences in ion energy loss (as indicated in Fig. 2e), show differences in the shape of etch pits. Near the irradiated surface etch pits have mainly square-like shape (Fig. 2a), whereas in the region of the Bragg maximum, where the energy loss of ions reaches extreme, etch pits have rectangular shape elongated in the direction of ion beam (Fig. 2b). Nonetheless, the density of dislocations (approx. $10^7$ cm$^{-2}$) is similar in both regions. With the increase of fluence, the count of etch pits increases, many tiny pits occur and at fluence of $4 \times 10^{13}$ S cm$^{-2}$ the density of dislocations approaches $10^{10}$ cm$^{-2}$ (Fig. 2c). For heavily irradiated samples the contrast of selective etching decreases due to increase of chemical activity of the irradiated crystal.

The average size of dislocation loops estimated from the Fig. 2b is about 200 nm. The etch pits for the smallest loops are almost square shaped. The resolution of etching technique is too low to determine the size of such loops. During the etching smallest loops quickly vanish. Thus in Fig. 2a and b a large number of sites with a low contrast, which correspond to contours of previous etch pits, can be seen.

Dislocation loops created in LiF by $^{36}$S ions at moderate fluences maintain some mobility. This is confirmed by a following experiment. To induce local mechanical stresses, the irradiated samples prior to chemical etching were exposed to microindentation. The impressions were located at the vicinity of irradiated zone. Etching of these samples showed that in the stressed region around the impression majority of irradiation induced defects (etch pits) are repulsed from the indent (Fig. 2d). In turn, the corresponding dislocation arms of the imprint are reduced due to such interaction. The mobility of dislocations in samples irradiated to higher fluences was strongly reduced.

Since dislocations from other kinds of defect aggregates are distinguished by their ability to move under the influence of mechanical stresses, the obtained result can be considered also as an additional evidence for identification of the etch pits as dislocations.

## 4. Discussion

Formation of dislocations under irradiation of LiF crystals with SHI is not surprising. Prismatic dislocation loops in alkali halide crystals irradiated with electrons were observed already in the 1970's performing *in situ* transmission electron microscopy (TEM) experiments (see Fig. 2g) [7,14,15]. As it is known an intensive electron radiation in the form of delta-electrons is emitted in the process of SHI interaction with the matter as well.

It is widely accepted that, taking into account the high mobility of interstitials, in irradiated LiF crystals at room temperature mainly interstitial type dislocation loops can be formed. The prismatic dislocations are of the edge dislocation type with the Burgers vector $b = 1/2 <1\,1\,0>$ directed normal to the plane of the loop.

A perfect interstitial dislocation loop in ionic crystal is formed by the aggregation of equal numbers of anion and cation interstitials as required to maintain the charge neutrality [7]. However, all previous work showed that in alkali halides SHI creates damage in the halogen sublattice, whereas the alkali sublattice remains nearly intact. Since there is little evidence for the direct production of cation Frenkel pairs by ionizing radiation, alternative models were presented in which the planar dislocation loop forms primarily as a result of the initial aggregation of halogen interstitials alone. Hobbs proposed a model in which the growth of dislocations occurs when di-halide molecule occupies a lattice position and as a result expels an anion and a cation [7]. This reaction is unlikely to occur in the ideal lattice but becomes exothermic on edges of dislocation loops [16] thus providing anions and cations required for the perfect dislocations.

An alternative way for formation of extended defects deduced from the Hobbs model is the growth of colloids at temperatures where the F-centres become mobile [17]. However, LiF crystals irradiated at room temperature with SHI (up to uranium) do not show Li colloids [4]. In the present study additionally to the results of chemical etching also EPR measurements were performed on LiF crystals irradiated with $8 \times 10^{10}$ U cm$^{-2}$ and $2 \times 10^{13}$ S cm$^{-2}$. EPR spectra didn't show the presence of colloids. Their formation in LiF has been observed at elevated irradiation temperatures or after post-irradiation annealing, when the mobility of F-centers becomes sufficiently high [6,18].

The Hobbs model can explain the growth of dislocations, however, gives no information about their nucleation. Formation of dislocations in irradiated LiF was experimentally studied by Gilman [19]. In the particular work it has been shown that the pre-existing dislocations and precipitates serve as dislocation sources. As another possible mechanism formation of dislocations under shear stresses which are generated in tracks during relaxation processes after Coulomb explosion is considered [20]. However, our observations do not confirm the formation of perfect dislocations within isolated tracks. The chemical etching reveals only the presence of possible nuclei for dislocations. Rows of small etching pits are clearly seen along the tracks of $^{238}$U ions (Fig. 1a). Such rows appear also in the separate tracks of lighter $^{36}$S ions, however, with a lower etching contrast. The observed etch pits can be ascribed to small aggregates of radiation defects or impurity complexes, or even to very small dislocation loops. Yet, classical square shaped dislocation etch pits were observed only at the stage of track overlapping as it is shown for $^{238}$U ions in Fig. 1b and for $^{36}$S ions in Fig. 2a and b. In the latter case the shape of dislocation etch pits varies in dependence on the distance from the irradiated surface and the energy loss of projectile. Such behavior can be related to change of the track radii along the ion path. It was observed in the study of depth profiles of F-centers and track size [21]. The results showed variation of the track radii along the ion trajectories. The peak values are observed at the Bragg maximum. Obviously this is a reason why the experimentally observed dislocation etch pits are smaller in the initial part of the ion pass (Fig. 2a) than around the Bragg maximum (Fig. 2b) where a higher extent of track overlapping is suggested and the average size of loops reaches saturation value around 200 nm. Such differences in the structure along the ion path are observed only in samples irradiated with ions exhibiting pronounced maximum in the energy loss.

To evaluate the contribution of prismatic dislocation loops it was calculated what fraction of total radiation defects is included in dislocations. Estimation on LiF samples irradiated with $^{36}$S ions,

which is based on the data in Fig. 2b, shows that from the total number of radiation defects at saturation (up to 4–5 $\times$ $10^{19}$ $cm^{-3}$) [22] substantial part (around 10%) is embedded in dislocations. For $^{238}U$ ions even higher contribution of dislocations is expected.

Our recent studies show that significant role in ion-induced hardening of LiF crystals is played by formation of sessile dislocations [23]. As it is known, dislocations, especially electrically charged jogs around their perimeter, can serve as binding sites for the radiation defects and nuclei for the growth of defect complexes and aggregates [24]. Thus there is a reason to consider SHI-induced dislocations as defect aggregates of complex nature. It is known that the absorption of defects and impurities on dislocations lowers their mobility. In heavily irradiated LiF crystals the mobility of dislocations decreases to such an extent that it causes a change in the mechanism of plastic deformation. The dislocation mechanism is replaced by plastic deformation *via* rearrangement of atoms in localized shear bands [23]. Such mechanism of plastic deformation is observed in metallic glasses and other related materials. The initiation of shear banding mechanism determines the upper threshold (4–4.5 GPa) for the hardness of irradiated LiF crystals.

The growth and arrangement of dislocations is strongly affected by the stress fields of tracks as it can be observed in the vicinity of U tracks exhibiting core damage. An additional factor promoting the growth of dislocations along tracks is their location close to the track core which serves as a path for facilitated diffusion of defects [25]. We suggest that the SHI induced ordering of dislocations in rows along the ion trajectory plays a significant role in the formation of the bulk nanostructure. It has been established that the mosaic-type nanostructure in LiF crystals irradiated with SHI is formed under the conditions when the energy loss of ions surpasses the critical threshold value of 10 keV/nm and when the fluence is sufficient to ensure overlapping of tracks [2,9]. As observed in this study, formation of dislocations and their ordering in rows along the ion trajectory occurs precisely at these conditions. Obviously such arrangement can be considered as an initial stage of sub-grain boundary formation. This self-organized process intensifies with the increase of fluence. In LiF crystals irradiated with $^{36}S$ ions dislocations are arranged irregularly, which hinders formation of the bulk nanostructure as it has been shown also in cases of other light ions [2].

Another source of dislocations in crystals irradiated with SHI is swelling – induced long range stresses. The swelling of irradiated crystal creates substantial shear stresses along the interface between the irradiated layer and unirradiated crystal as well as bending stresses in whole sample. At high fluences the stresses can exceed the threshold for generation of dislocations that leads to formation of ordinary edge and screw dislocations (not the dislocation loops). Such dislocations are mainly generated in softer unirradiated part of sample, particularly near the interface where the gliding of dislocations along <1 1 0> direction inclinated at 45° to (0 0 1) plane is observed [26]. Swelling-induced dislocations are readily formed under irradiation with heavy ions which create stronger effect of swelling.

## 5. Conclusions

This study confirms the formation of prismatic dislocation loops in LiF crystals under high-fluence irradiation with SHI.

- It has been shown that prismatic dislocations are formed in the stage of track overlapping. In separate tracks, chemical etching reveals small aggregates of defects which might serve as nuclei for dislocations.
- Differences of the main parameters of dislocations created by heavy ($^{238}U$) and light $^{36}S$ ions is observed due to difference of energy loss, track structure and track diameter.
  - The threshold fluence for formation of dislocations is $\Phi \approx 10^9$ U $cm^{-2}$ and $\Phi \approx 10^{10}$ S $cm^{-2}$;
  - The diameter of dislocation loops reaches 600–1000 nm for $^{238}U$ ions and 200 nm for $^{36}S$ ions;
  - Dislocations created by $^{238}U$ ions are arranged in rows along the direction of ion beam, whereas $^{36}S$ ions create freely distributed dislocation loops each of them being oriented along the beam.

## Acknowledgements

The research is carried out within the framework of the ERAF project Nr. 2010/0253/2DP/2.1.1.1.0/10/APIA/VIAA//079 and European Social Fund within the project Support for Doctoral Studies at University of Latvia.

## References

[1] M. Toulemonde, C. Trautmann, E. Balanzat, K. Hjort, A. Weidinger, Nucl. Instrum. Methods B 216 (2004) 1–8.
[2] J. Maniks, I. Manika, R. Zabels, R. Grants, E. Tamanis, K. Schwartz, Nucl. Instrum. Methods B 282 (2012) 81–84.
[3] W.J. Soppe, H. Donker, A. Garcia Celma, J. Prij, J. Nucl. Mater. 217 (1994) 1–31.
[4] C. Trautmann, K. Schwartz, J.M. Costantini, T. Steckenreiter, M. Toulemonde, Nucl. Instrum. Methods Phys. Res. B 146 (1998) 367–378.
[5] V.I. Dubinko, A.A. Turkin, D.I. Vainshtein, H.W. den Hartog, Nucl. Instrum. Methods Phys. Res. B 153 (1999) 163–166.
[6] E.A. Kotomin, A.I. Popov, in: K.E. Sickafus et al. (Eds.), Radiation Effects in Solids, Springer, Amsterdam, 2007, pp. 153–192.
[7] L.W. Hobbs, A.E. Hughes, D. Pooley, Proc. R. Soc. London A 332 (1973) 167–185.
[8] J. Maniks, I. Manika, R. Grants, R. Zabels, K. Schwartz, M. Sorokin, R.M. Papaleo, Appl. Phys. A 104 (2011) 1121–1128.
[9] A. Dauletbekova, J. Maniks, I. Manika, R. Zabels, A.T. Aklibekov, M.V. Zdorovets, Y. Bikert, K. Schwartz, Nucl. Instrum. Methods B 286 (2012) 56–60.
[10] K. Schwartz, C. Trautmann, T. Steckenreiter, O. Greiβ, M. Krämer, Phys. Rev. B 58 (1998) 11232–11240.
[11] C. Trautmann, K. Schwartz, O. Geiβ, J. Appl. Phys. 83 (1998) 3560–3564.
[12] C. Trautmann, M. Toulemonde, K. Schwartz, J.M. Costantini, A. Müller, Nucl. Instrum. Methods B 164–165 (2000) 365–376.
[13] I. Manika, J. Maniks, K. Schwartz, J. Phys. D Appl. Phys. 41 (2008) 074008.
[14] L.W. Hobbs, J. Phys. 34 (C9) (1973) 227–241.
[15] Y. Kawamata, J. Phys. 37 (C7) (1976) 502–506.
[16] C.R.A. Catlow, K.M. Diller, L.W. Hobbs, Philos. Mag. A 42 (1980) 123–150.
[17] U. Jain, A.B. Lidiard, Philos. Mag. 35 (1977) 245–259.
[18] K. Schwartz, A.E. Volkov, M.V. Sorokin, R. Neumann, C. Trautmann, Phys. Rev. B 82 (2012) 231–240.
[19] J.J. Gilman, W.G. Johnston, G.W. Sears, J. Appl. Phys. 29 (1958) 747–754.
[20] D.A. Young, Nucl. Instrum. Methods B 225 (2004) 231–240.
[21] A. Perez, E. Balazant, J. Dural, Phys. Rev. B 41 (1990) 3943–3950.
[22] K. Schwartz, C. Trautmann, A.S. El-Said, R. Neumann, M. Toulemonde, W. Knolle, Phys. Rev. B 70 (2004) 184104.
[23] J. Maniks, R. Zabels, I. Manika, IOP Conf. Ser. Mater. Sci. Eng. 38 (2012) 012017.
[24] R. Smoluchowski, J. Phys. 27 (C3) (1966) 3–11.
[25] S. Abu Saleh, Y. Eyal, Nucl. Instrum. Methods B 230 (2005) 246–250.
[26] I. Manika, J. Maniks, K. Schwartz, C. Trautmann, M. Toulemonde, Nucl. Instrum. Methods B 209 (2003) 93–97.

Appl. Phys. A
DOI 10.1007/s00339-015-9145-9

Applied Physics A
Materials Science & Processing

# Depth profiles of indentation hardness and dislocation mobility in MgO single crystals irradiated with swift $^{84}$Kr and $^{14}$N ions

R. Zabels[1] · I. Manika[1] · K. Schwartz[2] · J. Maniks[1] · R. Grants[1] · M. Sorokin[3] · M. Zdorovets[4]

Received: 8 October 2014 / Accepted: 30 March 2015


**Abstract** The depth dependence of damage and modification of micromechanical properties in MgO single crystals irradiated with 150 MeV $^{84}$Kr and 24.5 MeV $^{14}$N ions (specific energy 1.75 MeV/u) at fluences up to $10^{15}$ ions/cm$^2$ has been studied. The effects of ion-induced increase in hardness and reduction in dislocation mobility, magnitude of which varies along the ion range, were observed. These effects are related to ion-induced dislocations which were revealed by chemical etching. The results confirm a joint contribution of electronic excitations and atomic displacements by elastic collisions in the structural damage of MgO. The excitation mechanism in hardening dominates in the incoming part of ion range (up to the Bragg's maximum), while the role of impact mechanism becomes dominant only at the end of ion range.

## 1 Introduction

MgO single crystals exhibit a high resistance to radiation damage and withstand high temperatures, therefore having a potential in nuclear applications, such as a host of inert matrix fuels, a component material for fusion devices and others. An actual topic in the studies of suitability of radiolysis-resistant refractory oxides is their reliability under conditions of severe irradiation with high-energy particles, particularly with swift heavy ions (SHI), energy loss of which is of the same order as for nuclear fission fragments.

In radiation-sensitive ionic crystals, such as LiF, efficient formation of radiation defects occurs mainly via ionization and excitation processes, while the contribution of displacements caused by elastic collision mechanism is negligible [1]. In contrast to LiF, MgO single crystals have an energy gap $E_g = 7.8$ eV that is below the critical energy for the creation of stable Frenkel defects in anion sublattice ($E_{FD} = 15.2$ eV). As a result, the excitons, holes and electrons in pure MgO do not undergo self-trapping and their decay in the bulk of a crystal does not create Frenkel defects. Such suppression of radiation damage production by ionization and excitation processes was confirmed in experiments on high purity (1–10 ppm) MgO crystals which were grown using arc fusion technique (3 recrystallization cycles and subsequent annealing at 3000 K) [2]. This means that radiation defects in high-purity MgO are created primarily by less efficient elastic collision (impact) mechanism. However, in commercial MgO crystals with a higher content of impurities, some contribution of the non-impact damage under conditions of ion-induced high-density electronic excitations becomes possible [2, 3]. This is due to impurity ions such as $Ca^{2+}$ and $Be^{2+}$ which substitute $Mg^{2+}$ and serve as hole traps ensuring formation of Frenkel defects. In such crystals, a joint contribution of electronic and impact mechanisms in production of color centers was found to occur [2].

For nuclear applications of MgO, the basic criterion is structural and mechanical integrity. MgO is known as brittle material under conditions of macroscopic deformation while exhibiting plasticity at microscale and nanoscale

✉ R. Zabels
rzabels@gmail.com

[1] Institute of Solid State Physics, University of Latvia, Riga, Latvia

[2] GSI Helmholtzzentrum für Schwerionenforschung, Darmstadt, Germany

[3] National Research Centre Kurchatov Institute, Moscow, Russia

[4] Institute of Nuclear Physics, Almaty, Kazakhstan

Published online: 17 April 2015

[4, 5]. Severe irradiation of MgO with SHI leads to aggregation of primary radiation defects and formation of extended defects, e.g., dislocations which play a significant role in mechanical behavior. However, the SHI-induced damage processes in MgO, accumulation of extended defects and modification of its micromechanical properties have not been extensively studied.

Formation of dislocations in MgO and related spinel structures under high-dose irradiation with swift ions was confirmed in TEM studies [6, 7]. A characteristic feature of the aggregation stage of radiation defects in ionic crystals is the ion-induced increase in hardness [8]. It has been shown that dislocations and other aggregates of primary radiation defects are responsible for hardening, while single defects are of a minor importance [9].

In the present work, the structural damage and modification of micromechanical properties of MgO single crystals irradiated with high doses of swift $^{84}$Kr and $^{14}$N ions has been studied. The attention is focused on the role of electronic excitation and impact mechanisms in radiation damage. To distinguish them, the indentation hardness as a local and structure-sensitive probe was used. The indentation technique allows measurements on profile surfaces prepared by cleaving samples along the direction of ion beam. In such a way, we can trace the ion-induced changes from the incoming part of the ion range, where electronic excitation processes are dominating, to the end of the ion range, where calculations show the maximum contribution of the impact mechanism.

## 2 Experimental

MgO single crystals (MTI, CA, USA) were used for experiments. The density of grown-in dislocations in unirradiated crystals was $10^4$ cm$^{-2}$. About 1-mm-thick samples of 10 × 10 mm$^2$ size were prepared by cleaving and irradiated at the DC-60 cyclotron accelerator (Astana, Kazakhstan) with 150 MeV $^{84}$Kr and 24.5 MeV $^{14}$N ions of specific energy 1.75 MeV/u at fluences up to $10^{15}$ ions/cm$^2$. All irradiations were performed under normal incidence of the ions to the (100) face of crystals. The temperature of samples during irradiation did not exceed 360 K. The energy loss and the range of ions were calculated using SRIM 2013 [10].

Nanoindentation tests were performed by a G200 nanoindenter (Agilent, USA) with a Berkovich and Vickers diamond tips (curvature < 20 nm) in ambient air at room temperature using the basic and continuous stiffness measurement techniques. The strain rate was 0.05 s$^{-1}$. The nanoindenter was calibrated using a reference sample of fused silica. The hardness, Young's modulus and standard deviation of the measurements were calculated from experimentally obtained loading–unloading curves and averaged from ten individual measurements. The depth profiles of hardness and modulus at a constant indentation load (20 mN) were measured on sample cross sections prepared by cleaving the samples along the direction of ion beam. The distance of indents from the irradiated surface was measured using optical microscopy.

The indentation hardness tests were complemented with the measurements of the mobility of indentation-induced dislocations in irradiated MgO. For this purpose, the technique based on the arm length measurements of dislocation rosette around indent was used ([11] and references therein). The shape of dislocation rosette on (100) indentation plane is determined by the indentation activated {110} < (110) slip system [12]. The ion-induced effect in dislocation mobility was expressed as the relative variation of dislocation arm length: $(l_0 - l)/l_0$, where $l_0$ and $l$ are the arm lengths in unirradiated and irradiated crystal, respectively.

The indentation-induced dislocations as well as the ion-induced dislocations were revealed by chemical etching in a saturated aqueous $FeCl_3$ solution and inspected by AFM (CPII, Veeco, USA) in a tapping mode. To distinguish between indentation-induced large dislocation half-loops and the small ion-induced prismatic dislocation loops with nanoscale dimensions, the former in further text are named simply as dislocations and the latter as prismatic dislocation loops.

The etching of fresh indentation-induced dislocations provided good AFM images of dislocation rosettes [13]. Nevertheless, the selectivity of etching in irradiated MgO was rather poor as has been reported earlier for "old" dislocations, etching of which is inhibited by segregated impurities [14, 15].

## 3 Results and discussion

### 3.1 Optical absorption spectroscopy

The results of optical spectroscopy confirm ion-induced coloring of crystals which increases with the fluence (Fig. 1). The absorption spectra show formation of a strong ~250-nm band, which is assigned to important amount of neutral and charged oxygen vacancy centers, such as $F$ centers (oxygen vacancy with two trapped electrons) and $F^+$ centers (oxygen vacancy with a single trapped electron) as previously reported in the literature [2, 16]. The results show stronger coloring in the case of Kr ions for which at fluences above $10^{14}$ Kr/cm$^2$ the measurable absorbance limit of 250 nm band is exceeded. Besides, for irradiations with Kr ions, a weak 570-nm band ascribed to aggregated centers is also present (Fig. 1a, inset).

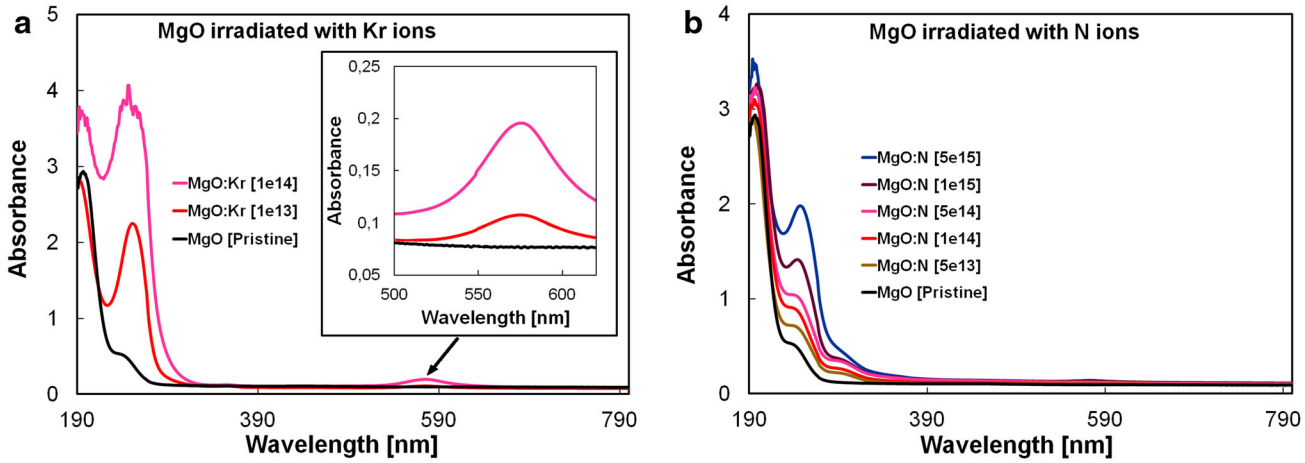


**Fig. 1** Optical absorption spectra of MgO crystal irradiated with **a** 150 MeV $^{84}$Kr and **b** 24.5 MeV $^{14}$N ions at different fluences

### 3.2 Nanoindentation study

Nanoindentation tests on the irradiated surface of MgO crystals irradiated with Kr and N ions to high fluences show an increase in hardness. The surface hardness increases with the fluence and saturates at fluences above $10^{14}$ ions/cm$^2$ where the effect of hardening reaches about 50 %, which is considerably lower than in the case of radiation-sensitive materials, such as LiF, in which the hardening of about 200 % is observed [8, 9]. Ion-induced change of modulus is small. Thus, the Young's modulus for unirradiated MgO was 310 GPa, whereas after high fluence, irradiation with Kr ions increased to 350 GPa (an increase by 13 %). The increase in hardness indicates that radiation damage includes not only a formation of primary color centers but also a formation of defect aggregates responsible for hardening.

Also, the depth profiles of ion-induced hardening on surfaces cleaved along the ion path have been investigated. The results for $^{84}$Kr and $^{14}$N ions are shown in Figs. 2 and 3, respectively. The indentation tests were complemented with the measurements of dislocation mobility (characterized by the size of dislocation rosette around indents) which is even more sensitive to defect aggregates and extended defects than hardness [9]. For the comparison, also the data of calculated electronic and nuclear energy loss for Kr and N ions have been plotted. Additionally, we performed a more accurate calculation on damage produced in nuclear stopping taking into account full damage cascades as described in [17, 18]. It was taken into account that the primary knocked target atoms have the energy high enough to deposit a considerable fraction of the energy in inelastic collisions inside the material.

As seen in Figs. 2 and 3, the hardness of irradiated MgO varies along the ion path and displays a maximum at the

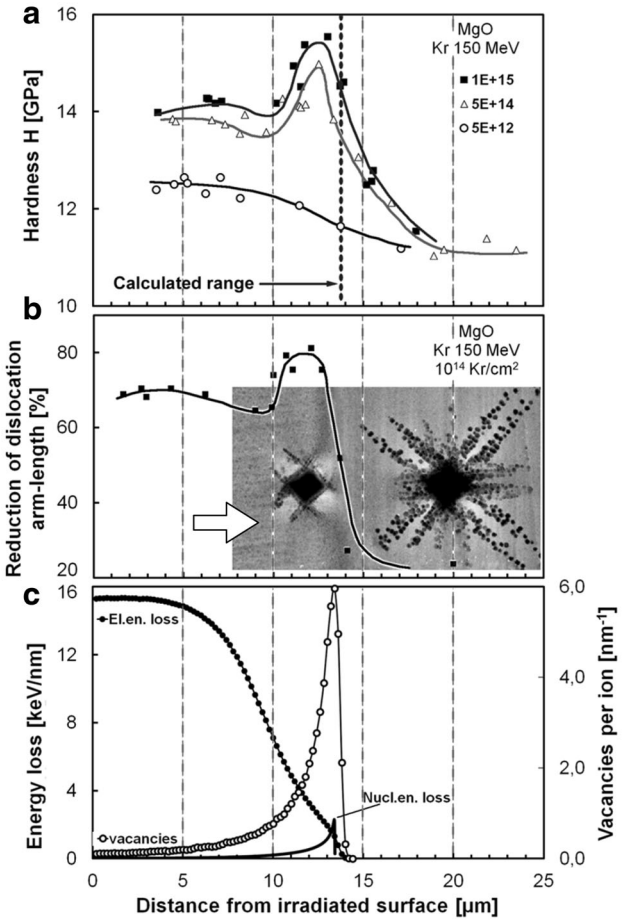


**Fig. 2** **a** The depth profile of hardness of MgO irradiated with 150 MeV $^{84}$Kr ions at fluences $5 \times 10^{12}$, $5 \times 10^{14}$ and $5 \times 10^{15}$ Kr/cm$^2$; **b** the depth profile of the dislocation mobility for fluence $10^{14}$ Kr/cm$^2$; inset shows the AFM image of dislocation rosettes in the zone of maximum hardening (*arrow* indicates the direction of ion beam); **c** the calculated depth profiles of electronic and nuclear energy loss (*left axis*) and a number of oxygen and magnesium vacancies per incident Kr ion (*right axis*)

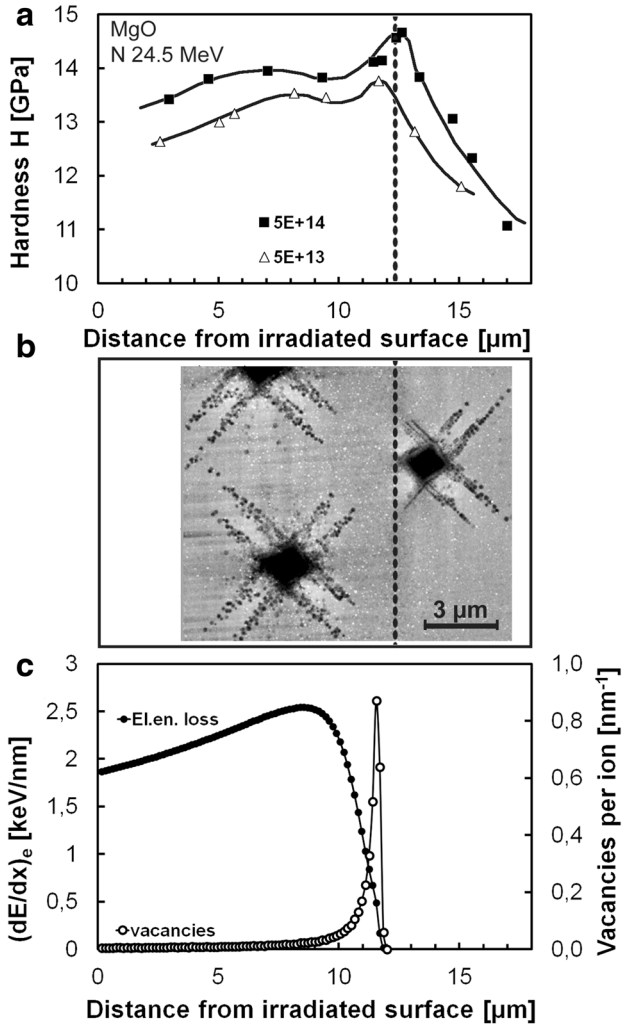


**Fig. 3** **a** The depth profile of hardness of MgO irradiated with 24.5 MeV $^{14}$N ions at $5 \times 10^{13}$ and $5 \times 10^{14}$ N/cm$^2$; **b** AFM image of dislocation rosettes in the zone of maximum hardening, fluence $\Phi = 10^{15}$ N/cm$^2$; **c** the calculated depth profiles of electronic energy loss (*left axis*) and a number of oxygen and magnesium vacancies per incident $^{14}$N ion (*right axis*)

end of the ion range. This provides evidence for a non-uniform distribution of defect clusters and aggregates along the ion range.

The dislocation mobility measurements in irradiated samples show the reduction in the size of dislocation rosette due to pinning of dislocations by aggregates of radiation defects. The change of the dislocation mobility ($\Delta l/l_0$, %) along the ion path for the fluence of $10^{14}$ Kr/cm$^2$ is presented in Fig. 2b. The maximum decrease in dislocation mobility (about 80 %) is reached at the end of the ion range where the maximum of hardness is observed. Insets in Figs. 2b and 3b demonstrate a sharp reduction in the size of dislocation rosette inside a narrow (1–2 μm) zone of maximum hardening compared to that in its close vicinity.

The damage production is known to be strongly affected by the energy loss of ions. The energy deposition is commonly described by the stopping power d$E$/d$x$ which gives the energy transfer per path length of a projectile along its trajectory. According to SRIM data, the calculated electronic energy transfer in a major part of the ion range exceeds the nuclear stopping power by an order of magnitude for both $^{84}$Kr and $^{14}$N ions, as it is commonly observed for swift heavy ions. As it is seen from the comparison of the hardness and electronic energy loss data, in the large part of the ion range, there is a correlation between them. An exception is the tail part of the ion range where the calculated number of vacancies per incident ion in damage cascades (Figs. 2c, 3c) as well as the calculated nuclear energy loss in terms of keV/nm reaches a maximum. Results allow us to conclude that both electronic and nuclear stopping mechanisms of Kr and N ions contribute not only to the creation of color centers as was established earlier [2, 19] but also to the creation of defect aggregates and extended defects responsible for hardening. The contribution of electronic stopping is dominating in the major part of the ion range, including also measurements on the irradiated surface, whereas the contribution of elastic displacements dominates close to the end of the projectile range.

The damage through ionization and electronic excitations in MgO under SHI irradiation is known to be impossible in ultra-pure crystals; however, it takes place if the content of metal impurities (Be, Ca, etc.) responsible for self-trapping of excitons is sufficiently high. Such conditions are met in the present work performed on MgO crystals containing Ca, Fe and Cr impurities (above 10 ppm). Despite the fact that only a small part of ions (impurity ions in substituting positions) is involved in the production of Frenkel defects through the exciton mechanism, its resulting contribution in hardening exceeds that from the impact mechanism. The latter dominates only in a narrow zone at the end of the ion range.

The dependence of electronic and nuclear components of hardening on fluence has been studied, and the results for irradiations with Kr ions are presented in Fig. 4, where the hardness data at the Bragg's maximum (depth 6 μm) and at the maximum of nuclear stopping (depth 13 μm) have been plotted. The results in both cases show a power law behavior. Generally, the hardening by impact mechanism, as less efficient, requires higher fluences. From the extrapolation of results, it follows that the threshold fluence of ion-induced hardening is expected above $10^{10}$ and $10^{12}$ ions/cm$^2$ (dose of 48 and 4.8 MGy) for electronic and nuclear stopping, correspondingly. In agreement with this, nanoindentation tests at the end of the ion range show no maximum of hardness for the lowest fluence of $5 \times 10^{12}$ Kr/cm$^2$ because the contribution of the impact mechanism to hardening becomes small (Fig. 2a). Taking

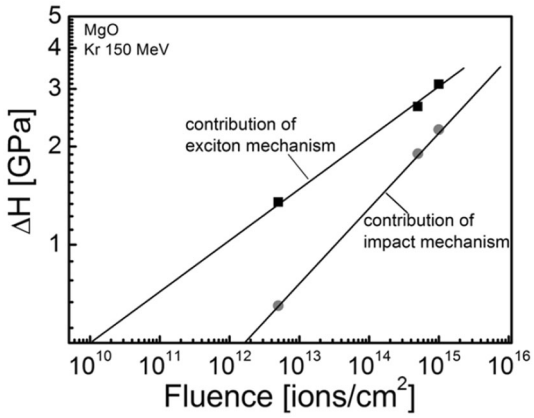


**Fig. 4** Contribution of electronic excitation and impact mechanisms in ion-induced hardening, dependence on fluence for irradiations with $^{84}$Kr ions

into account that the hardening is observed at the stage of track overlapping [9, 20–22], we can estimate the effective radii of tracks using the Poisson's law [23].

$$A/A_0 = 1 - \exp\left(-\pi r_F^2 \times \Phi\right) \quad (1)$$

where $A$ is the overlapped area, $A_0$ is the nominal area, $\Phi$ is the ion fluence, and $r_F$ is the effective track radius involved in excitonic or impact processes. From the estimates obtained by extrapolation of track overlapping curves, it follows that track radii responsible for hardening are about 17 nm in the case of electronic excitations and 1.5–2 nm in the case of impact damage cascades. Note that these values give the lower limit of track radii estimation since single-ion tracks can be far from saturation with the radiation defects responsible for hardening [24]. In particular, the damage cascades of single projectiles certainly provide non-saturated defect concentration. As a result, comparatively high fluences, ensuring multiple track overlapping, are required for hardening.

A comparison of the efficiency of Kr and N ions in damage production on the irradiated surface where ionization and electronic excitation mechanisms play a dominating role has been performed. As expected, the hardening effect at the same irradiation dose ($\sim$900 MGy) was by approximately 17 % stronger in the case of Kr ions. Irradiation with Kr ions displays higher efficiency also in the case when the nuclear mechanism dominates. The calculated number of produced vacancies per Kr ion by a factor of seven exceeds that for N ion (see Figs. 2, 3). Similarly, a stronger effect of hardening at the same dose is reached.

Nanoindentation tests for $^{14}$N ions at high-fluence irradiation reveal some hardening beyond the ion range assessed by SRIM code [10]. The effect can be explained partially by the edge effect in the hardness measurements due to definite size of deformation zone around indents. On the other hand, the adjacent unirradiated zone can be hardened by formation of dislocations under swelling-induced long-range stresses as it was observed in LiF crystals irradiated with SHI [25]. Other possible mechanisms are discussed in [26].

Instrumented nanoindentation is applicable also for the characterization of plasticity of materials. Nanoindentation tests on irradiated surface as well as on profile surfaces show no pop-in events related to crack formation and give smooth loading and unloading curves. No cracks around indents in the investigated range of indentation depth (up to 2 μm) were observed also in AFM images from as-cleaved and chemically etched samples irradiated at different fluences. We conclude that MgO crystals maintain microplasticity even after high-fluence irradiation with $^{84}$Kr and $^{14}$N ions. However, the observed variation of hardness along ion trajectory points to non-uniformity of damage. The concentration of strong damage in local areas, namely at the end of the ion range, can create mechanical stresses facilitating brittleness at macroscopic loading.

### 3.3 Study of dislocation structure

Structural study performed by chemical etching on profile surfaces of irradiated MgO revealed etching pits which can be attributed to ion-induced prismatic dislocation loops. The etching of dislocations is clearly seen in Fig. 5a where indentation-induced dislocation rosette is presented. The density of prismatic dislocation loops in a large part of the ion range (up to the Bragg's maximum) was comparatively low (about $10^8$ cm$^{-2}$) (Fig. 5). In the narrow zone of maximum hardening, the density of etching pits was remarkably higher. For irradiations with N ions, their density at fluence $10^{15}$ N/cm$^2$ exceeded $10^9$ cm$^{-2}$. The increase in density of ion-induced dislocation loops leads to a reduction in dislocation mobility and increase in hardness as it is demonstrated in Figs. 2 and 3.

Recent experiments on LiF crystals irradiated with SHI showed that the production of primary radiation defects as well as formation of extended defects at the stage of track overlapping is strongly affected by the structure of ion tracks. Tracks consisting of strongly damaged core region surrounded with halo of color centers exhibit stress field that facilitates the arrangement of dislocations and formation of bulk nanostructures, while the tracks exhibiting only the halo damage produce randomly distributed dislocations [20–22]. In the present study, the maximum electronic energy loss for Kr ions (15 keV/nm) and N ions (2 keV/nm) is below the threshold for core damage in MgO, which is reported as 22 keV/nm [27]. In agreement with this, the only defects revealed by chemical etching were ion-

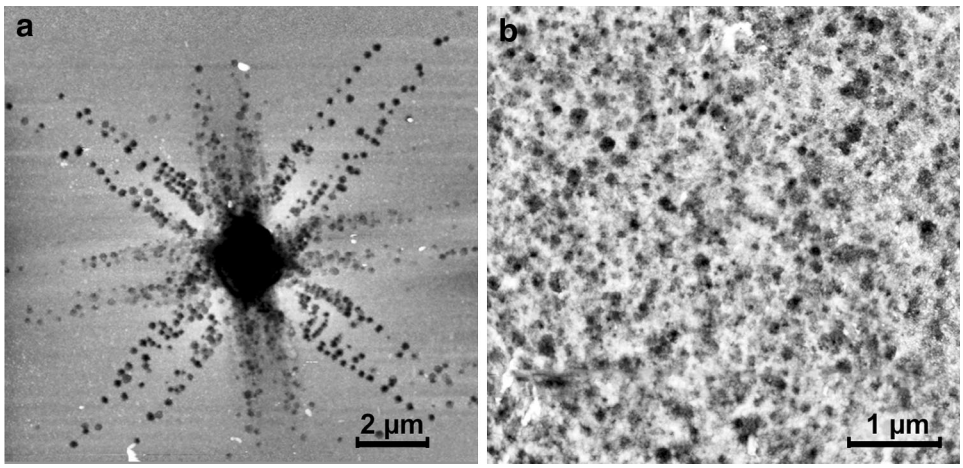


**Fig. 5** AFM image of the dislocation rosette on pristine MgO (**a**) and dislocation etching pits on profile surface after irradiation with $10^{14}$ Kr/cm$^2$ (**b**)

induced dislocation loops. No evidence for etching of tracks or ion-induced nanostructuring was obtained.

The evidence for the formation of SHI-induced prismatic dislocation loops in MgO was obtained in previous TEM studies, where small interstitial dislocation loops (around 10 nm) having the Burgers vector $\boldsymbol{b} = a/2\ [1\bar{1}0]$ and lying on {110} plane were observed [6, 7].

The size of dislocation rosette in heavily irradiated MgO (Fig. 2b, inset) is strongly reduced which indicates localization of plastic deformation in the vicinity of indents. Under such conditions, not only the dislocation plasticity but also the non-dislocation mechanisms of plastic deformation could be initiated. Some contribution of the point defect-assisted plasticity was detected even in unirradiated MgO [28, 29]. In irradiated MgO, such mechanism based on rearrangement of atomic groups at indentation tests can be facilitated by the swelling (increase in free volume) and increase in pressure beneath the indenter [30].

## 4 Conclusions

The irradiation of MgO single crystals with energetic $^{84}$Kr and $^{14}$N ions at high fluences leads to ion-induced formation of dislocations and ion-induced increase in hardness. The ion-induced hardening manifests at fluences above $10^{10}$ - ions/cm$^2$ corresponding to the stage of track overlapping. Its magnitude varies along the ion range following the depth dependence of calculated total energy loss of ions. A joint contribution of electronic excitations and atomic displacements by elastic collisions in the structural damage and hardening of MgO is confirmed. Results allow us to conclude that both electronic and nuclear stopping mechanisms of Kr and N ions contribute not only to the creation of color centers as was established earlier but also to the creation of defect aggregates and extended defects responsible for hardening. The electronic excitation mechanism prevails on the major part of ion range, while impact mechanism becomes dominant at the end of the ion range, where the nuclear energy loss displays a maximum and density of ion-induced dislocations reaches about $10^9$ cm$^{-2}$.

The obtained results characterize MgO as a material which survives severe irradiation with swift $^{84}$Kr and $^{14}$N ions, maintains integrity and microplasticity and exhibits improved hardness.

**Acknowledgments** The work has been supported by the ESF project Nr. 2013/0015/1DP/1.1.1.2.0/13/APIA/VIAA/010 and the National Research Program IMIS2.

## References

1. N. Itoh, A.M. Stoneham, *Materials Modification by Electronic Excitation* (Cambridge University Press, Cambridge, 2001)
2. A. Lushchik, E. Feldbach, S. Galajev, T. Kärner, P. Liblik, Ch. Lushchik, A. Maaroos, V. Nagirnyi, E. Vasil'chenko, Radiat. Meas. **42**, 92 (2007)
3. A. Lushchik, Ch. Lushchik, K. Schwartz, F. Savikhin, E. Shablonin, A. Shugai, E. Vasil'chenko, Nucl. Instr. Meth. B **277**, 40 (2012)
4. I. Richter, R. Gheewala, S.D. Smith, J. Kenny, K.Sickafus Valdez, J. Nucl. Mater. **382**, 176 (2008)
5. M.Y. Khan, L.M. Brown, M.M. Chaudhri, J. Phys. D Appl. Phys. **25**, 257 (1992)
6. C. Kinosita, in *Radiation Effects in Solids. NATO Science Series*, eds. by K. Sickafus, E. Kotomin, B.P. Uberuaga (Springer, Netherlands, 2007) vol. 235, pp. 45–64
7. J. Ohta, K. Suzuki, T. Suzuki, J. Mater. Res. **9**, 2953 (1994)
8. I. Manika, J. Maniks, K. Schwartz, C. Trautmann, Nucl. Instr. Meth. B **196**, 299 (2002)
9. I. Manika, J. Maniks, K. Schwartz, J. Phys. D: Appl. Phys. **41**, 074008 (2008)
10. F. Ziegler, P. Biersack, U. Littmark, *The Stopping and Range of Ions in Matter* (Pergamon Press, New York, 1985)
11. I. Manika, J. Maniks, K. Schwartz, Nucl. Instr. Meth. B **266**, 2741 (2008)
12. A.S. Keh, J. Appl. Phys. **31**, 1538 (1960)
13. Y. Gaillard, C. Tromas, J. Woirgard, Acta Mater. **51**, 1059 (2003)
14. J.J. Gilman, W.G. Johnston, G.W. Sears, Appl. Phys. **29**, 747 (1958)

15. K. Sangwal, T.C. Patel, M.D. Kotak, J. Mater. Sci. **14**, 509 (1979)
16. B.D. Evans, J. Comas, P.R. Malmberg, Phys. Rev. B **6**, 2453 (1972)
17. M.V. Sorokin, R.M. Papaleo, K. Schwart, Appl. Phys. A **97**, 143 (2009)
18. J. Maniks, I. Manika, R. Grants, R. Zabels, K. Schwartz, M. Sorokin, R.M. Papaleo, Appl. Phys. A **104**, 1121 (2011)
19. A. Lushchik, T. Kärner, Ch. Lushchik, K. Schwartz, F. Savikhin, E. Shablonin, A. Shugai, E. Vasil'chenko, Nucl. Instr. Meth. B **266**, 200 (2012)
20. J. Maniks, I. Manika, R. Zabels, R. Grants, E. Tamanis, K. Schwartz, Nucl. Instr. Meth. B **282**, 81 (2012)
21. A. Dauletbekova, J. Maniks, I. Manika, R. Zabels, A.T. Aklibekov, M.V. Zdorovets, Y. Bikert, K. Schwartz, Nucl. Instr. Meth. B **286**, 56 (2012)
22. R. Zabels, I. Manika, K. Schwartz, J. Maniks, R. Grants, Nucl. Instr. Meth. B **326**, 318 (2014)
23. P. Thevenard, G. Guiraud, C.H.S. Dupuy, B. Delaunay, Radiat. Eff. **32**, 83 (1977)
24. M.V. Sorokin, K. Schwartz, C. Trautmann, A. Dauletbekova, A.S. El-Said, Nucl. Instr. Meth. B **326**, 307 (2014)
25. I. Manika, J. Maniks, K. Schwartz, M. Toulemonde, C. Trautmann, Nucl. Instr. Meth. B **209**, 93 (2003)
26. M.V. Sorokin, K. Schwartz, K.O. Voss, O. Rosmej, A.E. Volkov, R. Neumann, Nucl. Instr. Meth. B **285**, 24 (2012)
27. S.J. Zinkle, V.A. Skuratov, Nucl. Instr. Meth. B **141**, 737 (1998)
28. M.S. Akchurin, V.R. Regel, Chem. Rev. **23**, 59 (1998)
29. M.M. Chaudrhi, Phil. Mag. Lett. **77**, 7 (1998)
30. J. Maniks, R. Zabels, I. Manika, IOP Conf. ser. Mater. Sci. Eng. **38**, 012017 (2012)